



Universitat Autònoma de Barcelona

**ADVERTIMENT.** L'accés als continguts d'aquesta tesi queda condicionat a l'acceptació de les condicions d'ús establertes per la següent llicència Creative Commons:  [http://cat.creativecommons.org/?page\\_id=184](http://cat.creativecommons.org/?page_id=184)

**ADVERTENCIA.** El acceso a los contenidos de esta tesis queda condicionado a la aceptación de las condiciones de uso establecidas por la siguiente licencia Creative Commons:  <http://es.creativecommons.org/blog/licencias/>

**WARNING.** The access to the contents of this doctoral thesis it is limited to the acceptance of the use conditions set by the following Creative Commons license:  <https://creativecommons.org/licenses/?lang=en>



Universitat Autònoma de Barcelona

PhD Thesis

**A study of multi-parametric MRI as a prognostic and response biomarker in patients with castration resistant prostate carcinoma and bone metastases.**

**Raquel Perez Lopez**

PhD supervisor:  
Prof. Johann S. de Bono

PhD tutor:  
Dr. Albert Selva O'Callaghan

**Universitat Autònoma de Barcelona  
Doctorate Program in Medicine  
Barcelona, 2017**



## Acknowledgments

---

Primero de todo gracias a mi jefe y mentor Johann de Bono. Gracias por creer en la radiología tanto como yo, apostando por las técnicas de imagen como herramienta fundamental en el avance de nuevos tratamientos contra el cáncer; por confiar en mí y darme su apoyo.

Gracias a todos los profesionales del Institute of Cancer Research y The Royal Marsden Hospital y en especial al Drug Development Unit, Prostate Cancer Targeted Therapy Group, Magnetic Resonance Unit y al servicio de Radiología, porque todos y cada uno de ellos están poniendo un granito de arena en la lucha contra el cáncer y han hecho posible, de una u otra forma, los estudios que aquí se presentan.

A los pacientes y a sus familias por su generosidad, comprensión y paciencia al aceptar participar en estos estudios.

A todos los grandes amigos que he hecho en Londres, en especial a David Olmos, Elena Castro, David Lorente, Desam Roda, Begoña Jiménez y Pasquale Rescigno, por ser mi familia cuando los míos estaban lejos. A mis compañeros y amigos de Barcelona, porque también forman parte del largo camino que me ha llevado hasta aquí.

A mi hermana, Laura, por ser mi amiga, mi consejera, mi apoyo, mi referente.

A mis padres por haber hecho de mí lo que soy, por inculcarme el esfuerzo, la perseverancia, la curiosidad y la honradez. Gracias por vuestro amor incondicional, dedicación, enseñanzas, comprensión y por tantas cosas que no caben en palabras. Papá, este trabajo te lo dedico especialmente a ti; sé que hubieras disfrutado con cada nuevo descubrimiento y cada avance en mi carrera tanto o más que yo.

Por último, mi más sentido agradecimiento a Quim, mi compañero de viaje, gracias por sacar lo mejor de mí; y a mis queridísimos hijos Gabriel y Martín por, a pesar del agotamiento, darme fuerzas para seguir adelante, por darle sentido a todo esto.

## Abbreviations

---

ADC	Apparent Diffusion Coefficient
BS	Bone Scintigraphy
DWI	Diffusion-Weighted Imaging
cfDNA	cell-free Deoxyribonucleic Acid
CRPC	Castration Resistant Prostate Cancer
CT	Computed Tomography
CTC	Circulating Tumour Cell
FF	Fat Fraction
ICC	Intraclass Correlation Coefficient
IVIM	Intravoxel Incoherent Motion
mCRPC	metastatic Castration Resistant Prostate Cancer
MIP	Maximum Intensity Projection
MP	Multiparametric
MRI	Magnetic Resonance Imaging
RECIST	Response Evaluation Criteria in Solid Tumours
ROI	Region Of Interest
PARP	Poly(ADP-ribose) Polymerase
PCWG	Prostate Cancer Working Group
PET	Positron Emission Tomography
PSA	Prostate-Specific Antigen
PSMA	Prostate-Specific Membrane Antigen



## Summary

---

Multiple new drugs have been approved for advanced prostate cancer treatment over the last decade including novel endocrine therapies (abiraterone acetate and enzalutamide), taxane-based chemotherapies (docetaxel and cabazitaxel) and radiopharmaceuticals (Rad 223). Moreover, many other treatments such as PARP-inhibitors and immunotherapy are currently being developed; these have shown promising results in early trials. However, despite the exciting progress achieved in the management of prostate cancer, metastatic prostate cancer remains a fatal condition, causing marked morbidity and mortality worldwide.

The development of all these treatments has brought a wide range of opportunities for patients with advanced prostate cancer, but also challenges physicians to optimize treatment selection and pursue a rational and efficient sequence of drugs for each patient. Therefore, there is a need for predictive and prognostic biomarkers that help in treatment decision-making.

Assessment of response to anticancer therapy in patients with advanced prostate cancer represents a challenge. The skeleton is the most frequent organ of distal metastases in prostate cancer patients, representing very often the only site of metastatic disease. The currently used standard imaging techniques, computed tomography and bone scan, do not depict the true extent of bone metastases and are suboptimal in capturing biological changes occurring in response to treatment. Treatment switch decisions are too often being made based on PSA changes, which are neither a survival surrogate biomarker nor a good response biomarker for non-hormonal agents. Therefore, the development of accurate response biomarkers for bone metastases remains an unmet medical need.



MRI including functional sequences allows the study of anatomical and as well molecular and metabolic features. Diffusion-weighted imaging is a functional MRI technique that studies the movement of water molecules within a tissue and informs of tissue microstructure and cellularity. In my PhD studies I evaluated multiparametric MRI including diffusion-weighted imaging as a prognostic and response biomarker in patients with castration resistant prostate cancer and bone metastases.

The study presented in the manuscript “Volume of bone metastasis assessed with whole-body diffusion-weighted imaging is associated with overall survival in metastatic castration-resistant prostate cancer” showed that the burden of bone metastases assessed with whole body DWI is a prognostic biomarker in patients with advanced prostate cancer.

The study presented in the manuscript “Diffusion-weighted imaging as a treatment response biomarker evaluating bone metastases in prostate cancer” represents the first study of whole-body diffusion-weighted imaging in the setting of a prospective clinical trial in patients with metastatic prostate cancer. Changes in quantitative variables derived from diffusion-weighted imaging of bone metastases are indicators of response to the PARP inhibitor olaparib.

I also studied the correlation of multiparametric MRI features with histological findings in bone biopsies. This is crucial towards the validation of DWI as a biomarker for bone metastases in prostate cancer.

The positive results of these studies contribute towards the eventual implementation of DWI in prostate cancer care.

## Resumen

---

Múltiples drogas han sido aprobadas para el tratamiento de cáncer de próstata avanzado en las últimas décadas, incluyendo innovadoras terapias hormonales (abiraterona y enzalutamida), quimioterapias basadas en taxanos (docetaxel y cabazitaxel) y radiofármacos (Rad 223). Además, se han desarrollado muchos otros tratamientos como inhibidores de PARP e inmunoterapias; éstos han demostrado resultados prometedores en ensayos clínicos precoces. Aunque, a pesar del fascinante progreso conseguido en el manejo del cáncer de próstata, su forma metastásica sigue siendo una condición fatídica, causando elevada morbilidad y mortalidad en todo el mundo.

El desarrollo de todos estos tratamientos ha aportado nuevas oportunidades para los pacientes con cáncer de próstata avanzado pero, también significa un reto para los médicos a la hora de optimizar la selección de tratamientos y llevar a cabo una secuencia de tratamientos razonable y eficiente. Es por ello que existe la necesidad de desarrollar biomarcadores predictivos y pronósticos que ayuden en la toma de decisiones terapéuticas.

La valoración de respuesta en pacientes con cáncer de próstata avanzado representa un reto. El esqueleto es el órgano en el que ocurren con mayor frecuencia las metástasis en pacientes con cáncer de próstata, representando en muchas ocasiones la única localización de enfermedad metastásica. Las técnicas de imagen estándares utilizadas en la actualidad, tomografía computarizada y gammagrafía ósea, no muestran la verdadera extensión de las metástasis óseas y presentan de forma subóptima cambios biológicos como respuesta a tratamientos. El cambio de terapia se basa muchas veces en cambios de PSA, el cual no es ni un biomarcador pronóstico ni de respuesta en tratamientos no hormonales. Por ello, hay una necesidad médica imperiosa de desarrollar biomarcadores de respuesta precisos.

La RNM incluyendo secuencias funcionales permite el estudio de características anatómicas así como moleculares y metabólicas. Los estudios de difusión son una secuencia funcional de RNM que evalúa el movimiento de las moléculas de agua en los tejidos e informa de la microestructura y celularidad tisular. En mi programa de doctorado he analizado el papel de la RNM multiparamétrica, incluyendo imagen de difusión, como biomarcador pronóstico y de respuesta en pacientes con cáncer de próstata resistente a castración y metástasis óseas.

El estudio presentado en el manuscrito “El volumen de metástasis óseas evaluado mediante estudio de difusión de cuerpo entero se asocia con supervivencia en el cáncer de próstata resistente a castración” muestra que la carga de metástasis óseas cuantificada por imagen de difusión de cuerpo entero es un biomarcador pronóstico en pacientes con cáncer de próstata.

El estudio presentado en el manuscrito “Imagen de difusión como biomarcador de respuesta evaluando metástasis óseas en cáncer de próstata” representa el primer estudio de difusión de cuerpo entero dentro de un ensayo clínico prospectivo en pacientes con cáncer de próstata metastásico. Cambios en parámetros cuantificables derivados de las imágenes de difusión de las metástasis óseas son un indicador de respuesta al inhibidor de PARP olaparib.

También he estudiado la correlación de las características de RNM multiparamétrica con parámetros histológicos de biopsias óseas. Esto es crucial para la validación de la imagen de difusión como biomarcador de metástasis óseas en cáncer de próstata.

Los positivos resultados de estos estudios contribuyen a la eventual puesta en práctica de la imagen de difusión en el tratamiento del cáncer de próstata.

# Table of Contents

---

<b>Acknowledgments</b> .....	<b>3</b>
<b>Abbreviations</b> .....	<b>5</b>
<b>Summary</b> .....	<b>7</b>
<b>Resumen</b> .....	<b>9</b>
<b>1. Introduction</b> .....	<b>15</b>
1.1. Prostate cancer: need for biomarkers for precision medicine and challenges in assessing bone metastases.....	15
1.2. Diffusion-weighted imaging (DWI), a promising functional magnetic resonance imaging (MRI) technique for bone metastases assessment.....	17
1.3. MRI fat fraction (FF) quantification and its role in the evaluation of bone metastases .....	24
<b>2. Justification of the thesis theme</b> .....	<b>29</b>
<b>3. Hypothesis</b> .....	<b>33</b>
<b>4. Objectives</b> .....	<b>37</b>
4.1 General objectives.....	37
4.2 Specific objectives .....	37
<b>5. Methods: Whole-body MRI protocol</b> .....	<b>41</b>
5.1. Anatomical sequences.....	41
5.1.1. T1-weighted imaging.....	41
5.1.2. DIXON .....	43
5.2. Diffusion-weighted imaging.....	44
5.3. ADC and volume of bone metastases reproducibility.....	46
<b>6. Whole-body MRI analyses</b> .....	<b>51</b>
<b>Results and published studies</b> .....	<b>57</b>
7.1. Correlation of MP MRI with histological and molecular characteristics of bone marrow biopsies.....	57
7.2. Published manuscripts.....	83
7.2.1. Whole-body DW-MRI as prognostic biomarker in mCRPC with bone metastases .....	85

7.2.2. Whole-body DW-MRI as response biomarker of bone metastases in patients with mCRPC .....	99
<b>Discussion</b> .....	<b>119</b>
<b>Conclusions</b> .....	<b>129</b>
9.1. <i>General conclusions</i> .....	129
9.2. <i>Specific conclusions</i> .....	129
<b>10. Bibliography</b> .....	<b>135</b>
<b>11. Annexes</b> .....	<b>143</b>
<i>Other publications co-authored by the candidate during the PhD program</i> .....	143

# Introduction



# 1. Introduction

---

## 1.1. Prostate cancer: need for biomarkers for precision medicine and challenges in assessing bone metastases

---

The aim of precision medicine is to select the best treatment option for each patient at each time during the natural evolution of the disease based on understanding the clinical, pathology and molecular make-up of the tumour. Applied to cancer medicine, the ultimate objective of precision medicine is to improve patient survival and quality of life based on the individualisation of treatment. In order to achieve that goal, physicians need robust biomarkers to guide treatment decisions. These include prognostic, predictive, response and resistance biomarkers. Imaging has always played a critical role in guiding clinicians' decisions on cancer. The advent of functional imaging techniques, which not only describes anatomical characteristics but could also study the metabolic, vascular or molecular features of the disease, offers new opportunities for more precise patient care as well as a more efficient drug development process.

Since Huggins and Hodges demonstrated the effectiveness of hormonal manipulations over 70 years ago, androgen deprivation therapy has remained the mainstay of treatment for advanced prostate cancer (1). However, despite the significant and sometimes complete remissions with chemical or surgical castration, all patients with metastatic prostate cancer will eventually relapse to a fatal condition known as castration-resistant prostate cancer (CRPC). Several treatments have been approved over the past 10 years since the improvement in overall survival have been demonstrated by randomised trials in CRPC; these include novel endocrine therapies (abiraterone acetate and enzalutamide) (2, 3), taxane-based chemotherapies (docetaxel and cabazitaxel) (4, 5) and radiopharmaceuticals (Rad 223) (6). However, resistances to these therapies invariably appear and CRPC remains an incurable disease. To improve outcomes from CRPC, there is currently a tremendous effort



worldwide to develop further therapies for these patients. Recently, the antitumour activity of several target therapies such as the poly(ADP-ribose) polymerase (PARP) inhibitor olaparib (7), platinum-based chemotherapies (8, 9), radiolabelled prostate-specific membrane antigen (PSMA) (10) and different immunotherapies (11) have been reported in patients with metastatic CRPC (mCRPC). Treatment stratification based on predictive biomarkers is crucial to optimise therapy and eventually improve the survival of patients with CRPC as well as for the optimal development of further therapeutic agents, which is a costly and lengthy process. However, so far, no predictive biomarkers have been clinically validated for treatment selection in prostate cancer. Although there is great interest in non-invasive circulating biomarkers [circulating tumour cells (CTC) and circulating cell-free deoxyribonucleic acid (cfDNA)], archival tumour samples and fresh biopsies of primary or metastatic disease remain the gold standard for histological and molecular tumour evaluation. The optimisation of image-guided tumour sampling thus offers the possibility to increase biopsy efficacy and reduce patient discomfort of unsuccessful biopsies.

Bone metastases are the most frequent site of distal metastases in patients with CRPC, occurring in up to 84% of patients with mCRPC (12). In fact, the skeleton frequently represents the only organ of metastatic disease. Standard imaging techniques such as computed tomography (CT) and technetium-99 bone scintigraphy (BS) fail to accurately evaluate the burden of bone metastases and detect changes in response to treatment. Actually, the Response Evaluation Criteria in Solid Tumours (RECIST) 1.1 consider bone metastases with no lytic component, the most common type in prostate cancer, to be non-measurable (13). The Prostate Cancer Working Group 3 (PCWG3) criteria define progression in bone metastases based on the appearance of new lesions in BS, but fail to state any criteria for response in bone metastases (14). Therefore, tumour responses in patients with bone-only metastatic disease rely solely on prostate-specific antigen (PSA) falls; the latter have not been proven to be a surrogate for improved survival, challenging the assessment of response to therapy and the use of standard imaging techniques (i.e. CT and BS) as clinical trial endpoints for CRPC (15, 16).

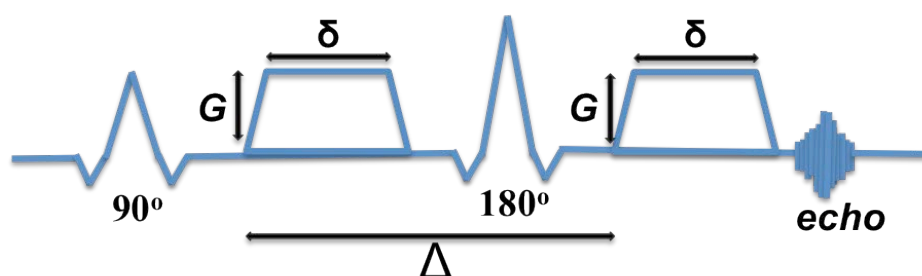
Therefore, there is an urgent unmet need to identify, develop and validate biomarkers for bone metastases in prostate cancer. The development of quantitative imaging biomarkers that can accurately elucidate the burden and nature of bone metastases will help to individualise patient risk stratification and treatment selection. Moreover, changes in the imaging-quantified burden of bone disease and/or conversion of other bone imaging biomarkers may have utility in evaluating response to treatment. Finally, in order to fully understand and ultimately validate an imaging biomarker, histological and molecular correlation with imaging findings is crucial.

## 1.2. Diffusion-weighted imaging (DWI), a promising functional magnetic resonance imaging (MRI) technique for bone metastases assessment

---

DWI is a functional MRI technique that studies the movement of water molecules within a tissue; the contrast between tissues is based on differences in the motion of water molecules within different compartments: intracellular, transmembrane, extracellular and intravascular. The DWI acquisition is based on the application of two gradients. The b value depends on the amplitude of the gradients ( $G$ ), duration of the applied gradients ( $\delta$ ) and spacing between the pulsed gradients ( $\Delta$ ) (17). Normally, b-values available on current MRI scanners range from in order of 0 to 4000 s/mm<sup>2</sup>.

**Figure 1. DWI sequence scheme based on the application of two strong gradient pulses of magnitude ( $G$ ) and duration ( $\delta$ ), separated by a time interval ( $\Delta$ );  $\gamma$  is the gyromagnetic ratio (42.58 MHz/Tesla for H<sup>1</sup>).**



***Formula to calculate b values based on the Stejskal-Tanner pulse gradient diffusion method:  $b = \gamma^2 G^2 \delta^2 (\Delta - \delta/3)$ .***

Depending on the chosen diffusion-weighted b value, we will enhance the influence of water molecules in different compartments. Low b values evaluate large diffusion distances and are, therefore, sensitive to the motion of intravascular water protons, allowing us to study vascular perfusion. Larger b values assess small diffusion distances in relation to the movement of water molecules between cells and, therefore, will be directly related to tissue cellularity. In theory, with very large b values (>4000 s/mm<sup>2</sup>), it is possible to evaluate the movement of water molecules within cells; however, in practice, there are technical challenges to achieving such high b values as the signal to noise is poor, requiring lengthy multiple acquisitions; that hinders clinical implementation due to the time-consuming nature and discomfort for the patient. Consequently, in order to evaluate bone marrow, a b value of 900 s/mm<sup>2</sup> is often chosen as a compromise between robust data and whole-body coverage achievable in a reasonable time frame.

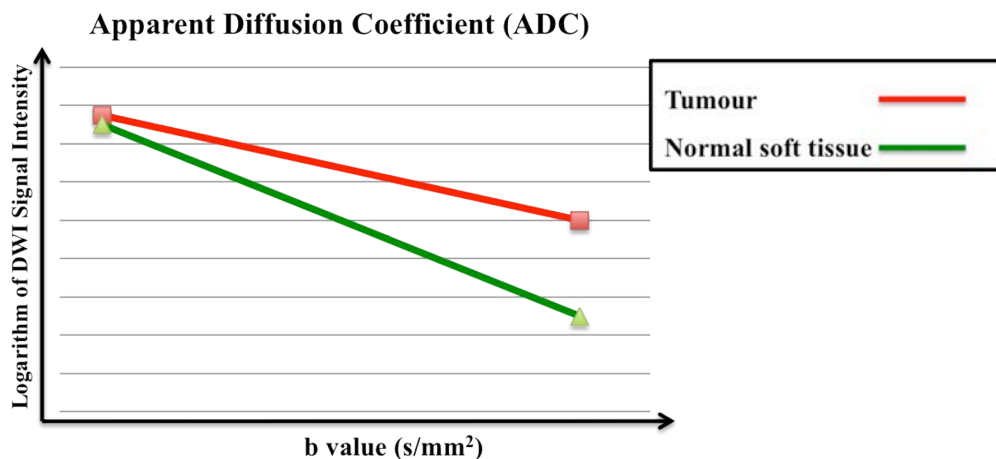
The apparent diffusion coefficient (ADC) is a parameter derived from the objective measurement of the water diffusion capabilities assessed using DWI. The calculation of the ADC is based on the changes in the signal attenuation of a tissue while increasing the DWI b values. Imaging with at least two diffusion weightings allows determining the differential signal attenuation.

$$\frac{S(b)}{S(0)} = e^{-b.ADC}$$

***Signal intensity after applying a b value [S(b)], normalised to the signal intensity without applying gradients, no b values, [S(0)].***

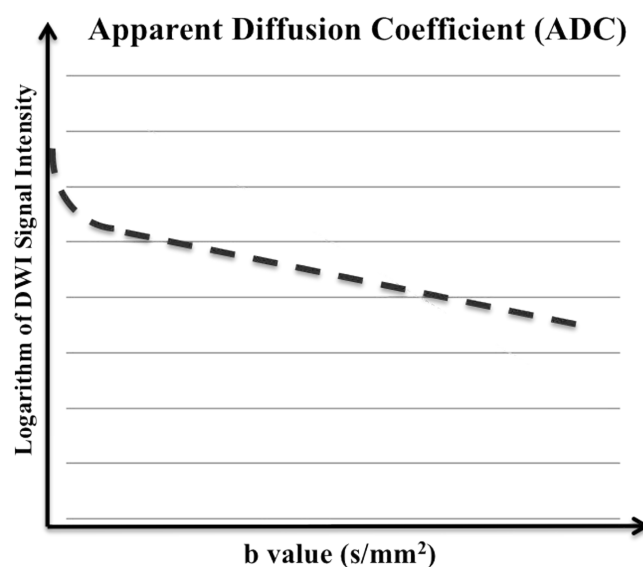
By increasing the number of acquired DWI sequences at multiple b values, the calculation of the ADC errors will be reduced. The slope of the line that describes the relationship between the logarithm of the signal intensity (on the y-axis) and the b value (on the x-axis) is the ADC. Therefore, when the movement of water molecules is not restricted within a tissue, the signal intensity of DWI will drop as we increase the b value. Hence, the slope of the line will be high and the ADC value will be high as well. Conversely, when there is restricted diffusion of the water molecules within a tissue, the signal intensity will not drop as much as we increase the DWI b value and therefore, the slope of the line will be lower and the ADC will be low. We can then obtain the automated calculation of an ADC for each pixel in the image and quantitative ADC maps can be produced and displayed as parametric ADC maps.

**Figure 2. Representation of the monoexponential fitting calculation of the ADC values in normal soft tissue with lower cellular density (green line) and highly cellular tumour (red line).**



The ADC is a complex function of tissue microarchitecture that is influenced by several components. Some of the factors that may influence the ADC are cellular architecture, cell size, membranes, macromolecules, viscosity of cytoplasm, flow in capillaries and active transport. It is simplistic to assume that the attenuation of the signal intensity with increasing b values occurs linearly in tissues. In fact, the signal intensity attenuates rapidly at low b values in many tissues such as the liver, while the attenuation is less marked at higher b values. This is due to the influence of water diffusibility within the blood vessels. Thus, diffusion-weighted data acquired over a range of b values that include low b values ( $< 50 \text{ s/mm}^2$ ) are sensitive to signal attenuation from perfusion. If we acquire the DWI sequences through only the high b values (i.e.,  $b=150\text{--}500 \text{ s/mm}^2$ ) we may provide a more accurate estimate of the cellularity of the tumour microenvironment by minimising any vascular contributions. The ADC values are theoretically independent of magnetic field strength.

**Figure 3. Representation of the intravoxel incoherent motion (IVIM) based biexponential calculation of the ADC values.**



Since DWI was described for the first time in 1985, it has mostly been implemented in the study of brain alterations; however, in the past decade there has been a surge in the study of DWI applications, particularly in the setting of oncology in multiple cancer types. Previous studies have demonstrated that ADC values are inversely correlated with cellularity in different tumour types including primary tumours and haematological malignancies (12–16). Recently, it has been shown that the use of DWI can optimise tissue acquisition in primary prostate tumour biopsies, helping identify aggressive tumours to improve diagnostic and therapy decisions for patients with suspicions of localised disease (18).

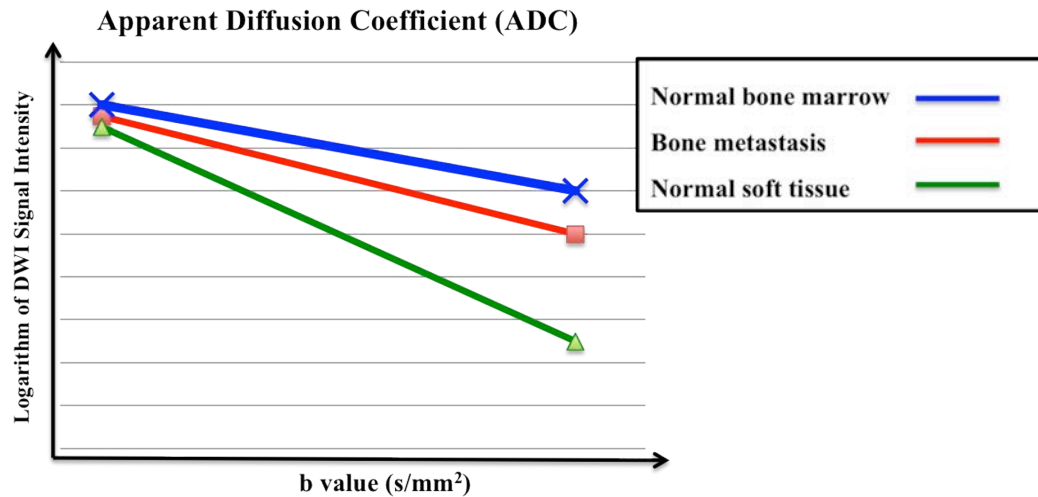
In response to treatment, the damage to cellular membranes, decrease in cellularity and increase in extracellular spaces within a tumour are expected to result in increasing motion capacities for water molecules, therefore resulting in ADC increases. Accordingly, changes in the ADC values after treatment have been correlated with tumour responses in different tumour types including myeloma, ovarian carcinoma, primary peritoneal carcinoma and rhabdomyosarcoma (19-21).

One of the most promising roles of DWI is the evaluation of bone marrow, particularly in the detection, prognosis and response evaluation of bone metastases. This is of particular interest for prostate cancer, where bone marrow represents the main site of metastatic spread in advanced disease, making the evaluation of response to therapy challenging. DWI has high sensitivity and specificity for the detection of bone metastases. DWI has been shown to be superior to CT, BS and <sup>11</sup>C-methionine positron emission tomography (PET) for the diagnosis of bone metastases (22). Other major advantages of DWI include the fact that no ionising radiation is administered and no injection of isotopes or any contrast medium is necessary. Importantly, whole-body DWI examinations with two b values are possible in reasonably short data acquisition times (25 minutes). Critically, DWI can be implemented using standard MRI equipment available at most major hospitals in the western world, facilitating the widespread use of these techniques in the near future, compared with the logistical hurdles for generalising certain techniques requiring of

short-living radioisotopes (23). There is particular interest in achieving agreement about the acquisition, interpretation and reporting of whole-body DWI scans that enables technique standardisation and facilitate longitudinal, multicentre studies and eventually the implementation of whole-body DWI into clinical practice (24). Whole-body DWI also allows the easy delineation of areas of signal abnormality with semi-automated segmentation software, providing the opportunity to more accurately determine the true extent of bone metastases; this is critical for homogenising assay interpretation (25, 26). Thus, signal intensity-depicted disease can be volumetrically quantified and tissue water diffusivity maps can enable the quantitative assessment of changes in the metastatic bone following therapy.

However, the presence of adipocytes in the bone marrow makes the evaluation of bone marrow with DWI somehow more complex. In normal adult bone marrow, particularly in the elderly population, fat marrow predominates and there is a paucity of free water. The motion of the small amount of water present is restricted by the large volume adipocytes and hence normal adult bone marrow has a very low signal on DWI and a very low ADC. At an early stage, bone metastases responding to treatment are expected to suffer massive cell death and a reduction in cellularity may translate into an increase in water diffusion. However, if response to treatment is maintained throughout a period of time, the fat marrow is expected to come back and replace the malignant cells. This may result in an “unexpected” ADC drop within the bone marrow in a responding patient. Hence, it is crucial to understand the normal bone marrow characteristics in our population and the evolution of the tumour-infiltrated bone marrow in response to treatment.

**Figure 4. Representation of the monoexponential fitting calculation of the ADC values in normal soft tissue (green line), bone metastases (red line) and normal bone marrow (blue line).**



Limited but promising data on the value of DWI in the assessment of response to bone metastases in mCRPC are currently available. Previous studies have shown that increases in the ADC and decreases in the volume of bone metastases assessed by DWI are indicators of response in patients with mCRPC (25, 27). Further prospective studies in a larger population are needed in order to validate these results.

Moreover, there is a need for imaging-pathology correlative studies to assess the relevance of these changes. Multiple studies have shown a strong correlation between the ADC values and tissue cellularity in soft tissue tumours (28-32). However, limited data are available for bone metastases, with only two studies providing histological correlation, not including prostate cancer patients (33, 34).



### 1.3. MRI fat fraction (FF) quantification and its role in the evaluation of bone metastases

---

One of the main components of bone marrow is fat; this represents approximately 80% of the bone marrow in the elderly population. Therefore, those MRI sequences able to detect and quantify the fat content within a tissue are particularly suited for the identification of bone marrow metastases and other infiltrative processes. These sequences, such as DIXON FF, are able to depict early cellular infiltration confined to the bone marrow space prior to the development of trabecular destruction.

The DIXON chemical shift imaging method utilises the fact that  $^1\text{H}$  nuclei in fat ( $\text{CH}_2$ ) and water ( $\text{H}_2\text{O}$ ) molecules precess at different rates due to the presence of different chemical environments. Fat and water are imaged when their  $^1\text{H}$  nuclei are spinning in phase with each other ( $\text{TE}=4.2$  msec in a 1.5T scanner) and out of phase with each other ( $\text{TE}=2.1$  msec in a 1.5T scanner). Thus, it is possible to depict the fat and water component of tissues. The in-phase and out-of-phase images can be combined so that fat-only and water-only images can be created. By definition:

Because of the different chemical environments of  $^1\text{H}$  in fat ( $\text{CH}_2$ ) and water ( $\text{H}_2\text{O}$ ),  $^1\text{H}$  precesses at different rates.

$$\text{in-phase} = (\text{water} + \text{fat})$$

$$\text{out-of-phase} = (\text{water} - \text{fat})$$

By averaging sum and difference data from each point, "pure water" and "pure fat" images can be reconstructed.

$$\text{fat only} = \frac{1}{2} (\text{in-phase} - \text{opposed phase}) = \frac{1}{2} [(\text{water} + \text{fat}) - (\text{water} - \text{fat})] = \frac{1}{2} (2\text{fat})$$

$$\text{water only} = \frac{1}{2} (\text{in-phase} + \text{opposed phase}) = \frac{1}{2} [(\text{water} + \text{fat}) + (\text{water} - \text{fat})] = \frac{1}{2} (2\text{water})$$

Previous studies have shown a strong correlation of the MRI FF and fat content within tissues such as the liver. However, limited information is available about the correlations of the histologically proven bone marrow fat content with the DWI signal intensity, the ADC or the FF.



# **Justification of the thesis theme**



## 2. Justification of the thesis theme

---

The research conducted during this PhD program aimed to advance the clinical qualification of multiparametric (MP) MRI including DWI as a prognostic and response biomarker in bone metastases from patients with mCRPC.

My work was divided into three projects within the same thematic unit: 1) to study how the volumetric assessment of bone metastases by DWI informs on disease burden and is a prognostic marker in mCRPC; 2) to study changes in the DWI of bone metastases in response and resistance to targeted therapies and 3) to study how MP MRI data translate the biological and pathology parameters of bone metastases.



# Hypothesis





### 3. Hypothesis

---

DWI studies the random movement of water within a tissue. DWI has shown outstanding performance in the detection of malignant bone marrow infiltration. Moreover, the ADC (an objective parameter derived from DWI) has been correlated with tumour cellularity.

I hypothesised that the evaluation of bone metastases by whole-body MP MRI would have utility as a prognostic and response biomarker in CRPC patients with bone metastases.

I also hypothesised that MP MRI including DWI would provide accurate *in vivo* information about bone metastases pathology and molecular features.



# Objectives



## 4. Objectives

---

### 4.1 General objectives

---

To assess the value of whole-body DWI as a prognostic and response biomarker of bone metastases in patients with mCRPC and evaluate the correlation of MP MRI with DWI with histological and molecular parameters from bone biopsies.

### 4.2 Specific objectives

---

- To establish the correlation between the burden of bone metastases assessed by whole-body DWI and known prognostic factors in patients with mCRPC.
- To study how the burden of bone metastases assessed by whole-body DWI associates with survival in patients with mCRPC.
- To assess if changes in the volume of bone metastases or in the ADC values assessed with DWI are indicators of response to therapy in patients with mCRPC.
- To study the correlation between the ADC and normalised DWI signal intensity of bone metastases and tumour cellularity in bone metastases biopsies.
- To study the correlation between FF assessment from MRI and the fat content in bone metastases biopsies.



## **Methods: Whole-body MRI protocol**





## 5. Methods: Whole-body MRI protocol

---

For the purpose of the research projects presented in this thesis, the whole-body MRI examinations were performed with a 1.5-T MR imaging unit (Aera or Avanto; Siemens Healthcare, Erlangen, Germany) by using surface and body coils in patients positioned supine. Patients were imaged from the skull vertex or the 2<sup>nd</sup> cervical vertebrae, depending on the study protocol in which they were included, to mid-thigh in all cases. The whole-body MRI protocol included the following sequences: axial T1-weighted turbo spin-echo and DWI in all the patients and DIXON quantitative chemical imaging shift in some of the patients, depending on the study protocol.

### 5.1. Anatomical sequences

---

#### 5.1.1. T1-weighted imaging

---

Whole-body axial T1-weighted fast low-angle shot gradient-echo (FLASH) imaging throughout four or five stations, depending on the study protocol and height of the patient, was performed. The T1-weighted imaging was acquired on inspiration and during breath hold. Patients were given directed breathing instructions and then requested to hold their breath on inspiration while the imaging block was acquired.

PARAMETER	T1-weighted imaging
Type of pulse sequence	Spoiled gradient echo (FLASH)
Respiration	Breath-hold on inspiration
Acquisition plane	Axial
Type of acquisition	2D

<b>Field of view (mm)</b>	380-420
<b>Section thickness (mm)</b>	5
<b>In-plane resolution (mm<sup>2</sup>)</b>	1.6 x 1.6
<b>Repetition time (ms)</b>	380
<b>Echo time (ms)</b>	5
<b>Inversion time (ms)</b>	NA
<b>Flip angle</b>	70
<b>Fat suppression</b>	NA
<b>Receiver bandwidth (Hz/pixel)</b>	331
<b>Number of signal average</b>	1
<b>Parallel imaging factor</b>	2
<b>Partial Fourier</b>	None
<b>b factors (s/mm<sup>2</sup>)</b>	NA
<b>Number stations</b>	4 (50 slices each)

### 5.1.2. DIXON

---

Whole-body axial or coronal DIXON T1-weighted volume interpolated breath-hold gradient-echo (VIBE) imaging was acquired.

PARAMETER	DIXON fat/water
Type of pulse sequence	fl3d_vibe
Respiration	Breath-hold on inspiration
Acquisition plane	Axial or coronal
Type of acquisition	3D
Field of view (mm)	450
Section thickness (mm)	5
In-plane resolution (mm <sup>2</sup> )	1.6 x 1.6
Repetition time (ms)	7
Echo time (ms)	TE1=2.39; TE2=4.78
Inversion time (ms)	NA
Flip angle	3
Fat suppression	NA
Receiver bandwidth (Hz/pixel)	400
Number of signal average	1
Parallel imaging factor	4
Partial Fourier	None
b factors (s/mm <sup>2</sup> )	NA
Number stations	2 (52 slices each)

## 5.2. Diffusion-weighted imaging

---

Whole-body axial DWI was acquired with free breathing and echo-planar DWI sequences from the skull base to the mid-thigh level, sequentially across three to six imaging stations, each consisting of 30-50 slices respectively. Two equal gradient pulses were applied (one on each side of the 180° radiofrequency pulse in echo-planar sequences). Two b values (b=50 and b=900) were chosen to obtain an accurate ADC value. Quantitative ADC maps were generated via manufacturer-provided software.

PARAMETER	DWI
Type of pulse sequence	Single-shot twice-refocused echo-planar imaging
Respiration	Free-breathing
Acquisition plane	Axial
Type of acquisition	2D
Field of view (mm)	380-420
Section thickness (mm)	5
In-plane resolution (mm <sup>2</sup> )	2.5 x 2.5
Repetition time (ms)	14000
Echo time (ms)	68
Inversion time (ms)	180
Flip angle	90
Fat suppression	STIR
Receiver bandwidth (Hz/pixel)	1800
Number of signal average	4

<b>Parallel imaging factor</b>	2
<b>Partial Fourier</b>	6/8
<b>b factors (s/mm<sup>2</sup>)</b>	50 and 900
<b>Number stations</b>	4 (50 slices each)

### 5.3. ADC and volume of bone metastases reproducibility

---

Measuring the reproducibility of an objective measurement is crucial to be able to determine the limits of error or expected technical or biological variations; therefore, we can better understand the magnitude of change that can be confidently detected and thus define the threshold above which values of measurement will be trustworthy. Ultimately, knowing the reproducibility of an objective parameter will allow us to validate this as a biomarker. The reproducibility of DWI signal intensity and the ADC is particularly important if DWI measurements are to be routinely used as a surrogate biomarker in oncologic patients.

Several methods can be considered to calculate reproducibility. Bland-Altman plots are commonly used to assess repeatability. Coefficient of Variation,  $CoV = \sigma/\mu$ , can be converted into percentage repeatability:  $100\% \times 1.96 \times \sqrt{2} \times CoV$  ( $p < 0.05$ , two-tailed test). We can also calculate the intra- and inter-observer intraclass correlation coefficients (ICCs)

As previously described, it is currently possible to perform whole-body DWI and analyse these data with semi-automated tools, thereby obtaining information about the total volume of DWI bone metastases and global ADC values. We showed there is nice agreement when calculating the total volume of bone metastases on DWI with the OsiriX semi-automated segmentation tool in patients with mCRPC; the intra- and inter-observer ICCs were 0.99 (95% CI: 0.95, 0.99) and 0.949 (95% CI: 0.86, 0.98), respectively (26). Likewise, *Blackledge et al.* (35) showed a good concordance of whole-body DWI measurements between observers by using in-house software developed by IDL (Exelis Visual Information Solution, Inc.) in patients with prostate and breast cancer; the inter-observer ICCs for the logarithm of total diffusion volume and median global ADC were 1.00 (0.97–1.00) and 0.99 (0.89–0.99), respectively; the intra-observer concordance of these measurements was similar [ICC 0.99 (0.95–1.00) for the logarithm of total diffusion volume and 0.98 (0.89–0.99) for the median global ADC]. *Giles et al.* (21) also showed similar ICCs when intra- and inter-observer comparisons of bone marrow ADC value calculations were performed with Onco-

Treat software (Siemens Healthcare) in a group of healthy volunteers and myeloma patients. They showed that the intra-observer percentage repeatability was in the order of 5.5–13.5% for the median global ADC and total diffusion volume.





# **Whole-body MRI analyses**



## 6. Whole-body MRI analyses

---

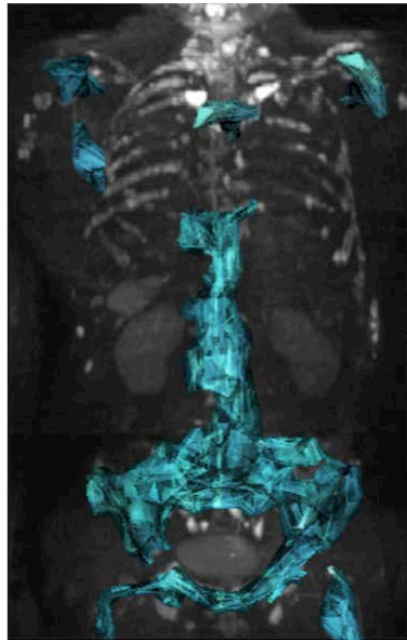
In these studies all the images were anonymised. We processed and analysed the images with the open-access imaging assistant software OsiriX version 5.6 (PixmeoSARL, Bernex, Switzerland). In all cases, the presence of bone metastases was assessed based on the T1-weighted and DWI (DWI b values of 50 and 900 s/mm<sup>2</sup> and ADC maps) features.

- **Whole-body metastatic bone disease** in the studies titled “Metastatic bone disease volume assessed by whole body diffusion weighted imaging associates with overall survival in metastatic castration-resistant prostate cancer” and “Diffusion-weighted imaging as a treatment response biomarker evaluating bone metastases in prostate cancer”, were calculated as follows:

Regions of interest (ROIs) including all the areas of abnormal signal intensity on DWI images, which corresponded to high signal intensity on DWI images obtained with b values of 900 s/mm<sup>2</sup> and low signal intensity on T1-weighted images, in keeping with metastatic bone disease in the axial skeleton (spine and pelvis, not including the ribs) between C4 and the mid-thighs, were delineated.

A semi-automated segmentation tool from OsiriX version 5.6 (PixmeoSARL, Bernex, Switzerland) was used for delineating ROIs. I performed all the delineation techniques for whole-body DWI images; I also performed the manual correction of the segmentation mask that corresponded to the ROIs where necessary.

**Figure 5. The ROI mask including whole-body bone metastases is superimposed on the DWI b900 maximum intensity projection (MIP) reconstruction.**



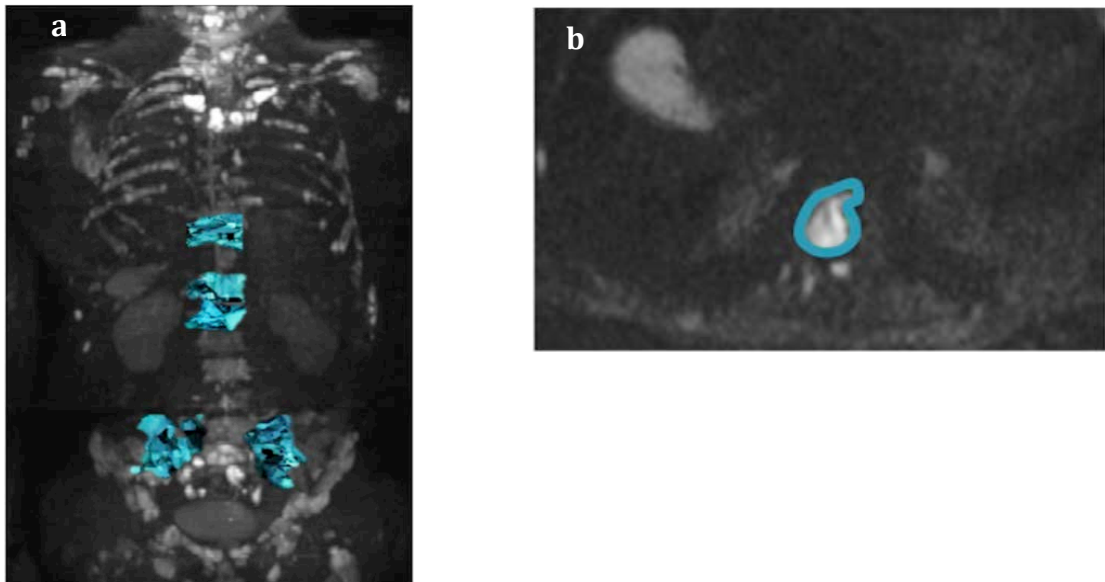
The volume of metastases was calculated as the number of voxels for all ROIs multiplied by the voxel volume in each case. The ADC value for every pixel included in the ROIs was recorded, and histogram representations of the ADC values of bone metastases for each patient were generated by using Microsoft Excel 2010 (Microsoft, Redmond, Wash).

- In order to evaluate **simpler delineation techniques** for evaluating DWI changes in bone metastases in response to treatment that could eventually be implemented into clinical practice, we also explored other bone metastases manual delineation techniques in the study “Diffusion-weighted imaging as a treatment response biomarker evaluating bone metastases in prostate cancer”:

A RECIST approach of a maximum of five target lesions representative of the metastatic bone disease was chosen using the following criteria: maximum axial dimension >1 cm, well-defined lesion border and representing different skeletal areas.

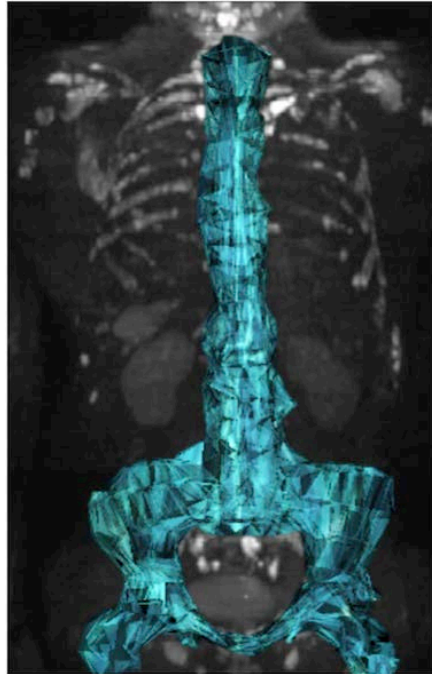
- ROIs including the total volume of up to five target lesions.
- ROIs including the central slice of the same target lesions.

**Figure 6. a) The ROI mask including five bone metastases is superimposed on the DWI b900 MIP reconstruction. b) Axial DWI b900 with an ROI delineating the central slice of a bone metastasis in a vertebral body.**



- Delineation of the entire axial skeleton (spine and pelvis) enclosing normal and abnormal bone marrow from C4 to lesser trochanters. This delineation technique was included in view of its possible advantage for the automated segmentation of the skeleton.

**Figure 7. The ROI mask including the entire axial skeleton is superimposed on the DWI b900 MIP reconstruction.**



The volume of metastases was calculated as the number of voxels for all ROIs multiplied by the voxel volume in each case. The bone metastases volume and diameter were recorded. The ADC value for every pixel was recorded, and histogram representations of the ADC values of bone metastases for each patient were generated by using Microsoft Excel 2010 (Microsoft, Redmond, Wash).

# **Results and published studies**





## Results and published studies

---

### 7.1. Correlation of MP MRI with histological and molecular characteristics of bone marrow biopsies

---

#### Research in context

Therapeutic options for patients with metastatic castration resistant prostate cancer (mCRPC) have increased over the last decade with the approval of several agents improving overall survival (2-4, 6). Yet, as progression on these treatments inevitably ensues, mCRPC remains a fatal condition. For optimal development of more precise therapeutic strategies, there is a need for the clinical qualification of predictive biomarkers, which requires acquisition of tumour material, and better response biomarkers to guide therapeutic decisions.

Bone metastases are the commonest metastatic site in advanced mCRPC; in more than 40% patients these represent the sole site of metastatic spread (36). Although bone marrow biopsies have been successfully implemented in prior studies (37), acquiring these samples remains difficult as bone marrow biopsies can yield specimens with poor tumour content due to increased sclerosis or response to previous therapies. Imaging that could increase the likelihood of obtaining high-quality tumour samples remains a highly desirable goal (38). Furthermore, standardized imaging response criteria for bone metastases remain a major unmet medical need (13, 14).

Multi-parametric (MP) magnetic resonance imaging (MRI) including T1 weighted sequences, diffusion weighted imaging (DWI) and Dixon quantitative chemical shift imaging derived FF allows the study of anatomical and functional features of bone marrow. DWI studies the random movement of water molecules within a tissue and

has high sensitivity and specificity for the detection of bone metastases (39). Multiple studies have previously shown a strong correlation between Apparent Diffusion Coefficient (ADC), the quantitative parameter derived from DWI, and tissue cellularity in soft tissue tumours (28-32, 40, 41). Also, several studies have shown significant ADC differences between normal bone marrow and malignancies in bone (42-44). However, only limited data are available correlating DWI parameters with cellularity and other histological features in bone (33, 34) and these studies did not include prostate cancer patients. Translational studies correlating functional imaging and the underlying histology are critical for clinical qualification of MP-MRI as a prognostic and response biomarker in prostate cancer bone metastases. We have previously shown the prognostic value of bone metastases volume in mCRPC measured by MP-MRI (45) and how increases in ADC, and decreases in bone metastases volume, assessed by whole body DWI, are promising biomarkers of response to anticancer treatments in mCRPC (25, 46).

Normal bone marrow contains both fat and water (yellow marrow approximately 80% fat; red marrow approximately 40% fat) (47). Malignant cells displace the bone marrow fat cells causing a reduction in fat content; conversely successful therapies are associated with return of normal bone marrow fat (48). Dixon quantitative chemical shift imaging uses the difference in resonance frequency between water and fat to estimate FF of a tissue (47).

### **Specific aims**

We aim to correlate MRI quantitative parameters of mCRPC bone metastases within the biopsy tract, including ADC, normalized b900 DWI (nDWI) signal intensity and FF with histological and molecular bone biopsy features including tumour cell burden, immature osteoid burden, fibrosis, proportion of fat, PTEN status and Ki67 proliferation index. We also assessed the MP-MRI features of normal bone marrow in a subgroup of patients with prostate cancer and no evidence of bone metastases on multimodality imaging.

## **Specific methods**

This was a retrospective study conducted under Royal Marsden Research Ethics Committee approval. Written informed consent was obtained from all patients.

### *Patient population*

We reviewed all consecutive posterior iliac crest bone marrow biopsies and MP-MRI in mCRPC patients at The Royal Marsden Hospital (UK) performed between May 2012 and March 2016. Study inclusion criteria were: a) MP-MRI within 12-weeks prior to the bone biopsy and b) Presence of a visible bone biopsy tract in the posterior iliac crest on a subsequent computed tomography (CT). Cases were excluded if a) bone biopsy did not include bone tissue; or b) MP-MRI study had suboptimal DWI due to artefacts or was incomplete.

A second control cohort included 10 consecutive patients who underwent MP-MRI but had no detectable bone metastases by CT, bone scan (BS) or MRI; no bone biopsies were obtained in this cohort for ethical reasons.

### *Clinical data collection*

Data from patient records was collected into an anonymised database; these included age, prior treatments, and laboratory parameters at the time of the MRI. The presence of bone metastases was assessed based on contemporaneous CT, BS and MP-MRI in all cases.

### *Histological and molecular parameters*

Bone biopsies were decalcified in 14% EDTA and processed as previously described (38). Sections were cut at 2 $\mu$ m onto glass slides and stained with Haematoxylin & Eosin. A pathologist blinded to clinical and radiological data reviewed the biopsies. Tumour cellularity was semi-quantitatively scored into four tiers: 0 (no tumour cells); +1 ( $\leq$ 50 tumour cells); +2 (50-250 tumour cells); +3 ( $\geq$ 250 tumour cells) by section. Trabecular volume was semi-quantitatively calculated as described by Teman et al (49). Gross fibrosis and immature osteoid (woven bone)

content were semi-quantitatively scored: 0 (absent); +1 (present in <1/3 of biopsy); +2 ( $\geq 1/3$ -<2/3 of biopsy); and +3 ( $\geq 2/3$  of biopsy). Fat content was defined as: (area occupied by fat/ total biopsy area)  $\times 100$ . PTEN and Ki67 were assessed by immunohistochemistry as previously described (50). PTEN loss was defined as H-score  $\leq 10$ .

#### *MP-MRI parameters*

MP-MRI was performed on a 1.5-T MRI scanner (Magnetom Avanto or Aera Siemens Healthcare, Erlangen, Germany), using surface and body coils on patients positioned supine (**Supplementary Table 1**). DW imaging was performed in axial plane using b-values of 50 and 900 s/mm<sup>2</sup>. The FF maps were calculated using an in-house OsiriX plug-in [FF = 100%  $\times S_{\text{fat}} / (S_{\text{fat}} + S_{\text{water}})$  where S=signal at every voxel location].

#### *MRI and CT analysis*

Images were processed and analysed with open-access imaging assistant software (OsiriX v5.6) by a single radiologist, blinded to pathology and molecular data. The biopsy tract was identified on a post-biopsy axial CT; a 2D region of interest (ROI) delineating the biopsy tract was manually drawn. In the population with no bone metastases, two bilateral ROIs delineating the posterior-superior iliac crests at one level, representative for where bone marrow biopsies are usually performed, were manually drawn. The axial CT and DWI sequences (b900, ADC and FF maps) taken pre-biopsy were co-registered using the OsiriX Insight Segmentation and Registration Toolkit (ITK) (51, 52); the ROIs were then transferred to the b900 images, ADC and FF maps. In order to perform DWI signal normalisation, ROI muscle were delineated on b900 images within the gluteus maximus muscle at the same side and level as the iliac crest bone marrow biopsy; nDWI was defined as the ratio of biopsy tract b900 signal intensity to muscle ROI b900 signal intensity. The following data were collated for each ROI on MRI: nDWI signal intensity, ADC and FF.

If a CT was performed within 12-weeks of the bone biopsy, co-registration of the CT pre- and post-biopsy was performed; CT density (Hounsfield Units [HU]) of the ROI corresponding to the biopsy tract in the pre-biopsy CT scan images were recorded.

#### *BS analysis*

If a whole-body BS had been performed within 12-weeks prior to the bone biopsy, bone scan index (BSI) was calculated using an automated BSI scoring software (Exini Diagnostics, Lund, Sweden) (53).

#### *Statistical analysis*

Descriptive statistics were used to summarize the baseline clinical, histological and molecular characteristics and imaging features. Differences in MRI and CT parameters between regions positive and negative for tumour cells on bone biopsy were assessed using Mann-Whitney tests. Univariate analyses were performed using logistic regression models. Variables with a statistically significant association to bone biopsy positivity for tumour cells ( $p < 0.05$ ) were included in a multivariate logistic regression model. Correlations between MRI parameters, histological and molecular parameters were assessed using Spearman's correlation ( $r$ ). The performance of the imaging biomarkers was evaluated by ROC curve analysis and Linear Discriminant Analysis. Statistical analyses were performed with Stata version 13 (StataCorp) and SPSS version 20 (IBM).

## **Results**

### *Patient and bone biopsy characteristics*

The flowchart of the study selection process is shown in **Supplementary Figure 1**. In the cohort of patients with bone metastases, 43 bone biopsies from 33 patients (all male; median age 72 years, range 48-84 years) were evaluable. Thirty-one of these 43 (72.1%) biopsies were positive for tumour cells with 12/43 (27.9%) having no tumour cells. In the cohort of patients with no detectable bone metastases, 10 CRPC patients were included (all male; median age 69 years, range 53-75 years). The

population characteristics are summarized in **Table 1**. The histological and molecular characteristics of the bone biopsies are summarized in **Table 2**.

*MP-MRI of bone with or without metastatic prostate cancer*

The median ADC of bone metastases was significantly higher than in non-metastatic iliac crests:  $993 \times 10^{-6} \text{mm}^2/\text{s}$  (IQR  $872.5\text{-}1093.5 \times 10^{-6} \text{mm}^2/\text{s}$ ) and  $601.8 \times 10^{-6} \text{mm}^2/\text{s}$  (IQR  $545\text{-}667 \times 10^{-6} \text{mm}^2/\text{s}$ ) respectively ( $p < 0.001$ ). The median nDWI signal was 4 (IQR 2.6-6.7) in the bone metastases cohort and 1.6 (IQR 1.4-2.7) in the cohort without bone metastases ( $p < 0.001$ ). The median FF in bone metastases was 16% (IQR 9-45 %), significantly lower than in non-metastatic bone, which was 63% (IQR 60-76%;  $p < 0.001$ ).

*Bone metastases: MRI and histological parameters*

The median ADC in the region of bone biopsies containing tumour was  $898 \times 10^{-6} \text{mm}^2/\text{s}$  (IQR  $816\text{-}1019 \times 10^{-6} \text{mm}^2/\text{s}$ ), compared to  $1617 \times 10^{-6} \text{mm}^2/\text{s}$  (IQR  $1067\text{-}1787.5 \times 10^{-6} \text{mm}^2/\text{s}$ ) in bone with no visible tumour cells in the bone biopsy ( $p < 0.001$ ). The median nDWI signal was significantly higher in positive bone biopsies (5.3 [IQR 3.1-7.8] vs 2.3 [IQR 2-3.3],  $p < 0.001$ ). Moreover, the median FF in positive bone biopsies was 11.45% (IQR 8.5-17%) compared to 62% (IQR 45-82.9%) in bone biopsies not containing tumour ( $p < 0.001$ ) (**Figure 1; Supplementary Figure 2**). ROC AUC values were 0.86 (95%CI: 0.64-1.00) for median ADC, 0.87 (95%CI: 0.68-0.98) for median nDWI signal and 0.90 (95%CI: 0.74-1.00) for median FF (**Supplementary Figure 3**).

We then evaluated whether the combination of these parameters could improve their performance, using Linear Discriminant Analysis. Due to the high correlation between median nDWI and median ADC ( $p < 0.001$ ), only median ADC and median FF were considered in the model. The function combining median ADC and median FF was able to significantly discriminate biopsies with tumour from biopsies without tumour and non-metastatic bone (Wilks lambda = 0.31;  $p < 0.001$ ). The function combining median ADC and median FF had a sensitivity of 80% and a specificity of

96% for the detection of a positive bone marrow biopsy; 91.4% of the cases were correctly classified by the function **(Supplementary Table 2)**.

There was an inverse correlation between histological cellularity burden as an ordinal variable and ADC ( $p<0.001$ ) and FF ( $p<0.001$ ), as well as a positive correlation with nDWI signal intensity ( $p<0.001$ ). We also observed a positive correlation between the median FF on MP-MRI and percentage of histological fat content in the bone biopsies ( $p<0.001$ ) **(Table 3)**.

Immature osteoid and fibrosis in the bone biopsies were associated with positive biopsy results; in multivariate analysis, median ADC remained independently associated with biopsy positivity for tumour cells ( $p=0.050$ ) **(Table 4)**.

In our series, median ADC of bone metastases did not correlate with Ki67 proliferation index ( $r=0.28$ ,  $p=0.180$ ) or loss of PTEN expression ( $r=-0.34$ ,  $p=0.118$ ).

#### *Evaluating bone metastases by CT and BS*

For 39/43 (90.7%) biopsies in the bone metastases cohort, a CT scan performed within 12-weeks before the biopsy was also available. All 10-patients in the cohort without bone metastases also had a CT scan performed within 12-weeks of the MP-MRI.

CT density was significantly higher in the presence of metastatic disease than in the bone with no metastases (median 252 HU, IQR 191-337.50 HU vs 67 HU, IQR 35-85 HU;  $p<0.001$ ).

In the metastatic cohort, 29 of the 39 patients (74.4%) with a CT scan performed within 12-weeks of the bone biopsy had positive biopsies containing tumour cells. The median HU on CT was not significantly different for bone metastases with positive biopsy compared to those with negative biopsy without tumour cells present



(median 278 HU [IQR 139-348 HU] vs 241 HU [IQR 192-327 HU],  $p=0.966$ ) **(Supplementary Figure 4)**.

Furthermore, in 35/43 (81.4%) biopsies, a BS was performed within 12-weeks (median 2.7 weeks; IQR 0.5-7.3 weeks) of the biopsy with DICOM images allowing BSI calculation. Twenty-five of these 35 biopsies (71.4%) were positive for tumour cells. The BSI was not significantly different in the group of patients with a positive biopsy compared to those with negative biopsy (median 5.6 [IQR 3.6-9.2] vs 5.5 [IQR 1.0-10.2],  $p=0.812$ ).

#### *Features of serial bone biopsies*

In three cases, biopsies of the posterior-superior iliac crest were taken at more than one time point, prior to and during treatment with different anticancer therapies. Two of these cases were initially biopsied in the presence of disease responding to therapy; in these post-treatment biopsies median ADC were high with biopsy analyses identifying no tumour cells. At disease progression established according to PCWG 2 criteria, however, median ADC decreased and repeat bone biopsies detected tumour cells **(Figure 2)**.

In the third patient with serial bone biopsies, a 74 year-old man with mCRPC who had received previous radiotherapy to the pelvis prior to the first biopsy, the median ADC of the biopsied iliac crest was similar at the two time points ( $1668 \times 10^{-6} \text{ mm}^2/\text{s}$  and  $1968 \times 10^{-6} \text{ mm}^2/\text{s}$  respectively), with both biopsies being negative for tumour cells. These high ADC values were consistent with maintained response to previous radiotherapy.

#### **Discussion**

In this study we correlated MP-MRI parameters of bone metastases, and of non-malignant bone, with bone biopsy histological and molecular features in treated patients with CRPC. These findings contribute to the clinical qualification of MP-MRI as a biomarker of mCRPC. We have shown that MP-MRI features including nDWI

signal intensity, ADC values and FF successfully differentiate normal bone from bone metastases in mCRPC patients. The nDWI signal intensity and ADC values in normal bone marrow in our population were similar to those previously described (42); these are closer to the described values in yellow bone marrow than in red bone marrow, in line with the high FF observed in our study. These are consistent with the advanced age of our population, and chronic exposure to hormonal ablation for prostate cancer treatment. Low signal intensity and low ADC values of yellow bone marrow are likely to be related to an abundance of fat cells and reduced water proton density.

Within the bone metastases cohort, MP-MRI parameters predicted the presence and burden of metastatic disease in bone biopsies. In this heavily pre-treated population, the absence of tumour in negative biopsies likely reflects tumour cell kill following prior treatments. We have shown a significant inverse correlation of ADC and FF, and a significant positive correlation of nDWI signal intensity with bone metastasis tumour cellularity burden. This supports using MP-MRI to guide bone biopsy acquisition in mCRPC for molecular and histological studies. Our studies do indicate, however, that ADC values and nDWI signal are also influenced by other histological findings, such as the presence of osteoid and fibrosis in biopsies. Nevertheless, when controlling for fibrosis and osteoid in multivariate analysis, median ADC was still independently correlated with tumour cellularity. Furthermore, by using DWI b50 rather than b0 as our low b value in the DWI acquisition, we have reduce the influence of blood flow variability on calculated ADC values. Lastly, in our study, MRI parameters including ADC, nDWI and FF were more informative of active versus treated bone metastases when compared to CT scan bone HU.

We acknowledge potential limitations of our study; first, our pilot sample size is small, although still representing the largest series presented to date of bone biopsy to MP-MRI correlative studies for this disease. Furthermore, external validity of the performance of these biomarkers by ROC curve and Linear Discriminant Analysis is limited, due to the absence of a validation cohort. Analysing larger populations in

prospective, multi-centre validation studies is now warranted for validation of these results. Secondly, the retrospective nature of this study may have led to some bias; ideally the MRI, CT, BS and bone biopsy should have been obtained simultaneously. However, we consider that the 12-week maximum interval between the scans and biopsy is reasonable considering the retrospective nature of this study and should not have substantially impacted these results. Moreover, MRI, CT and BS assessments were always performed before the bone biopsy, avoiding artefacts secondary to the biopsy procedure. Finally, histo-pathological analyses were performed with core-needle biopsies and the small area of the drawn ROIs on MRI and CT may not have been representative of tumour heterogeneity.

Overall, MP-MRI is a powerful non-invasive biomarker of the histological features of bone metastases in prostate cancer. MP-MRI differentiates normal bone marrow from bone metastases, and also bone metastases with detectable tumour cells from those without tumour cells at biopsy, which can aid bone biopsy guidance. Finally, we have reported that changes in DWI parameters and histological features parallel response to treatment. Overall, these findings, together with recent published clinical studies (25, 46), further support the clinical utility of MP-MRI as a biomarker of bone metastases in this disease.

**TABLES**

**Table 1.** Population characteristics of patients with bone metastases and biopsies, (n=43) and those with no bone metastases who did not have biopsies (n=10).

<b>Previous treatments</b>	<b>Cohort with bone metastases and biopsies (n=43) N (%)</b>	<b>Cohort with no bone metastases and no biopsies (n=10) N (%)</b>
<b>Prostate radiotherapy</b>	14 (32.6%)	5 (50%)
<b>Pelvic bone radiotherapy</b>	19 (44.2%)	0 (0%)
<b>Abiraterone</b>	36 (83.3%)	0 (0%)
<b>Enzalutamide</b>	15 (34.9%)	0 (0%)
<b>Docetaxel</b>	32 (74.4%)	0 (0%)
<b>Cabazitaxel</b>	18 (41.9%)	0 (0%)
<b>Cabozantinib</b>	3 (7.0%)	0 (0%)
<b>Rad 223</b>	5 (11.6%)	0 (0%)
<b>Clinical characteristics</b>	<b>Median (IQR)</b>	<b>Median (IQR)</b>
<b>PSA (ng/mL)</b>	345 (126-806)	23 (6-26)
<b>CTC (cells per 7.5 mL of blood)</b>	18 (6-121)	-
<b>Haemoglobin (g/dL)</b>	112 (106-125)	140 (132-155)
<b>Alkaline Phosphatase (IU/L)</b>	164 (105-423)	56 (52-65)
<b>Lactate Dehydrogenase (IU/L)</b>	189 (165-239)	198 (162-200)
<b>Bone Scan Index (%)</b>	<b>Median (IQR)</b>	
<b>Total biopsy cohort (n=35)</b>	5.6 (2.6-10.2)	-
<b>Biopsy positive for tumour cells (n=25)</b>	5.6 (3.6-9.2)	-
<b>Biopsy negative for tumour cells (n=10)</b>	5.5 (1.0-10.1)	-

**Table 2.** Histological and molecular characteristics of the bone biopsies (n=43).

<b>Histological characteristics</b>	
<b>Osteoid</b>	<b>N (%)</b>
<b>0</b>	0 (0 %)
<b>1</b>	9 (20.9 %)
<b>2</b>	16 (37.2 %)
<b>3</b>	18 (41.9 %)
<b>Fibrosis</b>	<b>N (%)</b>
<b>0</b>	4 (9.3 %)
<b>1</b>	11 (25.6 %)
<b>2</b>	8 (18.6 %)
<b>3</b>	20 (46.5 %)
<b>Cellularity</b>	<b>N (%)</b>
<b>0</b>	12 (27.9 %)
<b>1</b>	6 (13.9 %)
<b>2</b>	9 (20.9 %)
<b>3</b>	16 (37.2 %)
<b>Fat area</b>	<b>Median (IQR)</b>
<b>%</b>	25% (5-50 %)
<b>Molecular characteristics</b>	
<b>PTEN expression (n=22; unknown n=21)</b>	<b>N (%)</b>
<b>PTEN loss</b>	8 (36.3 %)
<b>PTEN present</b>	14 (66.6 %)
<b>Ki67 (n=25; unknown n= 18)</b>	<b>Median (IQR)</b>
<b>%</b>	25 (10-50)

**Table 3.** Correlation between multi-parametric (MP) magnetic resonance imaging (MRI) and histological parameters generated from bone biopsy analyses (r Spearman correlation coefficient).

<b>Correlation with bone metastasis cellularity</b>		
	<b>r</b>	<b>p-value</b>
<b>Median ADC</b>	-0.57	<0.001
<b>Median nDWI signal intensity</b>	0.59	<0.001
<b>Fat fraction</b>	-0.59	<0.001
<b>Correlation with bone metastasis fat content</b>		
	<b>r</b>	<b>p-value</b>
<b>Fat fraction</b>	0.60	<0.001

**Table 4.** Univariate and multivariate logistic regression models with bone marrow positivity as the dependent variable.

<b>Univariate logistic regression model</b>			
<b>MRI parameters</b>	<b>OR</b>	<b>95%CI</b>	<b>p-value</b>
<b>Median ADC</b>	0.99	0.99-1.00	0.002
<b>Median nDWI signal intensity</b>	1.57	1.01-2.43	0.045
<b>Fat fraction</b>	0.96	0.94-0.99	0.008
<b>Histological parameters</b>	<b>OR</b>	<b>95%CI</b>	<b>p-value</b>
<b>Osteoid score</b>	3.14	1.19-8.31	0.021
<b>Fibrosis score</b>	4.02	1.68-9.61	0.002
<b>Trabecular volume</b>	1.02	0.98-1.06	0.276
<b>Fat content</b>	0.92	0.88-0.97	0.001
<b>Multivariate logistic regression model</b>			
	<b>OR</b>	<b>95%CI</b>	<b>p-value</b>
<b>Median ADC</b>	0.99	0.97-1.00	0.050
<b>Osteoid score</b>	6.34	0.04-1040.72	0.478
<b>Fibrosis score</b>	15.40	0.32-748.75	0.168

## FIGURES

**Figure 1.** Box plots of the distribution of (a) median ADC, (b) median nDWI signal intensity and (c) median FF of the bone marrow in patients with bone metastases and bone biopsy negative for tumour cells (green), bone metastases and bone biopsy positive for tumour cells (red) and no bone metastases (blue).

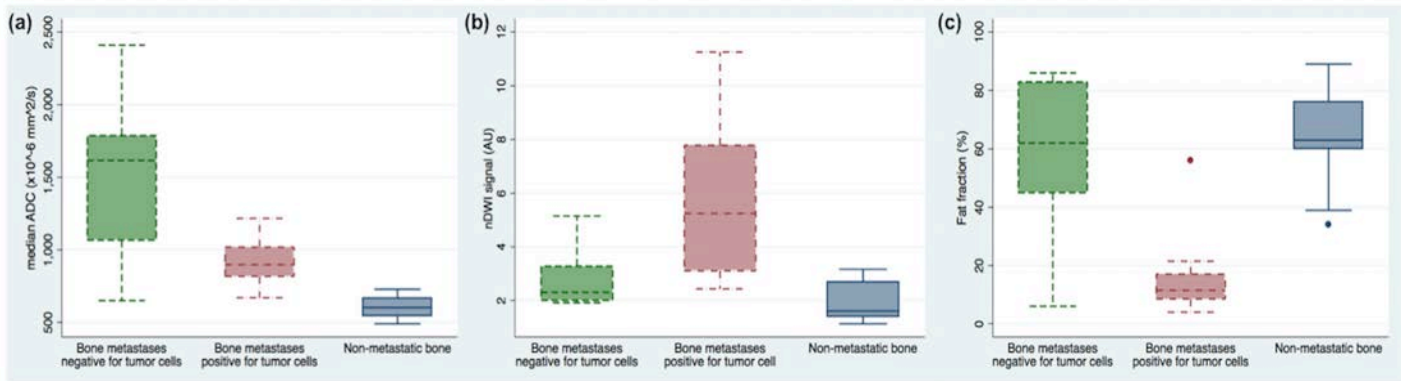


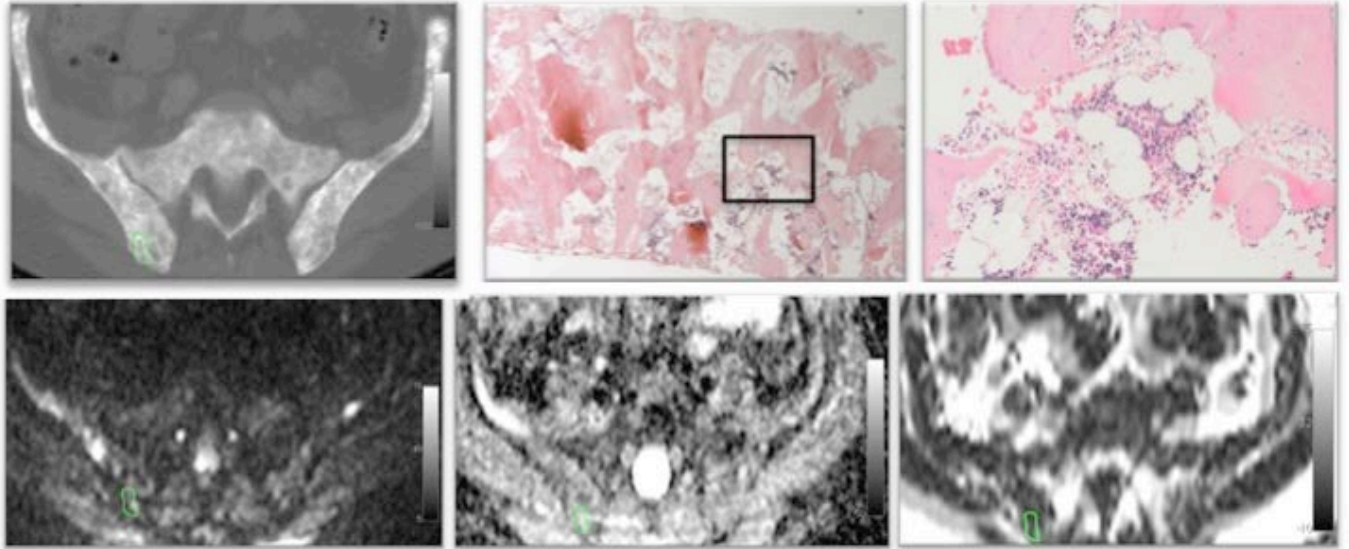


**Figure 2.** 79-year-old man with widespread bone metastases and MRI, CT and bone biopsies while responding (a) and after progressing (b) to abiraterone.

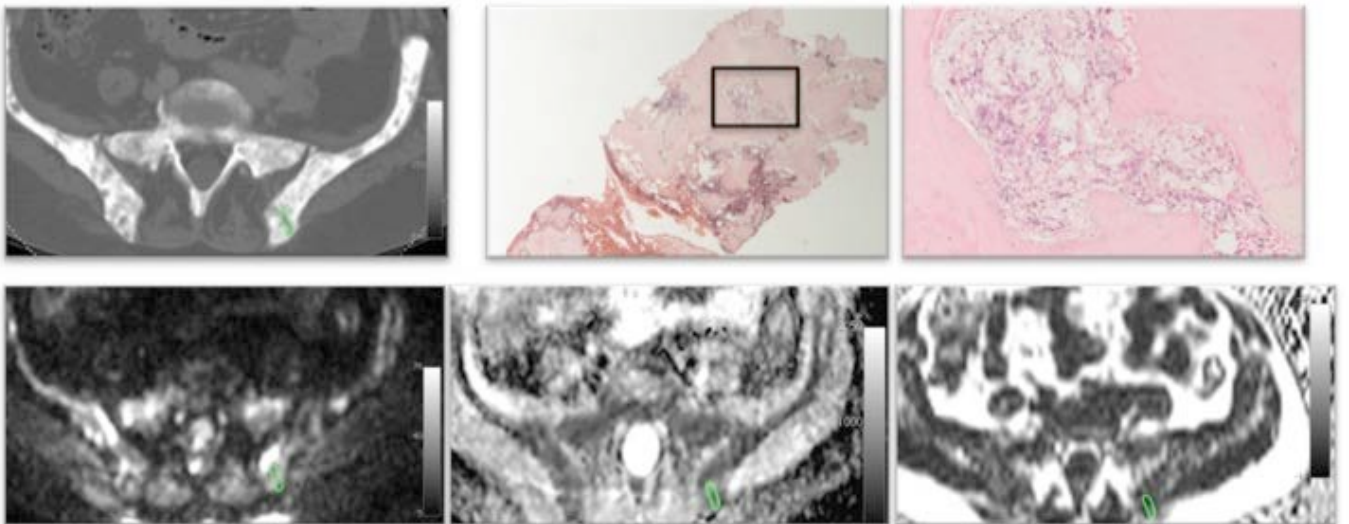
A green ROI delineating the biopsy tract on CT is shown as transferred on registered MRI sequences (DWI b900, ADC map and FF map). Median nDWI signal intensity in the area of the bone biopsy when responding was lower than at progression (2 vs 5), whilst median ADC values and FF were higher when responding than at progression ( $1342 \times 10^{-6} \text{ mm}^2/\text{s}$  vs  $899 \times 10^{-6} \text{ mm}^2/\text{s}$ ; 20% vs 13% respectively).

The bone biopsies were routinely processed and stained with Haematoxylin & Eosin (HE). A black rectangle in 40x panel marks the region depicted in 200x panel. In concordance with the MRI parameters, despite both biopsies were performed in areas of bone metastases, the bone biopsy when responding was negative for tumour cells and had 30% fat content; while at progression the bone biopsy was positive for tumour cells and had 5% fat content.

a.



b.



**SUPPLEMENTARY MATERIAL**

**Supplementary Table 1.** Whole body MRI acquisition parameters.

<b>PARAMETER</b>	<b>T1 weighted imaging</b>	<b>Diffusion weighted imaging</b>	<b>DIXON fat/water</b>
<b>MRI platform</b>	1.5-T scanner (Avanto or Aera, Siemens Healthcare)		
<b>Type of pulse sequence</b>	Spoiled gradient echo (FLASH)	Single-shot twice-refocused echo-planar imaging	f13d_vibe
<b>Respiration</b>	Breath-hold	Free-breathing	Breath-hold
<b>Acquisition plane</b>	Axial	Axial	Coronal
<b>Type of acquisition</b>	2D	2D	3D
<b>Field of view (mm)</b>	380-420	380-420	450
<b>In-plane resolution (mm<sup>2</sup>)</b>	1.6 x 1.6	2.5 x 2.5	1.6 x 1.6
<b>Section thickness (mm)</b>	5	5	5
<b>Repetition time (ms)</b>	380	14000	7
<b>Echo time (ms)</b>	5	68	TE1=2.38; TE2=4.76
<b>Inversion time (ms)</b>	NA	180	NA
<b>Flip angle</b>	70	90	3
<b>Fat suppression</b>	NA	STIR	NA
<b>Receiver bandwidth (Hz/pixel)</b>	331	1800	490
<b>Number of signal average</b>	1	4	1
<b>Parallel imaging factor</b>	2	2	4
<b>b factors (s/mm<sup>2</sup>)</b>	NA	50 and 900	NA
<b>Number stations</b>	4 (50 slices each)	4 (50 slices each)	2 (52 slices each)

**Supplementary Table 2.** Discriminant Function Analysis.

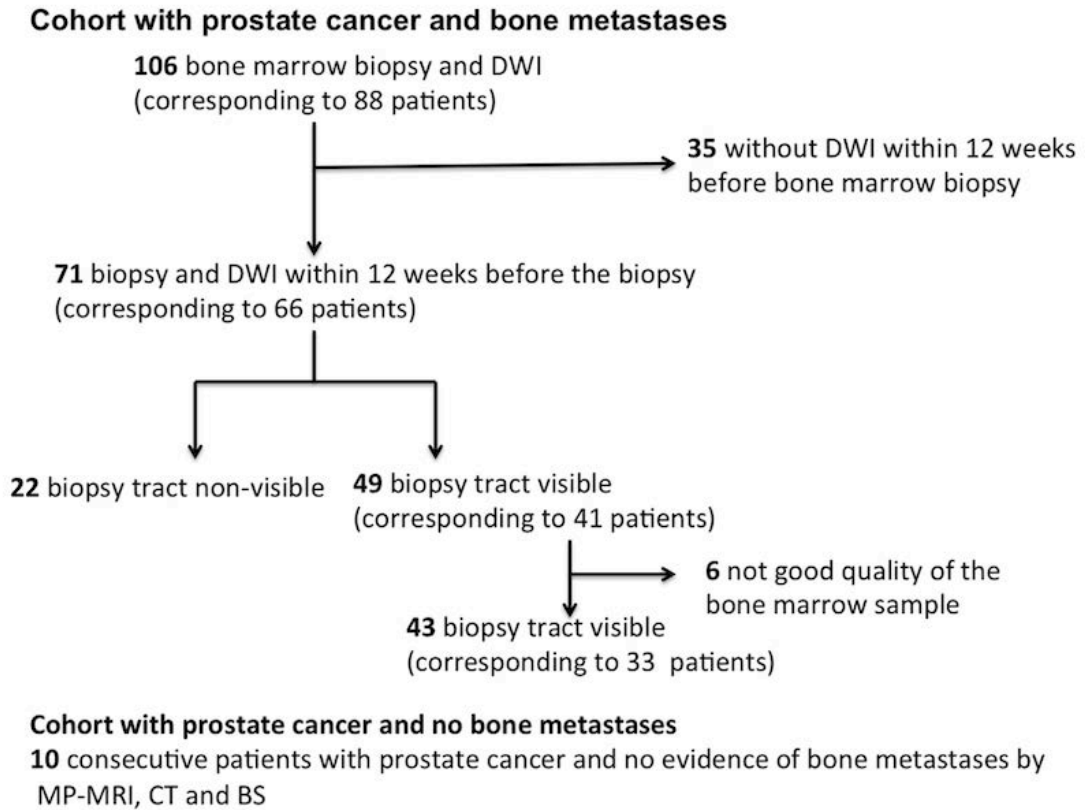
Summary of Canonical Discriminant Functions:

<b>Combined linear function</b>	-3.383 + 0.002*MedianADC + 0.047*MedianFF
<b>Eigen value:</b>	2.237
<b>Canonical Correlation:</b>	0.831
<b>Wilk's Lambda (p-value)</b>	0.309 (p<0.001)

Classification Results:

<b>Biopsy Result</b>	<b>Predicted Group Membership</b>		
	<b>Negative</b>	<b>Positive</b>	<b>Total</b>
<b>Negative</b>	8 (80%)	2 (20%)	10 (100%)
<b>Positive</b>	1 (4%)	24 (96%)	25 (100%)
<b>Ungrouped cases</b>	5 (50%)	5 (50%)	10 (100%)

**Supplementary Figure 1.** Flowchart of study selection process.

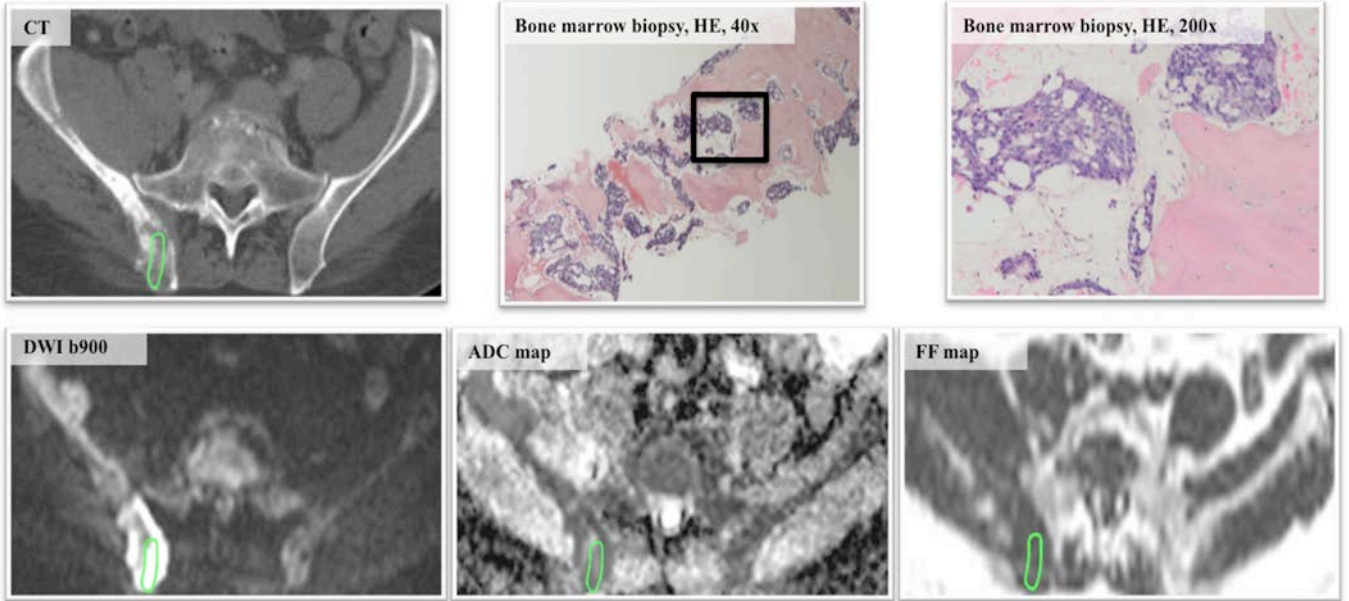


**Supplementary Figure 2.** Axial CT and MRI images and bone marrow biopsy sections of 2 patients with mCRPC included in the study. A green ROI delineating the biopsy tract on CT is also shown as transferred on registered MRI sequences (DWI b900, ADC map and FF map). The bone marrow biopsy sections were stained with Haematoxylin & Eosin (HE). A black rectangle in 40x panel marks the region depicted in 200x panel.

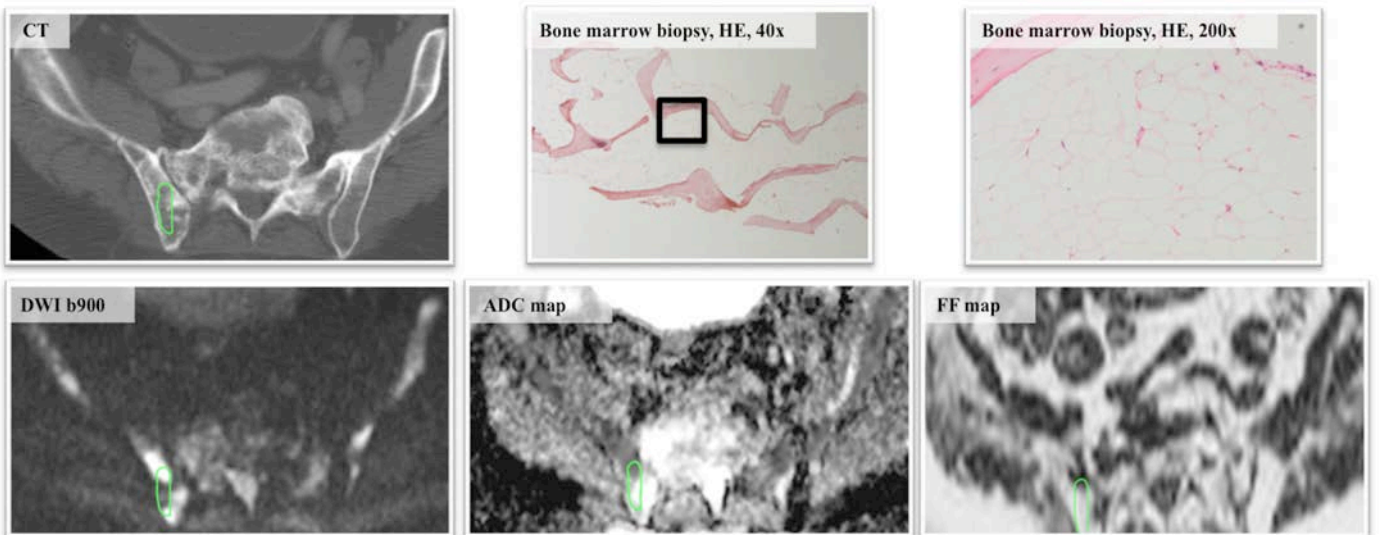
**(a)** 73-year-old man with mCRPC and bone metastases who underwent a bone marrow biopsy after progression on treatment with abiraterone, enzalutamide and cabazitaxel. His bone marrow biopsy showed high cellularity (3), high osteoid (2) and fibrosis (3) and low fat content (3%). DWI signal intensity from the area of the bone biopsy was high (7 AU), whilst median ADC was  $839 \times 10^{-6} \text{ mm}^2/\text{s}$  and FF was low (9%).

**(b)** 60-year-old man with mCRPC and bone metastases, previously treated with radiotherapy to the right pelvis for pain control in 2008. A bone biopsy was performed in 2014 after progression to therapy with abiraterone, cabazitaxel and Radium-223. His bone biopsy showed no evidence of tumour cells, low osteoid (0) and fibrosis (1) and high fat content (80%). DWI signal intensity in the area of the bone biopsy was lower than in case “a” (3 AU), whilst median ADC was high ( $1742 \times 10^{-6} \text{ mm}^2/\text{s}$ ) and, in line with the high fat content in the bone biopsy sample, FF was also high (83%).

**a.**

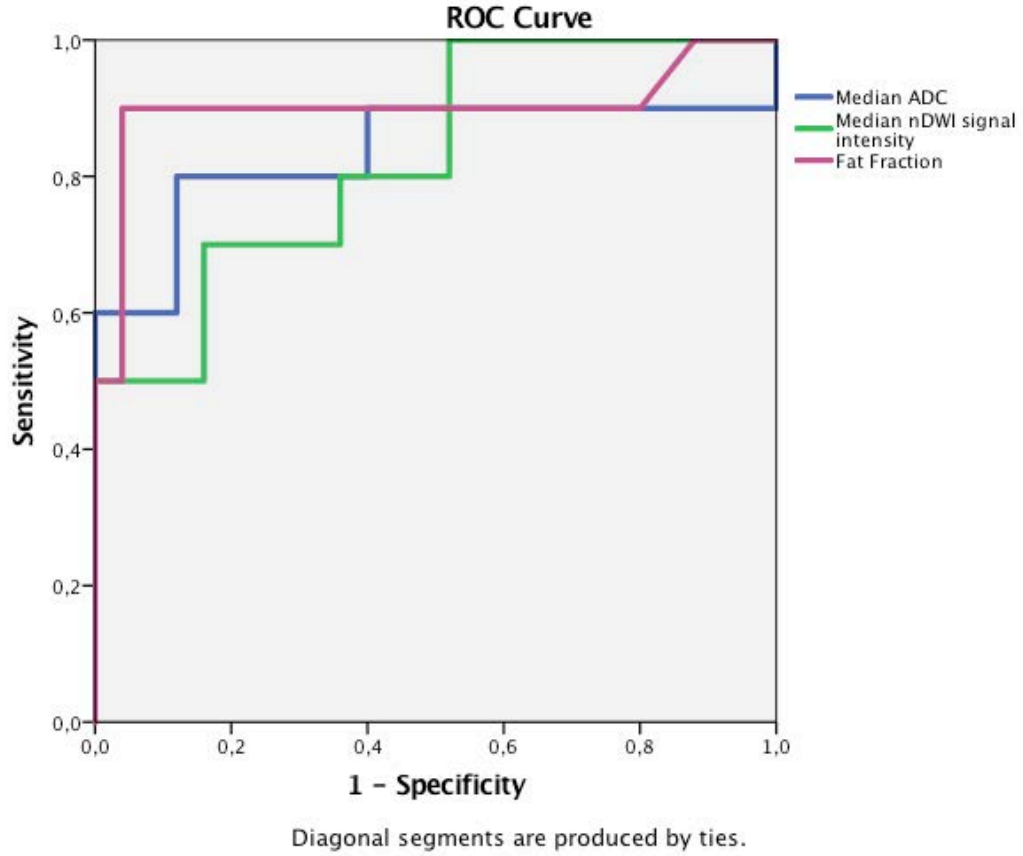


**b.**





**Supplementary Figure 3.** ROC Curves representing the performance of each parameter to predict the presence of detectable tumour cells in the bone biopsy.



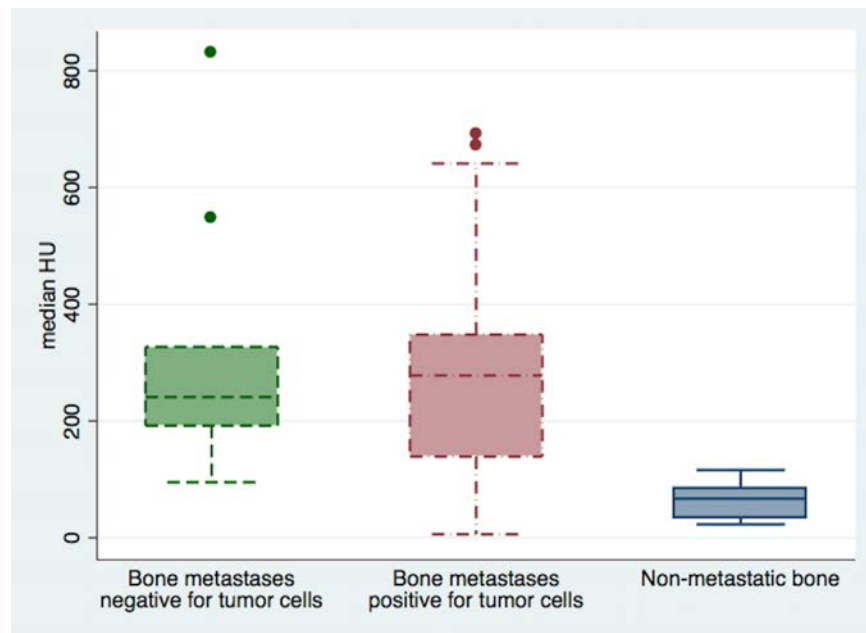
### Area Under the Curve

Variable	AUC	p-value	95% CI	
			Lower Bound	Upper Bound
Median ADC	,836	,002	,643	1,000
Median nDWI signal intensity	,828	,003	,677	,979
Fat Fraction	,900	,000	,742	1,000





**Supplementary Figure 4.** Box plots of the distribution of median Hounsfield Units (HU) on CT scans of the bone marrow in patients with bone metastases and biopsy negative for tumour cells (green), bone metastases and bone biopsy positive for tumour cells (red) and no bone metastases (blue).





## 7.2. Published manuscripts

---



### 7.2.1. Whole-body DW-MRI as prognostic biomarker in mCRPC with bone metastases

---

#### **Volume of Bone Metastasis Assessed with Whole-Body Diffusion-weighted Imaging Is Associated with Overall Survival in Metastatic Castration-resistant Prostate Cancer.**

Perez-Lopez R, Lorente D, Blackledge MD, Collins DJ, Mateo J, Bianchini D, Omlin A, Zivi A, Leach MO, de Bono JS, Koh DM, Tunariu N.

Radiology. 2016 Jul;280(1):151-60. doi: 10.1148/radiol.2015150799. Epub 2016 Jan 25.



Note: This copy is for your personal non-commercial use only. To order presentation-ready copies for distribution to your colleagues or clients, contact us at [www.rsna.org/hrsnavights](http://www.rsna.org/hrsnavights).

# Volume of Bone Metastasis Assessed with Whole-Body Diffusion-weighted Imaging Is Associated with Overall Survival in Metastatic Castration-resistant Prostate Cancer<sup>1</sup>

Raquel Perez-Lopez, MD, MSc  
David Lorente, MD  
Matthew D. Blackledge, PhD  
David J. Collins, BA, CPhys  
Joaquin Mateo, MD, MSc  
Diletta Bianchini, MD  
Aurelius Omlin, MD  
Andrea Zivi, MD  
Martin O. Leach, PhD  
Johann S. de Bono, MD, PhD  
Dow-Mu Koh, MD  
Nina Tunariu, MD, FRCR, MRCP

<sup>1</sup>From the Institute of Cancer Research and the Royal Marsden NHS Foundation Trust, Cancer Therapeutics Division, 15 Cotswold Rd, Sutton SM2 5NG, England. Received April 27, 2015; revision requested June 13; revision received October 21; accepted October 23; final version accepted November 2. Supported by Stand Up to Cancer funding reference SU2C-AACR-DT0712, Prostate Cancer Foundation grants reference 20131017 and 20131017-1, Prostate Cancer UK grant reference PG12-49, ECMC funding from Cancer Research UK and the Department of Health reference CRM064X, BRC Funding to the Royal Marsden reference BRC A38, NIHR postdoctoral fellowship NHR011X. Address correspondence to N.T. (e-mail: [Nina.Tunariu@icr.ac.uk](mailto:Nina.Tunariu@icr.ac.uk)).

© RSNA, 2016

## Purpose:

To determine the correlation between the volume of bone metastasis as assessed with diffusion-weighted (DW) imaging and established prognostic factors in metastatic castration-resistant prostate cancer (mCRPC) and the association with overall survival (OS).

## Materials and Methods:

This retrospective study was approved by the institutional review board; informed consent was obtained from all patients. The authors analyzed whole-body DW images obtained between June 2010 and February 2013 in 53 patients with mCRPC at the time of starting a new line of anticancer therapy. Bone metastases were identified and delineated on whole-body DW images in 43 eligible patients. Total tumor diffusion volume (tDV) was correlated with the bone scan index (BSI) and other prognostic factors by using the Pearson correlation coefficient ( $r$ ). Survival analysis was performed with Kaplan-Meier analysis and Cox regression.

## Results:

The median tDV was 503.1 mL (range, 5.6–2242 mL), and the median OS was 12.9 months (95% confidence interval [CI]: 8.7, 16.1 months). There was a significant correlation between tDV and established prognostic factors, including hemoglobin level ( $r = -0.521$ ,  $P < .001$ ), prostate-specific antigen level ( $r = 0.556$ ,  $P < .001$ ), lactate dehydrogenase level ( $r = 0.534$ ,  $P < .001$ ), alkaline phosphatase level ( $r = 0.572$ ,  $P < .001$ ), circulating tumor cell count ( $r = 0.613$ ,  $P = .004$ ), and BSI ( $r = 0.565$ ,  $P = .001$ ). A higher tDV also showed a significant association with poorer OS (hazard ratio, 1.74; 95% CI: 1.02, 2.96;  $P = .035$ ).

## Conclusion:

Metastatic bone disease from mCRPC can be evaluated and quantified with whole-body DW imaging. Whole-body DW imaging-generated tDV showed correlation with established prognostic biomarkers and is associated with OS in mCRPC.

© RSNA, 2016

Online supplemental material is available for this article.



**P**rostate cancer is the second most common cancer and the fifth leading cause of cancer death among men worldwide (1). Prostate cancer metastasizes primarily to the bone; skeletal dissemination occurs in up to 84% of patients (2), causing higher morbidity and mortality in this population (3–5). Despite notable advances in the management of metastatic castration-resistant prostate carcinoma (mCRPC) with new drugs, including abiraterone acetate and enzalutamide, which have been approved in the past 5 years (6,7), mCRPC remains ultimately a fatal condition. Current bone imaging is inadequate, relying largely on bone scintigraphy with technetium 99m, an isotope taken up primarily by osteoblasts that is unable to accurately depict and quantify the true extent of metastatic disease to bone. The development of quantitative imaging biomarkers that can accurately evaluate the burden of bone metastases may help individualize patient risk stratification and treatment selection and may ultimately be useful for evaluating the response to treatment.

The accuracy of magnetic resonance (MR) imaging in the detection of bone metastases is higher than that of bone scintigraphy and, possibly, choline

positron emission tomography (PET)/computed tomography (CT) (8,9). Moreover, functional MR imaging complements anatomic sequences that assess some biologic characteristics of the tumor. Diffusion-weighted (DW) imaging is a functional MR imaging technique that provides quantitative measurement of the random displacement of water molecules (10). Previous studies have established the high sensitivity of DW imaging in the identification of bone metastases (11,12). DW imaging also allows easy delineation of areas of signal abnormality with semiautomated segmentation software; this provides the opportunity to more accurately determine the true extent of bone metastases. In addition, the apparent diffusion coefficient (ADC) shows correlation with cell density in different tumor types, including prostate cancer (13–17).

As part of a broader effort to clinically qualify whole-body MR imaging of bone metastases for mCRPC, our study was conducted to determine the correlation between volume of bone metastasis as assessed with DW imaging and established prognostic factors in mCRPC and the association of volume of bone metastases with overall survival (OS).

#### Advances in Knowledge

- Semiautomated whole-body diffusion-weighted (DW) imaging signal abnormality delineation is feasible, enabling the assessment of the total volume of bone metastasis in patients with metastatic castration-resistant prostate cancer (mCRPC).
- Assessment of total volume of bone metastases with whole-body DW imaging informs on the overall survival of patients with mCRPC.
- In our data set, the volume of bone metastases assessed with whole-body DW imaging showed correlation with established prognostic biomarkers for patients with advanced mCRPC, including circulating tumor cell count.

#### Materials and Methods

This retrospective study was approved by the institutional review board. Verbal informed consent was obtained for the acquisition of the MR images, and written informed consent was obtained for the acquisition of biologic samples from all patients.

#### Patient Population

Fifty-four male patients with mCRPC who were receiving treatment at a single institution underwent whole-body



#### Implication for Patient Care

- Assessment of the volume of bone metastases with whole-body DW imaging in patients with mCRPC may help individualize patient risk stratification and, therefore, treatment selection.

MR imaging, including DW imaging, between June 2010 and February 2013 before starting a new line of anticancer therapy. Patients were included in the study if (a) whole-body MR imaging was performed within 4 weeks of starting a new line of anticancer therapy, (b) bone metastases were identified on the basis of a review of images from combined imaging modalities (MR imaging, CT [in all cases], and bone scintigraphy [when available]), (c) whole-body MR imaging was performed with a 1.5-T unit (according to the technical parameters described below), and (d) at least 1 year of clinical follow-up data were available (or the patient died during the follow-up period). Patients were excluded if assessment with MR imaging was suboptimal owing to artifacts or incomplete studies. Of 54 cases reviewed, 43 were eligible for our study (all men; mean age, 69 years; age range, 41–80 years). The mean time between MR imaging and the start of treatment was 2.2 weeks. One case was not included

#### Published online before print

10.1148/radiol.2015150799

Content codes:  

Radiology 2016; 000:1–10

#### Abbreviations:

ADC = apparent diffusion coefficient  
BSI = bone scan index  
CI = confidence interval  
CTC = circulating tumor cell  
DW = diffusion weighted  
IQR = interquartile range  
mCRPC = metastatic castration-resistant prostate carcinoma  
OS = overall survival  
tDV = total tumor diffusion volume

#### Author contributions:

Guarantors of integrity of entire study, R.P.L., A.Z., J.S.d.B., N.T.; study concepts/study design or data acquisition or data analysis/interpretation, all authors; manuscript drafting or manuscript revision for important intellectual content, all authors; manuscript final version approval, all authors; agrees to ensure any questions related to the work are appropriately resolved, all authors; literature research, R.P.L., D.L., M.D.B., D.J.C., J.M., D.B., J.S.d.B., N.T.; clinical studies, R.P.L., D.J.C., J.M., A.O., A.Z., M.O.L., J.S.d.B., N.T.; experimental studies, M.D.B., A.Z., J.S.d.B.; statistical analysis, R.P.L., D.L., M.D.B., D.J.C., M.O.L., J.S.d.B., D.M.K.; and manuscript editing, R.P.L., D.L., M.D.B., D.J.C., J.M., A.O., A.Z., M.O.L., J.S.d.B., D.M.K., N.T.

Conflicts of interest are listed at the end of this article.

because whole-body MR imaging was not performed within 4 weeks of starting a new line of treatment, six cases were excluded because there was no radiologic evidence of bone metastases, and four cases were excluded because of the presence of artifacts (eg, susceptibility artifacts) and/or incomplete studies (Fig 1).

#### Clinical Data Collection

Data were collected into an anonymized database. Patient characteristics included age, previous anticancer treatments, Eastern Cooperative Oncology Group performance status (18), and laboratory results (hemoglobin, prostate-specific antigen, lactate dehydrogenase, alkaline phosphate, and albumin levels) at the time of MR imaging. Circulating tumor cell (CTC) count (19) and bone scan index (BSI) were included only if obtained within 12 weeks of MR imaging (mean time from CTC count to MR imaging, 3.6 weeks; mean time from BSI to MR imaging, 3.0 weeks). Follow-up data collected from electronic patient records included survival status and OS (defined as time from MR imaging to death by any cause). For noncensored patients, follow-up data included the length of clinical follow-up.

#### Whole-Body MR Imaging Parameters

MR imaging was performed with patients in the supine position by using a 1.5-T unit (Avanto; Siemens Healthcare, Erlangen, Germany) with surface and body coils. Axial images were acquired by using free-breathing single-shot twice-refocused echo-planar DW imaging from vertex to midthighs, sequentially across four imaging stations, with each consisting of 50 sections. In addition to whole-body DW imaging, anatomic imaging was also performed by using a breath-hold axial T1-weighted sequence. The imaging parameters used to perform whole-body MR imaging are summarized in Table 1.

#### Image Analysis

Images were processed and analyzed with open-access imaging assistant software (OsiriX v5.6; OsiriX Foundation,

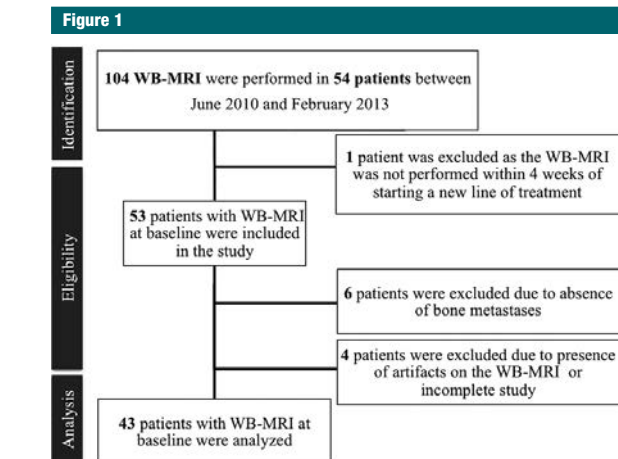


Figure 1: Flowchart of study selection process. WB = whole body.

Table 1

#### Imaging Parameters for Whole-Body DW Imaging

Parameter	T1-weighted Imaging	DW Imaging
Type of pulse sequence	Spoiled gradient echo (FLASH)	Single-shot twice-refocused echo-planar imaging
Respiration	Breath hold	Free breathing
Type of acquisition	2D	2D
Field of view (mm)	380–420	380–420
Repetition time (msec)	380	14 000
Echo time (msec)	5	68
Inversion time (msec)	NA	180
Flip angle (degrees)	70	90
Fat suppression	NA	STIR
Receiver bandwidth (Hz/pixel)	331	1800
No. of signals acquired	1	4
Section thickness (mm)	5	5
<i>b</i> value (sec/mm <sup>2</sup> )	NA	50 and 900
No. of stations	4 (from vertex to midthighs), 50 sections each	4 (from vertex to midthighs), 50 sections each

Note.—A 1.5-T unit (Avanto, Siemens Healthcare) was used for the imaging platform. FLASH = fast low-angle shot, NA = not applicable, STIR = short inversion time inversion recovery, 2D = two-dimensional.

Geneva, Switzerland). The T1-weighted and DW images (*b* value = 50 and 900 sec/mm<sup>2</sup> and ADC maps) were evaluated to assess the presence of metastatic bone disease. Regions of interest including all areas of signal intensity abnormality on DW images obtained with a *b* value of 900 sec/mm<sup>2</sup>, which corresponded to

high signal intensity on DW images obtained with a *b* value of 900 sec/mm<sup>2</sup> and low signal intensity on T1-weighted images, in keeping with metastatic bone disease, observed between C4 and midthighs were delineated. The skull vault and base were excluded owing to frequent artifacts, poor visualization of

disease, and lower incidence of metastases in these locations (20). A semiautomatic segmentation tool from the OsiriX software was used for delineating bone disease. The delineation of total tumor diffusion volume (tDV) was performed by a radiologist (R.P.L.) with 2 years of experience in whole-body DW imaging; manual correction of the segmentation mask corresponding to the volume of interest was performed when necessary (Fig 2). Pixel size and number of pixels for all volumes of interest were recorded to calculate the tDV for each patient. The ADC of every pixel was recorded, and

histogram representations of the ADCs of tDV for each patient were generated by using software (Excel 2010; Microsoft, Redmond, Wash).

Parameters analyzed at whole-body DW imaging included the tDV (defined as the number of pixels multiplied by the pixel volume in each case, accounting for differences in the size of the field of view), mean, median, skewness, and kurtosis of the ADC histogram for each patient.

A randomly selected subset of 10 cases was analyzed again by the primary radiologist (R.P.L.) at least 6 months

after the first assessment and by a second radiologist (N.T., with 6 years of experience in whole-body DW imaging) who was blinded to the initial analysis with the purpose of assessing the intra- and inter-observer reliability in tDV measurement.

#### CTC Count

CTCs were enumerated after isolation from blood samples by using a tumor cell kit (Cellsearch system; Janssen Diagnostics, Raritan, NJ), as described in a previous article (21). Results are expressed as the number of CTCs per 7.5 mL of blood.

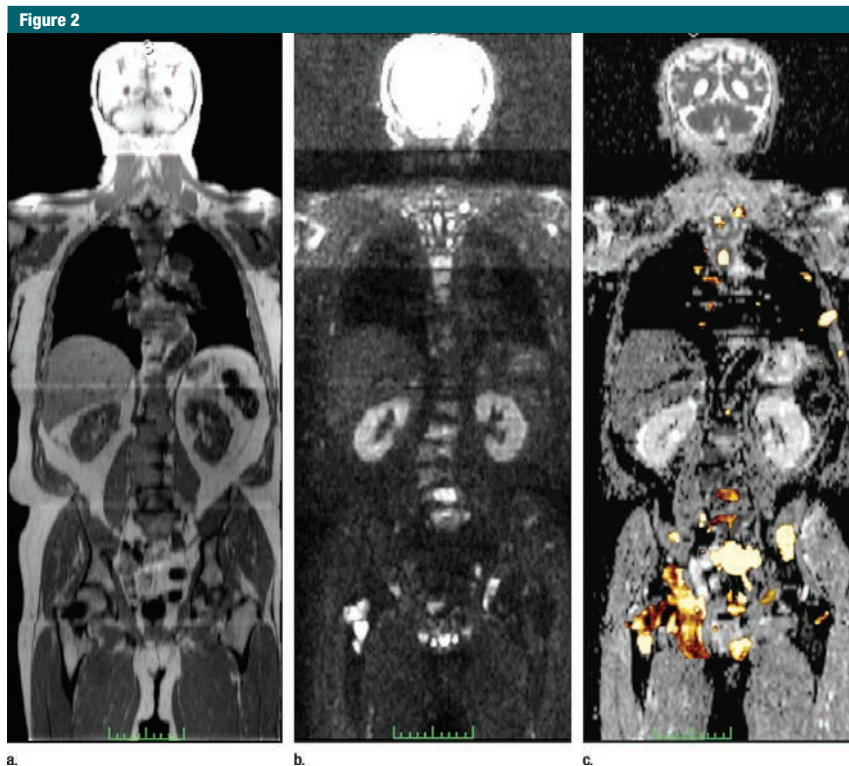


**Figure 2:** Images show metastatic bone disease segmentation steps in two-dimensional coronal views for illustrative purpose. Areas of signal abnormality corresponding to (a) high signal intensity on DW image ( $b = 900 \text{ mm}^2/\text{sec}^2$ ) and (b) low signal intensity on T1-weighted image, in keeping with bone metastases observed between C4 and the midthigh, were delineated and applied to the ADC map (c) to obtain ADCs in areas of interest. The overlaid colored mask is a three-dimensional representation of the tumor volume accounting for the apparent mismatch.

Table 2

**Baseline Characteristics and Previous Treatments of the Overall Population Included in the Final Analysis**

Parameter	Value*
<b>Baseline clinical characteristics (n = 43)<sup>†</sup></b>	
Hemoglobin level (g/dL)	43 [11] (10–13)
Prostate-specific antigen level (ng/mL)	43 [222] (69–1486)
Alkaline phosphatase level (IU/L)	43 [140] (88–586)
Lactate dehydrogenase level (IU/L)	43 [183] (151–247)
Albumin level (g/dL)	43 [37] (32–39)
BSI	32 [7.9] (2–11.5)
CTC count (cells per 7.5 mL of blood)	21 [35] (7–148)
<b>Prior treatments<sup>‡</sup></b>	
Docetaxel	29 (67.4)
Cabazitaxel	10 (23.3)
Abiraterone acetate	27 (62.8)
Enzalutamide	7 (16.3)
Radium-223	1 (2.3)
Bisphosphonates	6 (14)
Palliative radiation therapy to bone	22 (51.2)
<b>Sites of metastatic disease<sup>‡</sup></b>	
Bone only	20 (46.5)
Bone and nodal	17 (39.5)
Bone and viscera	6 (14)
<b>Metastatic bone disease characteristics</b>	
Median tDV (mL) <sup>§</sup>	503.1 (5.6–2242)
Median ADC (x10 <sup>-6</sup> mm <sup>2</sup> /sec) <sup>  </sup>	813 (780, 906)
Median OS (mo) <sup>  </sup>	12.9 (8.7, 16.1)

\* Unless otherwise specified, data are numbers of patients.

<sup>†</sup> Numbers in brackets are medians. Numbers in parentheses are the IQR.

<sup>‡</sup> Numbers in parentheses are percentages.

<sup>§</sup> Numbers in parentheses are the range.

<sup>||</sup> Numbers in parentheses are 95% CIs.

**BSI Calculation**

For those patients who underwent bone scintigraphy within 12 weeks of MR imaging and for whom Digital Imaging and Communication in Medicine images were available, the BSI was calculated by using an automated BSI scoring software system (Exini Diagnostics, Lund, Sweden) (22).

**Statistical Analysis**

The Pearson correlation coefficient (*r*) was determined to establish the correlation between variables. Kaplan-Meier analysis was used to study the OS of the population. Patients who were alive at the time of last follow-up were censored. Cox proportional hazards models were used to determine

the association of the variables with OS. The comparison between the discriminative ability of MR imaging and bone scintigraphy in the prediction of OS was performed by assessing the status of each patient (dead vs alive) at several time points (9, 12, and 15 months) and determining the area under the receiver operating characteristic curve (concordance index, or C-index). Comparison between receiver operating characteristic curves was performed with the method established by DeLong et al (23). The 95% confidence interval (CI) of the median ADC of the entire population was calculated by means of bootstrapping. tDV, BSI, prostate-specific antigen level, CTC count, alkaline phosphate level, and lactate dehydrogenase level

were log-transformed to account for the lack of normal distribution. The intra- and interobserver reliability of tDV measurements were assessed by using the Lin concordance correlation coefficient of absolute agreement and Bland-Altman analysis. Limits of agreement were defined as the mean difference  $\pm$  1.96 times the standard deviation of the differences. The coefficient of repeatability was calculated as 1.96 times the standard deviation of the differences between the two measurements. Software (SPSS, version 20; IBM, Armonk, NY) was used for statistical analyses.

**Results**

Forty-three patients were eligible and included in the analysis. Twenty of the 43 patients (46.5%) had metastatic disease limited to bone, 17 (39.5%) had bone and nodal disease, and six (14%) had visceral disease in addition to bone metastases.

Patients in our dataset had received a median of three (range, 0–7) lines of treatment for mCRPC at the time of MR imaging, including four patients (9.3%) who were treatment-naïve for mCRPC in whom MR imaging was performed within 4 weeks before their first systemic treatment for mCRPC. Twenty-eight of the 43 patients (65.1%) had undergone previous treatment with at least abiraterone acetate and/or enzalutamide and 29 (67.4%) were previously treated with taxane-based chemotherapy.

Thirty of the 43 patients (69.8%) died during the follow-up period, with 13 patients (30.2%) alive at the time of data analysis. The median OS of the overall population was 12.9 months (95% CI: 8.7, 16.1 months), with a median follow-up of 11.1 months (interquartile range [IQR]: 7.4–15.7 months). Patient and tumor characteristics, including treatment received before inclusion in our study, are summarized in Table 2.

The median tDV was 503.1 mL (range, 5.6–2242 mL), with a median global ADC for the regions of interest

for each individual of  $813 \times 10^{-6}$  mm<sup>2</sup>/sec (95% CI: 780,  $906 \times 10^{-6}$  mm<sup>2</sup>/sec), median skewness of 1.5 (IQR: 0.9–1.9), and median kurtosis of 3.5 (IQR: 1.4–7). Histograms of the global ADCs for each patient and the whole population are shown in Figure 3. Two patients had bimodal histograms, with a high density of ADCs within  $500\text{--}1500 \times 10^{-6}$  mm<sup>2</sup>/sec and a smaller peak within  $2000\text{--}3000 \times 10^{-6}$  mm<sup>2</sup>/sec. Both cases corresponded to patients who received focal palliative radiation therapy to the pelvis during the 6 months before MR imaging (Fig 4).

#### Correlation of tDV with Prognostic Factors

We investigated the correlation between tDV and known established prognostic factors, with special interest in those associated with bone disease (eg, hemoglobin and alkaline phosphate levels). Overall, tDV showed a significant correlation with all of the studied established prognostic factors for mCRPC (hemoglobin level:  $r = -0.521$ ,  $P < .001$ ; prostate-specific antigen level:  $r = 0.556$ ,  $P < .001$ ; lactate dehydrogenase level:  $r = 0.534$ ,  $P < .001$ ; and alkaline phosphate level:  $r = 0.572$ ,  $P < .001$ ) (Table 3).

Next, we explored the correlation between tDV and CTC count. Baseline CTC counts were available for 21 of the 43 patients (48.8%). The median CTC count was 35 cells per 7.5 mL (IQR: 7–148 cells per 7.5 mL). CTC count showed significant correlation with tDV ( $r = 0.613$ ,  $P = .004$ ), which is consistent with published evidence that high CTC count informs on worse prognosis in mCRPC (24) (Fig 5).

#### Association of tDV with OS

We hypothesized that the burden of bone disease would associate with OS in patients with mCRPC; tDV, as a continuous variable, showed a statistically significant association with OS, with patients with a higher tDV having an increased risk of death (hazard ratio: 1.74; 95% CI: 1.02, 2.96;  $P = .035$ ).

#### Association of Other Parameters Derived from Whole-Body DW Imaging with OS

Histogram parameters that describe the distribution of the global ADCs of

bone metastases, such as mean (hazard ratio: 1; 95% CI: 0.998, 1.001;  $P = .876$ ), median (hazard ratio: 1; 95% CI: 0.998, 1.002;  $P = .928$ ), skewness (hazard ratio: 0.92; 95% CI: 0.563, 1.504;  $P = .740$ ), or kurtosis (hazard ratio: 0.97; 95% CI: 0.89–1.06;  $P = .532$ ) did not show a significant association with OS in our population.

#### Comparison of the Predictive Ability of Whole-Body DW Imaging and BSI

Among the 43 patients, 32 (74.4%) had BSI data available for analysis from bone scans obtained within the prespecified time ranges. Seven of the 43 patients (16.3%) underwent bone scintigraphy more than 12 weeks apart from MR imaging and were therefore excluded from this subanalysis. Two of the 43 patients (4.7%) did not have results from bone scintigraphy available, and two (4.7%) did not have Digital Imaging and Communications in Medicine images, which are necessary for BSI calculation, available. The median BSI was 7.9 (IQR, 2–11.5). The tDV measured with whole-body DW imaging, as a continuous variable, and the estimation relative to total skeletal mass by the BSI were highly correlated ( $r = 0.565$ ,  $P = .001$ ) (Fig 5). To further assess the prognostic performance of BSI and tDV, we evaluated mortality rates at 9, 12, and 15 months (when approximately one-third, one-half, and two-thirds of patients had died). Receiver operating characteristic curve analysis was performed to determine the C-statistic (area under the receiver operating characteristic curve) with each of both imaging biomarkers at the specified time points. Although the area under the receiver operating characteristic curve for tDV was consistently superior to that for BSI for 9-month (0.745 vs 0.613, respectively;  $P = .141$ ), 12-month (0.686 vs 0.627;  $P = .533$ ), and 15-month (0.704 vs 0.607;  $P = .345$ ) mortality rates (Fig E1 [online]), these differences were not statistically significant.

#### Intra- and Interobserver Reliability of tDV Measurement

The intraclass correlation coefficients were 0.986 (95% CI: 0.945, 0.996) and

0.949 (95% CI: 0.857, 0.981) for intra- and interobserver comparison, respectively. The Bland-Altman-calculated intraobserver coefficient of repeatability was 0.302 L, and the interobserver coefficient of repeatability was 0.500 L. All values in the intra- and interobserver Bland-Altman analysis are within the 95% limits of agreement.

#### Discussion

Bone involvement in patients with advanced prostate cancer is extremely common, resulting in higher morbidity and mortality in patients with mCRPC. When we consider the limitations of CT and bone scintigraphy in the accurate assessment of the extent of bone metastases, it is imperative to develop new imaging biomarkers and pursue their analytical and clinical quantification, with the aim of providing new tools for guiding radiologists and clinicians in therapeutic decisions.

Our study shows an association between whole-body DW imaging parameters, OS, and prognostic factors in mCRPC, which was previously established in the literature. Notably, the volume of bone metastasis quantified with whole-body DW imaging correlates with prognostic biomarkers routinely implemented into standard physician's practice, such as hemoglobin level, prostate-specific antigen level, and the bone turnover marker alkaline phosphate level. Interestingly, we also detected a correlation with CTC count, an established prognostic biomarker in mCRPC, although these findings must be corroborated in larger populations.

Histogram representation of the ADCs of the burden of metastatic bone disease may also provide a useful representation of tissue cellularity. The median ADC for our population was  $813 \times 10^{-6}$  mm<sup>2</sup>/sec; this value is lower than the median ADC reported in previous studies in other tumor types, including multiple myeloma (25), a disease with predominately lytic disease. In this mCRPC population, conversely, metastases were mainly sclerotic (26). Studies in which DW imaging is used as a biomarker in



Figure 3

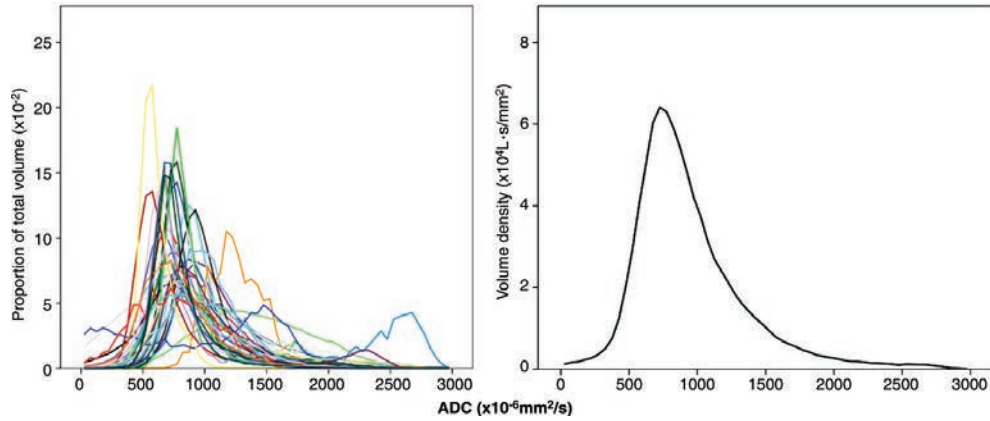


Figure 3: Left, histogram representation of ADCs for every patient included in analysis ( $n = 43$ ). Right, volume density plot, where the y-axis represents the volume density per unit ADC. The area under the curve thus represents the total volume of disease in the patient population.

Figure 4

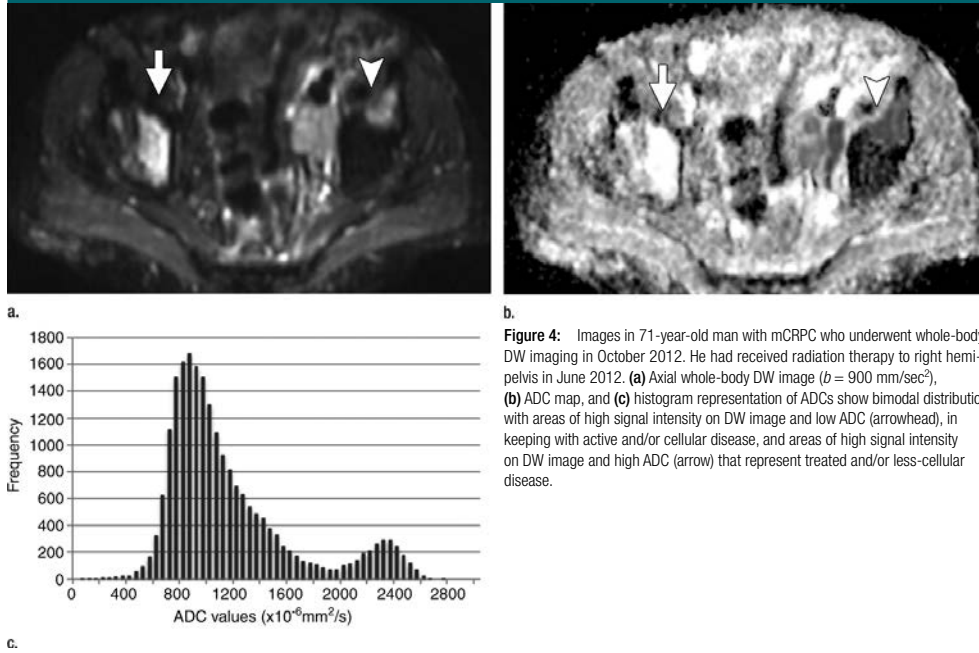


Figure 4: Images in 71-year-old man with mCRPC who underwent whole-body DW imaging in October 2012. He had received radiation therapy to right hemipelvis in June 2012. (a) Axial whole-body DW image ( $b = 900 \text{ mm}^2/\text{sec}^2$ ), (b) ADC map, and (c) histogram representation of ADCs show bimodal distribution with areas of high signal intensity on DW image and low ADC (arrowhead), in keeping with active and/or cellular disease, and areas of high signal intensity on DW image and high ADC (arrow) that represent treated and/or less-cellular disease.

cancer medicine, therefore, must account for such differences in disease biology among tumor types. Furthermore, bimodal histograms reflect the coexistence of two different patterns of disease with different cellular density distributions (27).

Parameters that help describe the distribution of the global ADCs of bone metastases, such as mean, median, skewness, or kurtosis, were not associated with OS in our population.

**Table 3**  
**Correlation of tDV and Other Prognostic Factors**

Prognostic Factor	Correlation Coefficient*	P Value
Hemoglobin level	-0.521	<.001
Prostate-specific antigen level	0.556	<.001
Lactate dehydrogenase level	0.534	<.001
Alkaline phosphatase level	0.572	<.001
Albumin level	-0.332	.030
CTC count	0.613	.004

Note.—The tDV, prostate-specific antigen level, lactate dehydrogenase level, alkaline phosphatase level, and CTC count were log-transformed.

\* Pearson correlation coefficient.

In the past few years it has been shown that indirect measurements of the burden of bone metastases, measured either as proportion of skeletal mass with BSI or the number of lesions visible at CT and PET/CT, provide prognostic information in prostate cancer (28,29). These examinations, however, only largely reflect bone turnover as a response to either benign or malignant processes. MR imaging has been previously shown to have higher sensitivity and specificity than bone scintigraphy and CT in the detection of bone metastases (12). In our data set, the receiver operating characteristic curves with bone scintigraphy were consistently inferior to those with whole-body DW imaging in the prediction of mortality, which suggests that the performance of DW imaging is superior. However, considering the limited population included in our study, formal comparisons in larger cohorts will be necessary to confirm this finding because the differences did not reach statistical significance.

We acknowledge the potential limitations of our study. First, the retrospective observational nature of our work, the variability in the number and type of treatments administered in the time between MR imaging and the start

of therapy, and the presence of nodal and visceral disease in some of our patients are limitations. Second, because of the limited sample size of our pilot study, it is important to note that we did not control for clinical factors in the evaluation of the association between tDV and OS. A larger population would be needed for future validation of these data, allowing for multivariate analysis—ideally in the setting of prospective studies. Third, there is a risk of underestimating the disease because the presented data included skeletal segmentation from the cervical spine to midthighs only. However, taking into account that the vast majority of bone metastases occur within the spine and pelvis (20), it is unlikely that this had a major effect on the assessment of the total burden of metastatic bone disease. Finally, it should be noted that delineation of the volume of interest is dependent on the quality of the acquired DW imaging data, the semiautomatic segmentation tool, and radiologist expertise. Despite these limitations, to our knowledge, our study represents the largest series assessing mCRPC bone metastasis with DW imaging and the data presented herein support further evaluation of whole-body DW imaging in this disease.

**Figure 5**

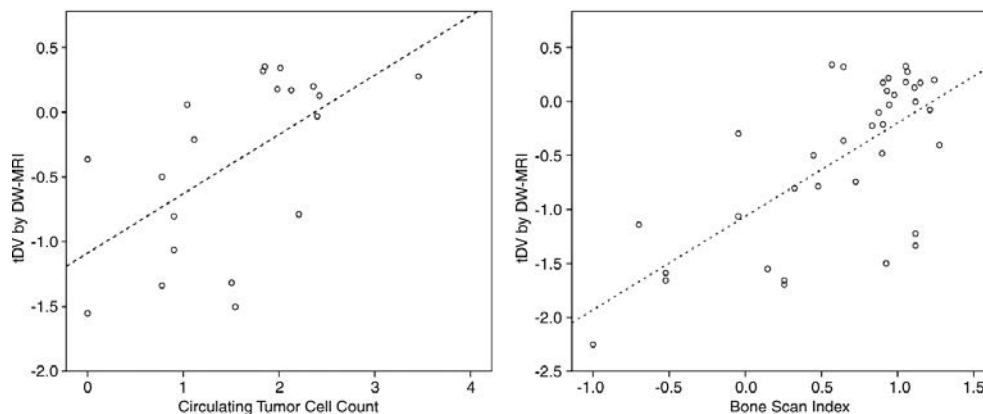


Figure 5: Scatterplots show relationship between tDV and CTC count and between tDV and BSI.

One practical conclusion of our study is the demonstration of the feasibility of assessing metastatic bone disease from prostate cancer with whole-body DW imaging; indeed, in 49 of 53 cases reviewed (92%) the outcome of DW imaging was fully suitable for assessment. We are currently able to perform whole-body DW imaging in reasonably short data acquisition times (24 minutes), thus analyzing whole-tumor burden and its spatial heterogeneity. Other advantages of whole-body MR imaging including DW imaging compared with the current standard of CT and bone scintigraphy are the avoidance of the need for radiation or radioactive materials, evaluation of both soft-tissue and bone metastases, and accurate depiction of complications such as cord compression or bone fractures. Whole-body MR imaging including DW imaging can be implemented in everyday clinical practice, as the technique is robust and the protocols can be implemented in most of the commonly used imaging units.

In conclusion, we have shown a strong correlation between tDV assessed with whole-body DW imaging and proved prognostic factors in mCRPC, including CTC counts, and present promising data that support an association between tDV and OS. Our results, taken together with those from previous reports that describe changes in DW imaging after exposure to anti-cancer treatments (30), raise the need for further evaluation of DW imaging as a prognostic and response biomarker in prospective cohorts of patients with mCRPC to acquire clinical qualification and, eventually, implementation in routine clinical practice.

**Acknowledgments:** This study was supported by Prostate Cancer UK and the Stand Up To Cancer-Prostate Cancer Foundation Prostate Dream Team Translational Cancer Research Grant; Stand Up To Cancer is a program of the Entertainment Industry Foundation administered by the American Association for Cancer Research (SU2C-AACR-DT0712). Raquel Perez-Lopez conducted this work in the Medicine Doctorate framework of the Universidad Autonoma de Barcelona. The authors thank other clinical research fellows at the Prostate Cancer Targeted Therapy Group and radiographers at The Royal Marsden NHS Foundation Trust and the Insti-

tute of Cancer Research. We acknowledge patients and their families for their collaboration toward research.

**Disclosures of Conflicts of Interest:** R.P. disclosed no relevant relationships. D.L. Activities related to the present article: disclosed no relevant relationships. Activities not related to the present article: receives consulting fees from Sanofi. Other relationships: disclosed no relevant relationships. M.D.B. disclosed no relevant relationships. D.J.C. disclosed no relevant relationships. J.M. disclosed no relevant relationships. D.B. disclosed no relevant relationships. A.O. disclosed no relevant relationships. A.Z. disclosed no relevant relationships. M.O.L. disclosed no relevant relationships. J.S.d.B. disclosed no relevant relationships. D.M.K. disclosed no relevant relationships. N.T. disclosed no relevant relationships.

#### References

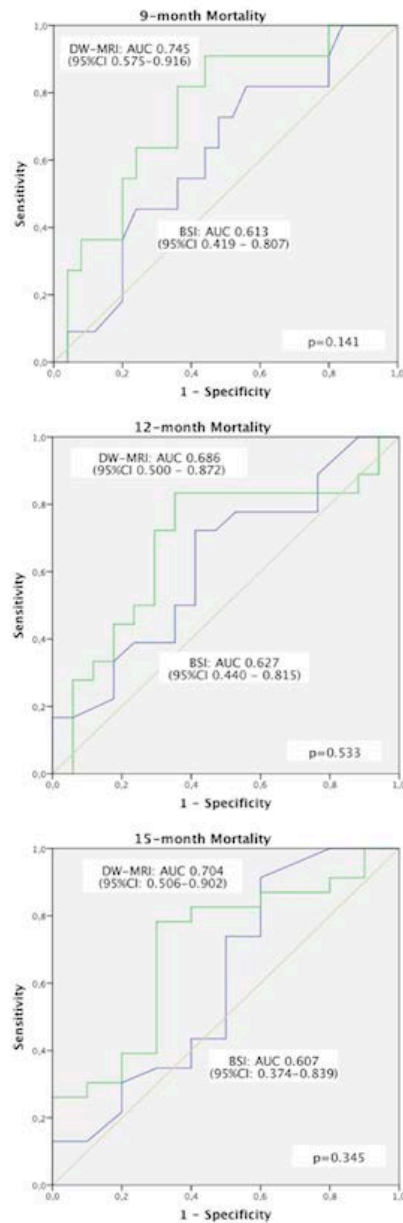
1. Ferlay J, Soerjomataram I, Dikshit R, et al. Cancer incidence and mortality worldwide: sources, methods and major patterns in GLOBOCAN 2012. *Int J Cancer* 2015;136(5):E359-E386.
2. Gandaglia G, Abdollah F, Schiffmann J, et al. Distribution of metastatic sites in patients with prostate cancer: a population-based analysis. *Prostate* 2014;74(2):210-216.
3. Carlin BI, Andriole GL. The natural history, skeletal complications, and management of bone metastases in patients with prostate carcinoma. *Cancer* 2000;88(12 Suppl):2989-2994.
4. Saad F, Lipton A, Cook R, Chen YM, Smith M, Coleman R. Pathologic fractures correlate with reduced survival in patients with malignant bone disease. *Cancer* 2007;110(8):1860-1867.
5. Sathiakumar N, Delzell E, Morrisey MA, et al. Mortality following bone metastasis and skeletal-related events among men with prostate cancer: a population-based analysis of US Medicare beneficiaries, 1999-2006. *Prostate Cancer Prostatic Dis* 2011;14(2):177-183.
6. de Bono JS, Logothetis CJ, Molina A, et al. Abiraterone and increased survival in metastatic prostate cancer. *N Engl J Med* 2011;364(21):1995-2005.
7. Scher HI, Fizazi K, Saad F, et al. Increased survival with enzalutamide in prostate cancer after chemotherapy. *N Engl J Med* 2012;367(13):1187-1197.
8. Shen G, Deng H, Hu S, Jia Z. Comparison of choline-PET/CT, MRI, SPECT, and bone scintigraphy in the diagnosis of bone metastases in patients with prostate cancer: a meta-analysis. *Skeletal Radiol* 2014;43(11):1503-1513.
9. Jambor I, Kuisma A, Ramadan S, et al. Prospective evaluation of planar bone scintigraphy, SPECT, SPECT/CT, (18)F-NaF PET/CT and whole body 1.5T MRI, including DWI, for the detection of bone metastases in high risk breast and prostate cancer patients: SKELETA clinical trial. *Acta Oncol* 2016;55(1):59-67.
10. Koh DM, Collins DJ. Diffusion-weighted MRI in the body: applications and challenges in oncology. *AJR Am J Roentgenol* 2007;188(6):1622-1635.
11. Luboldt W, Küfer R, Blumstein N, et al. Prostate carcinoma: diffusion-weighted imaging as potential alternative to conventional MR and 11C-choline PET/CT for detection of bone metastases. *Radiology* 2008;249(3):1017-1025.
12. Lecouvet FE, El Mouedden J, Collette L, et al. Can whole-body magnetic resonance imaging with diffusion-weighted imaging replace Tc 99m bone scanning and computed tomography for single-step detection of metastases in patients with high-risk prostate cancer? *Eur Urol* 2012;62(1):68-75.
13. Guo AC, Cummings TJ, Dash RC, Provenza JM. Lymphomas and high-grade astrocytomas: comparison of water diffusibility and histologic characteristics. *Radiology* 2002;224(1):177-183.
14. Hayashida Y, Hirai T, Morishita S, et al. Diffusion-weighted imaging of metastatic brain tumors: comparison with histologic type and tumor cellularity. *AJNR Am J Neuroradiol* 2006;27(7):1419-1425.
15. Zelhof B, Pickles M, Liney G, et al. Correlation of diffusion-weighted magnetic resonance data with cellularity in prostate cancer. *BJU Int* 2009;103(7):883-888.
16. Liu Y, Ye Z, Sun H, Bai R. Clinical application of diffusion-weighted magnetic resonance imaging in uterine cervical cancer. *Int J Gynecol Cancer* 2015;25(6):1073-1078.
17. Matsubayashi RN, Fujii T, Yasumori K, Muranaka T, Momosaki S. Apparent diffusion coefficient in invasive ductal breast carcinoma: correlation with detailed histologic features and the enhancement ratio on dynamic contrast-enhanced MR images. *J Oncol* doi: 10.1155/2010/821048. Published online September 2, 2010. Accessed April 15, 2015.
18. Oken MM, Creech RH, Tormey DC, et al. Toxicity and response criteria of the Eastern Cooperative Oncology Group. *Am J Clin Oncol* 1982;5(6):649-655.
19. Olmos D, Arkenau HT, Ang JE, et al. Circulating tumour cell (CTC) counts as intermediate end points in castration-resistant prostate cancer (CRPC): a single-centre experience. *Ann Oncol* 2009;20(1):27-33.



20. Kakhki VR, Anvari K, Sadeghi R, Mahmoudian AS, Torabian-Kakhki M. Pattern and distribution of bone metastases in common malignant tumors. *Nucl Med Rev Cent East Eur* 2013;16(2):66–69.
21. Kraan J, Sleijfer S, Strijbos MH, et al. External quality assurance of circulating tumor cell enumeration using the CellSearch(®) system: a feasibility study. *Cytometry B Clin Cytom* 2011;80(2):112–118.
22. Ulmert D, Kaboteh R, Fox JJ, et al. A novel automated platform for quantifying the extent of skeletal tumour involvement in prostate cancer patients using the bone scan index. *Eur Urol* 2012;62(1):78–84.
23. DeLong ER, DeLong DM, Clarke-Pearson DL. Comparing the areas under two or more correlated receiver operating characteristic curves: a nonparametric approach. *Biometrics* 1988;44(3):837–845.
24. de Bono JS, Scher HI, Montgomery RB, et al. Circulating tumor cells predict survival benefit from treatment in metastatic castration-resistant prostate cancer. *Clin Cancer Res* 2008;14(19):6302–6309.
25. Messiou C, Collins DJ, Morgan VA, Desouza NM. Optimising diffusion-weighted MRI for imaging metastatic and myeloma bone disease and assessing reproducibility. *Eur Radiol* 2011;21(8):1713–1718.
26. Messiou C, Collins DJ, Morgan VA, Bianchini D, de Bono JS, de Souza NM. Use of apparent diffusion coefficient as a response biomarker in bone: effect of developing sclerosis on quantified values. *Skeletal Radiol* 2014;43(2):205–208.
27. Padhani AR, van Ree K, Collins DJ, D'Sa S, Makris A. Assessing the relation between bone marrow signal intensity and apparent diffusion coefficient in diffusion-weighted MRI. *AJR Am J Roentgenol* 2013;200(1):163–170.
28. Kaboteh R, Damber JE, Gjerdtsson P, et al. Bone scan index: a prognostic imaging biomarker for high-risk prostate cancer patients receiving primary hormonal therapy. *EJNMMI Res* 2013;3(1):9.
29. Vargas HA, Wassberg C, Fox JJ, et al. Bone metastases in castration-resistant prostate cancer: associations between morphologic CT patterns, glycolytic activity, and androgen receptor expression on PET and overall survival. *Radiology* 2014;271(1):220–229.
30. Blackledge MD, Collins DJ, Tunariu N, et al. Assessment of treatment response by total tumor volume and global apparent diffusion coefficient using diffusion-weighted MRI in patients with metastatic bone disease: a feasibility study. *PLoS One* 2014;9(4):e91779.

## Supplemental material

**Supplemental Figure E1.** Receiver operating characteristic curve analysis. Receiver operating characteristic curves for tDV and BSI for discriminating (top) 9-month mortality, (middle) 12-month mortality, and (bottom) 15-month mortality. The area under the receiver operating characteristic curve (AUC) for tDV was consistently superior to that for BSI for 9-month (0.745 vs 0.613, respectively;  $P = .141$ ), 12-month (0.686 vs 0.627;  $P = .533$ ), and 15-month (0.704 vs 0.607;  $P = .345$ ) mortality rates, although these differences were not statistically significant.





### 7.2.2. Whole-body DW-MRI as response biomarker of bone metastases in patients with mCRPC

---

#### **Diffusion-weighted Imaging as a Treatment Response Biomarker for Evaluating Bone Metastases in Prostate Cancer: A Pilot Study.**

Perez-Lopez R, Mateo J, Mossop H, Blackledge MD, Collins DJ, Rata M, Morgan VA, Macdonald A, Sandhu S, Lorente D, Rescigno P, Zafeiriou Z, Bianchini D, Porta N, Hall E, Leach MO, de Bono JS, Koh DM, Tunariu N.

Radiology. 2017 Apr;283(1):168-177. doi: 10.1148/radiol.2016160646. Epub 2016 Nov 22.



# Diffusion-weighted Imaging as a Treatment Response Biomarker for Evaluating Bone Metastases in Prostate Cancer: A Pilot Study<sup>1</sup>

Raquel Perez-Lopez, MD, MSc  
 Joaquin Mateo, MD, MSc  
 Helen Mossop, MMathStat  
 Matthew D. Blackledge, PhD  
 David J. Collins, BMIP  
 Mihaela Rata, PhD  
 Veronica A. Morgan, MS  
 Alison Macdonald, MS  
 Shahneen Sandhu, MD  
 David Lorente, MD  
 Pasquale Rescigno, MD  
 Zafeiris Zafeiriou, MD  
 Diletta Bianchini, MD  
 Nuria Porta, PhD  
 Emma Hall, PhD  
 Martin O. Leach, PhD  
 Johann S. de Bono, MB, ChB, PhD  
 Dow-Mu Koh, MD, FRCR, MRCP  
 Nina Tunariu, MD, FRCR, MRCP

<sup>1</sup> From the Inst of Cancer Research and Royal Marsden NHS Foundation Trust, Cancer Therapeutics Div, 15 Cotswold Rd, Sutton SM2 5NG, England. Received March 16, 2016; revision requested May 3; revision received July 3; accepted July 22; final version accepted July 28. **Address correspondence to** N.T. (e-mail: [Nina.Tunariu@icr.ac.uk](mailto:Nina.Tunariu@icr.ac.uk)).

Supported by BRC (BRC A38), Stand Up to Cancer (SU2C-AACR-DT0712), ECOMC funding from Cancer Research UK and Dept of Health (CRM064X), Cancer Research UK (C12540/A12829, C12540/A13230, C1491/A15955, C1491/A9895), CRUK and EPSRC in association with MRC and Dept of Health (C1060/A10334, C1060/A16464), Prostate Cancer UK (PG14-016-TR2), Prostate Cancer Foundation (20131017), the Investigator-Sponsored Study Collaboration between AstraZeneca and the National Inst for Health Research Cancer Research Network, and NHS funding to the NIHR Biomedicine Research Ctr and Clinical Research Facility. J.M. supported by the MRC-Prostate Cancer UK Fellowship and a PCF Young Investigator Award. M.D.B. supported by the NIHR postdoctoral fellowship (NHR011X).

This work was undertaken at The Royal Marsden NHS Foundation Trust, which received a proportion of its funding from the NHS Executive; the views expressed in this publication are those of the authors and not necessarily those of the NHS Executive. M.O.L. is an NIHR senior investigator.

Published under a CC BY 4.0 license.

## Purpose:

To determine the usefulness of whole-body diffusion-weighted imaging (DWI) to assess the response of bone metastases to treatment in patients with metastatic castration-resistant prostate cancer (mCRPC).

## Materials and Methods:

A phase II prospective clinical trial of the poly-(adenosine diphosphate-ribose) polymerase inhibitor olaparib in mCRPC included a prospective magnetic resonance (MR) imaging substudy; the study was approved by the institutional research board, and written informed consent was obtained. Whole-body DWI was performed at baseline and after 12 weeks of olaparib administration by using 1.5-T MR imaging. Areas of abnormal signal intensity on DWI images in keeping with bone metastases were delineated to derive total diffusion volume (tDV); five target lesions were also evaluated. Associations of changes in volume of bone metastases and median apparent diffusion coefficient (ADC) with response to treatment were assessed by using the Mann-Whitney test and logistic regression; correlation with prostate-specific antigen level and circulating tumor cell count were assessed by using Spearman correlation ( $r$ ).

## Results:

Twenty-one patients were included. All six responders to olaparib showed a decrease in tDV, while no decrease was observed in all nonresponders; this difference between responders and nonresponders was significant ( $P = .001$ ). Increases in median ADC were associated with increased odds of response (odds ratio, 1.08; 95% confidence interval [CI]: 1.00, 1.15;  $P = .04$ ). A positive association was detected between changes in tDV and best percentage change in prostate-specific antigen level and circulating tumor cell count ( $r = 0.63$  [95% CI: 0.27, 0.83] and  $r = 0.77$  [95% CI: 0.51, 0.90], respectively). When assessing five target lesions, decreases in volume were associated with response (odds ratio for volume increase, 0.89; 95% CI: 0.80, 0.99;  $P = .037$ ).

## Conclusion:

This pilot study showed that decreases in volume and increases in median ADC of bone metastases assessed with whole-body DWI can potentially be used as indicators of response to olaparib in mCRPC.

Published under a CC BY 4.0 license.

Online supplemental material is available for this article.

**P**rostate cancer is the second most commonly diagnosed cancer among men worldwide (1). Bone metastases are highly prevalent in patients with metastatic castration-resistant prostate cancer (mCRPC), the late stage of prostate cancer that causes substantial disease-related morbidity and mortality in this population. Bone metastases occur in up to 84% of patients with mCRPC and frequently represent the only site of metastatic disease (2).

Standard imaging techniques, such as computed tomography (CT) and technetium 99m bone scintigraphy, fail to allow accurate evaluation of the burden of bone metastases and detection of changes in response to treatment (3). In fact, the widely used Response Evaluation Criteria In Solid Tumors (RECIST) version 1.1 (4) do not define response in bone metastases, as this is considered to be non-measurable disease. The Prostate Cancer Working Group 2 criteria define progression in bone metastases on the

basis of the appearance of new lesions at bone scintigraphy but fail to state any criteria for response in bone metastases (5). Therefore, evaluation of tumor response in patients with bone-only metastatic disease relies solely on decrease in prostate-specific antigen (PSA) level, which has not been proven to be a surrogate for improved survival (5–7). There is an urgent unmet need to identify, develop, and validate non-invasive response biomarkers for bone metastases in prostate cancer.

Diffusion-weighted imaging (DWI) is a functional magnetic resonance (MR) imaging technique used to study the motion of water molecules within tissue. Apparent diffusion coefficient (ADC) is an objective measurement of this water diffusion, which has been demonstrated to inversely correlate with cellularity in different tumor types, including bone marrow malignancies (8–13). Changes in ADC values after treatment have been correlated with tumor responses in different tumor types, including myeloma, ovarian carcinoma, primary peritoneal carcinoma, and rhabdomyosarcoma (14–16). Additionally, the volume of bone metastases assessed with whole-body DWI has prognostic value in patients with mCRPC (17). Limited data about the value of DWI in the assessment of response to bone metastases in mCRPC are currently available and come from small series of patients (18–21). In the setting of a prospective clinical trial, we aimed to determine the usefulness of whole-body DWI for the assessment of response of bone metastases to treatment in patients with mCRPC.

#### Advances in Knowledge

- All six patients who responded to the poly-(adenosine diphosphate-ribose) polymerase inhibitor olaparib showed a decrease in total diffusion volume (tDV) (median,  $-41.1\%$ ; range,  $-58.8\%$  to  $-6.3\%$ ), but no decrease was observed in any of the 15 nonresponders (median,  $+20.7\%$ ; range,  $+0.0\%$  to  $+76.9\%$ ); this difference between responders and nonresponders was significant ( $P = .001$ ).
- Increases in median apparent diffusion coefficient of the tDV after 12 weeks of treatment were associated with responses to olaparib (odds ratio, 1.08; 95% confidence interval [CI]: 1.00, 1.15;  $P = .037$ ).
- When analyzing up to five target bone metastases, changes in entire volume of the target bone metastases were also inversely associated with response (odds ratio, 0.89; 95% CI: 0.80, 0.99;  $P = .037$ ).

#### Implication for Patient Care

- Clinical qualification of whole-body diffusion-weighted imaging as a response biomarker in bone metastases would improve assessment of response to treatment in metastatic castration-resistant prostate cancer, allowing for optimization of patient care, treatment decision making, and drug development in this common disease.

#### Materials and Methods

We conducted a phase II trial of the poly-(adenosine diphosphate-ribose) polymerase inhibitor olaparib (Lynparza; AstraZeneca, Cambridge, United Kingdom) in mCRPC (Trial of Olaparib in Patients with Advanced Castration-Resistant Prostate Cancer [TOPARP-A], Cancer Research UK no. CRUK/11/029); patients were enrolled from July 2012 to September 2014. A prospective MR imaging substudy was conducted with institutional review board approval at The Royal Marsden NHS Foundation Trust. Enrollment in this MR imaging substudy was optional; written informed consent was obtained for MR imaging acquisition.

#### Study Design

The primary end point of the TOPARP-A trial was response rate, with response defined as any of the following: a response of soft tissue and/or visceral

#### Published online before print

10.1148/radiol.2016160646 Content codes: GU IMR IMK

Radiology 2017; 000:1–10

#### Abbreviations:

ADC = apparent diffusion coefficient  
 CI = confidence interval  
 CTC = circulating tumor cell  
 DWI = diffusion-weighted imaging  
 mCRPC = metastatic castration-resistant prostate cancer  
 PSA = prostate-specific antigen  
 RECIST = Response Evaluation Criteria In Solid Tumors  
 ROI = region of interest  
 tDV = total diffusion volume  
 TOPARP-A = Trial of Olaparib in Patients with Advanced Castration-Resistant Prostate Cancer

#### Author contributions:

Guarantors of integrity of entire study, R.P.L., S.S., J.S.D.B., N.T.; study concepts/study design or data acquisition or data analysis/interpretation, all authors; manuscript drafting or manuscript revision for important intellectual content, all authors; approval of final version of submitted manuscript, all authors; agrees to ensure any questions related to the work are appropriately resolved, all authors; literature research, R.P.L., D.J.C., D.L., P.R., J.S.D.B.; clinical studies, R.P.L., J.M., D.J.C., M.R., V.A.M., A.M., S.S., D.L., P.R., Z.Z., D.B., J.S.D.B., N.T.; experimental studies, R.P.L., M.R., J.S.D.B.; statistical analysis, J.M., H.M., M.D.B., D.J.C., N.P., E.H., J.S.D.B.; and manuscript editing, R.P.L., J.M., H.M., M.D.B., D.J.C., V.A.M., S.S., D.L., P.R., N.P., E.H., M.O.L., J.S.D.B., D.M.K., N.T.

Conflicts of interest are listed at the end of this article.

disease according to RECIST version 1.1 (4); a confirmed reduction of at least 50% in PSA level; or a conversion in the circulating tumor cell (CTC) count, with a reduction in the number of CTCs from at least five per 7.5 mL of blood at baseline to less than five per 7.5 mL of blood during treatment, with a confirmatory assessment at least 4 weeks later (22). Detailed information regarding the inclusion and exclusion criteria and the results of the TOPARP-A trial have been published and show a response rate of 33% (95% confidence interval [CI]: 20%, 48%) to olaparib in mCRPC (23).

Participation in the optional MR imaging substudy was offered to patients without contraindication to MR imaging at The Royal Marsden NHS Foundation Trust. Whole-body MR imaging was performed at baseline (within 28 days prior to starting treatment) and at cycle 4 day 1 (corresponding to 12 weeks after starting treatment) and every 12 weeks subsequently. The primary end point of the MR imaging substudy was to assess the association between changes in parameters derived from whole-body DWI (volume of bone metastases and median ADC) and response to olaparib. For MR imaging substudy purposes, patients were classified as responders if they met the definition of the primary end point of the TOPARP-A trial and if they had not experienced radiologic progression by 12 weeks.

#### Patient Population in the MR Imaging Substudy

Patients were included in this study if (a) signed informed consent was obtained for the MR imaging substudy in the setting of the TOPARP-A trial; (b) bone metastases were identified on images obtained with the combined imaging modalities of MR imaging, CT, and bone scintigraphy (in all cases); and (c) a minimum of two paired whole-body MR imaging studies were performed at baseline and after 12 weeks of treatment. Patients with whole-body MR images of suboptimal quality or incomplete studies were considered unevaluable for analysis and were excluded from the study.

#### Clinical Data Collection

Data were collated into an anonymized database and analyzed by the Institute of Cancer Research Clinical Trials and Statistical Unit, London, United Kingdom. PSA level and CTC counts were collected at baseline and every 12 weeks during treatment. CTC counts were also recorded at weeks 1, 2, 4, and 8. RECIST assessments were evaluated at baseline and every 12 weeks by using CT.

#### Whole-Body MR Imaging Parameters

Whole-body MR imaging was performed with a 1.5-T MR imaging unit (Avanto; Siemens Healthcare, Erlangen, Germany) by using surface and body coils in patients positioned supine. Axial images were acquired by using free-breathing single-shot twice-refocused echo-planar DWI from the upper cervical spine to the midthighs, sequentially across four imaging stations, each consisting of 50 sections. In addition to whole-body DWI, anatomic imaging was also performed by using breath-hold axial T1-weighted sequences. The imaging parameters are summarized in Table E1 (online).

#### Image Analysis

Images were processed and analyzed with open-access imaging assistant software (OsiriX version 5.6; PixmeoSARL, Bernex, Switzerland). Evaluation of T1-weighted and DWI images (ADC maps with  $b$  values of 50 and 900 sec/mm<sup>2</sup>) was performed to assess the presence of metastatic bone disease. Regions of interest (ROIs) were delineated and included areas of abnormal signal intensity on DWI images obtained with  $b$  values of 900 sec/mm<sup>2</sup>, which corresponded to high signal intensity on DWI images obtained with  $b$  values of 900 sec/mm<sup>2</sup> and low signal intensity on T1-weighted images, in keeping with metastatic bone disease. Different delineation techniques were undertaken for the abnormal signal intensity on DWI images obtained with  $b$  values of 900 sec/mm<sup>2</sup> that corresponded to bone metastases. First, ROI analyses were performed and included all areas of abnormal signal intensity on DWI images obtained with  $b$  values of 900 sec/mm<sup>2</sup> and T1-weighted MR images

that corresponded to bone metastases observed in the axial skeleton (spine and pelvis, not including the ribs) between C4 and the midthighs, labeled as total diffusion volume (tDV). Second, a more limited analysis was performed by using a RECIST approach with a maximum of five target representative bone metastases chosen by using the following criteria: maximum axial dimension larger than 1 cm, well-defined lesion border, and different skeletal areas represented. For this analysis, ROIs that included total volume of up to five target lesions and ROIs that included the central section of the same target lesions were chosen.

Additionally, one radiologist (R.P.L.) manually delineated the entire axial skeleton (spine and pelvis, not including the ribs) by including normal and abnormal bone marrow from C4 to the lesser trochanters. This delineation technique was included in view of its possible advantage for automated segmentation of the skeleton.

A semiautomated segmentation tool from OsiriX version 5.6 (PixmeoSARL) was used for delineating ROIs. All the delineation techniques for whole-body DWI images were performed by one radiologist (R.P.L.) with 3 years of experience in whole-body DWI; manual correction of the segmentation mask that corresponded to the ROIs was performed by the radiologist where necessary (Fig 1). The volume of metastases was calculated as the number of voxels for all ROIs, multiplied by the voxel volume in each case. The ADC value for every pixel was recorded, and histogram representations of the ADC values of bone metastases for each patient were generated by using Microsoft Excel 2010 (Microsoft, Redmond, Wash).

#### Statistical Analysis

Distribution of PSA level, CTC counts, median ADC values, tDV, volume, and diameter of the target lesions at baseline and percentage change after 12 weeks of treatment were presented by using descriptive statistics. Baseline distributions and median changes during treatment in ADC, tDV, volume, and diameter of the target lesions were compared between



Figure 1

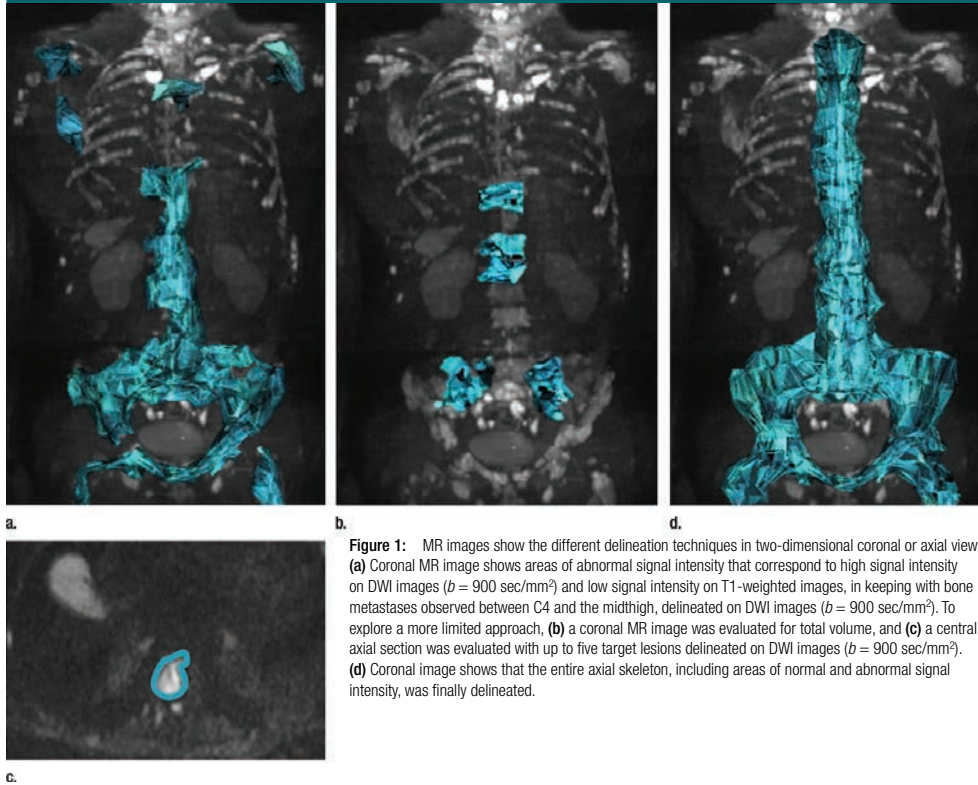


**Figure 1:** MR images show the different delineation techniques in two-dimensional coronal or axial views. **(a)** Coronal MR image shows areas of abnormal signal intensity that correspond to high signal intensity on DWI images ( $b = 900 \text{ sec/mm}^2$ ) and low signal intensity on T1-weighted images, in keeping with bone metastases observed between C4 and the midthigh, delineated on DWI images ( $b = 900 \text{ sec/mm}^2$ ). To explore a more limited approach, **(b)** a coronal MR image was evaluated for total volume, and **(c)** a central axial section was evaluated with up to five target lesions delineated on DWI images ( $b = 900 \text{ sec/mm}^2$ ). **(d)** Coronal image shows that the entire axial skeleton, including areas of normal and abnormal signal intensity, was finally delineated.

responders and nonresponders by using nonparametric Mann-Whitney tests, and their association with response to treatment was compared by using univariate and multivariate logistic regression models (adjusted for known prognostic factors of baseline PSA level, lactate dehydrogenase level, and alkaline phosphatase level). The correlation between *(a)* baseline tDV and changes in tDV after 12 weeks of treatment and *(b)* baseline and best percentage change in PSA level and CTC count, respectively, were assessed by using the Spearman correlation coefficient ( $r$ ), with  $r$  values of at least 0.4 and less than 0.6 indicating moderate correlation, at least 0.6

and less than 0.8 indicating strong correlation, and at least 0.8 indicating very strong correlation. A significance level of .05 and 95% confidence intervals (CIs) have been used. No adjustment for reporting of multiple analyses was performed; therefore, significant results must be interpreted with caution. The analyses are based on a data snapshot obtained on April 24, 2015, and were performed with Stata version 13 software (StataCorp, College Station, Tex).

#### Results

Thirty-two of the 42 patients (76.2%) enrolled in the TOPARP-A trial at The

Royal Marsden NHS Foundation Trust consented to the MR imaging substudy. Six patients did not undergo baseline whole-body MR imaging because of logistical or technical issues. All 26 patients with whole-body MR images at baseline had bone metastases. Of the 26 patients with baseline whole-body MR images, five did not undergo whole-body MR imaging at 12 weeks because of poor performance status. None of the cases were excluded for having suboptimal quality of the whole-body MR images or incomplete studies. Therefore, 21 patients had evaluable whole-body MR images at baseline and after 12 weeks of treatment (Fig 2); the

median age of all patients was 68.2 years (range, 40.8–79.3 years). The population characteristics at baseline are summarized in Table 1. The baseline CT images were also reviewed by using previously described terminology (24); 19 of the 21 patients had sclerotic bone metastases, whereas two patients had mixed osteoblastic and osteolytic disease with predominantly lytic metastases. The other sites of metastatic disease observed outside the bone were in lymph nodes (57.1%, 12 of 21 patients), liver (28.6%, six of 21 patients), and lung (23.8%, five of 21 patients). Seven patients had bone metastases only at baseline (33.3%, seven of 21). Six patients (28.6%, six of 21) were considered responders to olaparib per the primary end point definition and had not progressed prior to 12 weeks.

The median time between baseline whole-body MR imaging and the start of treatment was 6 days (1st quartile, 2.5 days; 3rd quartile, 11 days). The absolute value of the tDV, the sum of the five target lesion total volumes and of the central section diameters, and the median ADC at baseline assessed by using the different delineation techniques are summarized according to response status in Table 2. The percentage change of these parameters after 12 weeks of treatment is summarized according to response status in Table 3 and represented in box plots in Figure E1 (online).

**Analysis of Axial Skeleton DWI with a b Value of 900 sec/mm<sup>2</sup> and Abnormal Signal Intensity**

When delineating all the areas of abnormal DWI signal intensity, in keeping with bone metastases in the axial skeleton, the median tDV in this population was 0.45 L (range, 0.01–1.31 L), and median ADC was 782 × 10<sup>-6</sup> mm<sup>2</sup>/sec (range, [684–1121] × 10<sup>-6</sup> mm<sup>2</sup>/sec). These parameters, grouped according to responders and nonresponders, are summarized in Table 2; there were no statistically significant differences between baseline distribution of tDV and median ADC between the two groups (*P* = .243 and *P* = .312, respectively).

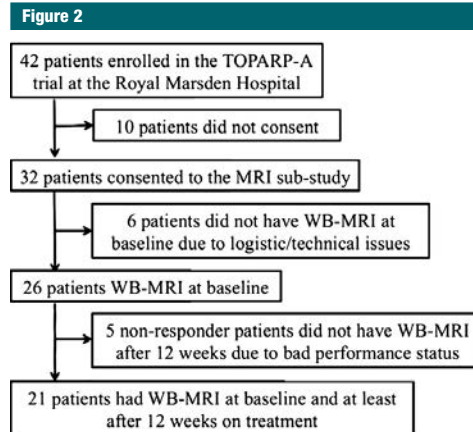


Figure 2: Consort diagram shows the study selection process. WB = whole-body.

Table 1

**Baseline Characteristics and Prior Treatments in All 21 Patients**

Parameter	Value
<b>Clinical characteristic</b>	
Hemoglobin level (g/dL)*	10.9 (10.2, 11.5) [9.2–14.2]
PSA level (ng/mL)*	411 (146, 806) [19–2949]
Alkaline phosphatase level (IU/L)*	147 (86, 363) [54–2652]
Lactate dehydrogenase level (IU/L)*	234 (176, 318) [109–862]
Albumin level (g/dL)*	3.5 (3.1, 3.7) [2.7–4.0]
CTC count (no. per 7.5 mL)*	46 (8, 102) [3–187]
<b>Prior treatment</b>	
Docetaxel	21 (100)
Cabazitaxel	11 (52.4)
Abiraterone acetate	19 (90.5)
Enzalutamide	4 (19.0)
Radium 223	1 (4.8)
Bisphosphonates	4 (19.0)
Palliative radiation therapy to bone	6 (28.6)
<b>Site of metastatic disease</b>	
Bone	21 (100)
Nodes	12 (57.1)
Liver	6 (28.6)
Lung	5 (23.8)
Bone only	7 (33.3)

Note.—Unless indicated otherwise, data are numbers of patients, with percentages in parentheses. To convert grams per deciliter to grams per liter, multiply by 10. To convert nanograms per milliliter to micrograms per liter, multiply by 1.0. To convert international units per liter to microkatal per liter, multiply by 0.0167.

\* Data are medians, with 1st and 3rd quartiles in parentheses and ranges in brackets.

Table 2

## Baseline Parameters of Bone Metastases Assessed in Responders and Nonresponders

Parameter	Responders		Nonresponders		P Value*
	No. of Patients	Median	No. of Patients	Median	
<b>Clinical characteristic</b>					
CTC count (no. per 7.5 mL)	6	63 (8, 102) [3–105]	15	46 (8, 104) [6–187]	.845
PSA level (ng/mL)	6	868 (34, 1847) [28–2949]	15	381 (146, 456) [19–1505]	.350
<b>Axial skeleton, abnormal DWI signal intensity</b>					
Volume (L)	6	0.83 (0.17, 1.01) [0.16–1.31]	15	0.44 (0.16, 0.79) [0.01–1.07]	.243
ADC ( $\times 10^{-6}$ mm <sup>2</sup> /sec)	6	847 (775, 921) [693–1121]	15	748 (726, 915) [684–1023]	.312
<b>Up to five target lesions</b>					
Volume (L)	6	0.05 (0.04, 0.06) [0.04–0.09]	15	0.05 (0.02, 0.12) [0.01–0.52]	.876
ADC ( $\times 10^{-6}$ mm <sup>2</sup> /sec)	6	859 (814, 900) [606–1712]	15	737 (695, 865) [624–1017]	.312
<b>Central section, five target lesions</b>					
Diameter (mm)	2	15.3 (14.3, 16.3) [14.3–16.3]	7	11.6 (7.5, 13.1) [2.8–20.2]	.143
Median ADC ( $\times 10^{-6}$ mm <sup>2</sup> /sec)	6	941 (867, 1002) [555–1263]	15	743 (673, 852) [575–1083]	.073
<b>Entire axial skeleton</b>					
ADC ( $\times 10^{-6}$ mm <sup>2</sup> /sec)	6	808 (650, 1093) [614–1182]	15	805 (751, 1002) [722–1039]	.938

Note.—Numbers in parentheses are 1st and 3rd quartiles. Numbers in brackets are ranges. To convert nanograms per milliliter to micrograms per liter, multiply by 1.0.

\* According to the Mann-Whitney test.

Table 3

## Percentage Change after 12 Weeks of Treatment in Responders and Nonresponders

Parameter	Responders		Nonresponders		P Value*
	No. of Patients	Median Change (%)	No. of Patients	Median Change (%)	
<b>Clinical characteristic</b>					
CTC count	6	−96.0 (−100, −82.9) [−100 to −60.5]	15	−2.9 (−37.5, 75.0) [−73.8 to 312.5]	NA†
PSA level	6	−68.6 (−80.1, −37.5) [−94.6 to −29.3]	15	89.9 (36.0, 239.0) [−14.4 to 525.6]	NA†
<b>Axial skeleton, abnormal DWI signal intensity</b>					
Volume	6	−41.1 (−52.9, −28.7) [−58.8 to −6.3]	15	20.7 (3.2, 53.0) [0.0–76.9]	.001
ADC	6	35.4 (3.8, 44.1) [1.3–59.5]	15	7.5 (3.7, 15.6) [−9.0 to 32.7]	.139
<b>Up to five target lesions</b>					
Volume	6	−25.5 (−57.0, −18.2) [−78.7 to 4.54]	15	14.6 (0.0, 47.5) [−20.2 to 76.9]	.002
ADC	6	26.3 (11.4, 47.4) [4.8–102.9]	15	7.4 (−2.3, 12.9) [−10.8 to 25.6]	.024
<b>Central section, five target lesions</b>					
Diameter	2	−59.2 (−88.3, −30.1) [−88.3 to −30.1]	7	3.8 (1.6, 41.4) [0.0–69.9]	.040
ADC	6	27.4 (14.0, 47.0) [12.8–52.3]	15	10.0 (3.2, 17.2) [−12.7 to 63.1]	.018
<b>Entire axial skeleton</b>					
ADC	6	7.4 (−0.8, 26.0) [−16.6 to 29.0]	15	5.6 (3.4, 12.5) [−21.6 to 16.7]	.876

Note.—Numbers in parentheses are 1st and 3rd quartiles. NA = not applicable. Numbers in brackets are ranges.

\* Changes in CTC count and PSA level were used to define response and nonresponse; therefore, formal comparisons have not been made.

† According to the Mann-Whitney test.

All six patients who responded to olaparib showed a decrease in tDV (median, −41.1%; range, −58.8% to −6.3%), but no decrease was observed in any of the 15 nonresponders (median, +20.7%; range, +0.0% to +76.9%); this difference between responders and nonresponders was significant ( $P = .001$ ) (Table 3, Fig E1 [online]). Patients who responded to olaparib showed a greater increase in median ADC after 12 weeks of treatment (median: +35.4%; range, +1.3% to +59.5%), compared with nonresponders (median, +7.5%; range,

−9.0% to +32.7%;  $P = .14$ ); increases in median ADC after 12 weeks of treatment were associated with increased odds of response (odds ratio, 1.08; 95% CI: 1.00, 1.15;  $P = .037$ ) (Table 4, Fig E2 [online]). An example of a responding patient is represented in Figure 3.

The two patients with mixed osteoblastic and osteolytic pattern with predominantly lytic bone metastases were nonresponders who had +55.5% and +24.6% increase in tDV and +3.40% and +15.6% increase in median ADC, respectively, after 12 weeks of treatment.

The correlation between PSA levels, CTC counts, and DWI parameters was also explored; baseline PSA levels and CTC counts showed strong and moderate positive association with baseline tDV ( $r = 0.64$  [95% CI: 0.29, 0.84] and  $r = 0.59$  [95% CI: 0.22–0.82], respectively), and there was a strong positive association between changes in tDV and best posttreatment percentage change in PSA level and CTC count ( $r = 0.63$  [95% CI: 0.27, 0.83] and  $r = 0.77$  [95% CI: 0.51, 0.90], respectively), indicating that changes in tDV correlate with response to therapy.

Of the six responding patients, four underwent further evaluable whole-body MR imaging at the time of radiologic progression and/or with PSA level increase. In all four patients, we observed a decrease in tDV while responding to olaparib, followed by a later increase in tDV at the time of radiologic progression and/or increase in PSA level. Three of these four responding patients also had an increase in median ADC while responding to treatment, followed by a decrease in median ADC at the time of radiologic progression and/or increase in PSA level. The fourth patient experienced minimal median ADC change at the PSA level nadir and at disease progression (Figs E3, E4 [online]).

#### Analysis of Five Target Lesions (Total Volume and Central Section)

With the aim of evaluating more limited radiologic analyses, to decrease workload, we correlated changes in up

**Table 4**

#### Logistic Regression Associations between Changes in Values after 12 Weeks with Binary Response to Treatment

Parameter	No. of Patients	Univariate Analysis		Multivariate Analysis*	
		Odds Ratio	P Value	Odds Ratio	P Value
<b>Axial skeleton DWI signal intensity abnormality</b>					
Volume	21	Not calculable <sup>†</sup>	...	Not calculable <sup>†</sup>	...
Median ADC	21	1.08 (1.00, 1.15)	.037	1.16 (1.01, 1.33)	.04
<b>Up to five target lesions</b>					
Volume	21	0.89 (0.80, 0.99)	.037	0.53 (0.09, 3.15)	.48
Median ADC	21	1.10 (1.00, 1.22)	.056	1.13 (0.95, 1.33)	.17
<b>Central section five target lesions</b>					
Median ADC	21	1.05 (0.99, 1.11)	.082	1.07 (0.99, 1.15)	.07
<b>Entire axial skeleton</b>					
Median ADC	21	1.03 (0.94, 1.12)	.518	1.03 (0.93, 1.15)	.56

Note.—Numbers in parentheses are 95% CIs.

\* Adjusted for baseline PSA level, lactate dehydrogenase level, and alkaline phosphatase level.

<sup>†</sup> Unable to fit model, as change in volume < 0% predicts data perfectly.

to five target lesions per patient with treatment response. We evaluated five target lesions in 19 of the 21 patients (90.5%); the remaining two patients had only one and three evaluable bone lesions, respectively. The median sum of total volumes that corresponded to the target lesions in the population at baseline was 0.05 L (range, 0.01–0.52 L), and the median ADC when delineating total volume of the target lesions was  $814 \times 10^{-6} \text{ mm}^2/\text{sec}$  (range, [606–1712]  $\times 10^{-6} \text{ mm}^2/\text{sec}$ ). In patients with nonwidespread bone disease ( $n = 9$ ), we also assessed the diameter of the target lesions in the central section. When assessing only the central section of the same target lesions, the median of the sum of diameters at baseline was 12.6 mm (range, 2.8–20.2 mm), and the median ADC was  $835 \times 10^{-6} \text{ mm}^2/\text{sec}$  (range, [554.5–1263]  $\times 10^{-6} \text{ mm}^2/\text{sec}$ ). These parameters, grouped according to responders and nonresponders, are summarized in Table 2; there were no statistically significant differences between the baseline distribution of volume, diameter, and median ADC (central section and volume) of the target lesions between the two groups ( $P = .876$ ,  $P = .143$ ,  $P = .312$ , and  $P = .073$ , respectively).

Then, we assessed the same target lesions for each patient on their follow-up whole-body MR images after 12 weeks of treatment; the percentage change of these parameters after 12 weeks of treatment is summarized according to response status in Table 3 and Figure E1 (online). Changes in entire lesion volume of the target bone metastases were also inversely associated with response (odds ratio, 0.89; 95% CI: 0.80, 0.99;  $P = .037$ ) (Table 4). The median ADC change at 12 weeks, when analyzing the target bone metastases (total volume and central section), was also associated with response, although these associations did not reach statistical significance ( $P = .056$  and  $P = .082$ , respectively) (Table 4). Results from the multivariate logistic regression analyses showed similar trends (Table 4).

#### Analysis of the Axial Skeleton (Including Normal and Abnormal Bone Marrow)

The baseline median ADC in our population when delineating the entire axial skeleton, including both normal and abnormal bone marrow, was  $805 \times 10^{-6} \text{ mm}^2/\text{sec}$  (range, [614–1182]  $\times 10^{-6} \text{ mm}^2/\text{sec}$ ). Median ADC values at baseline, grouped according to

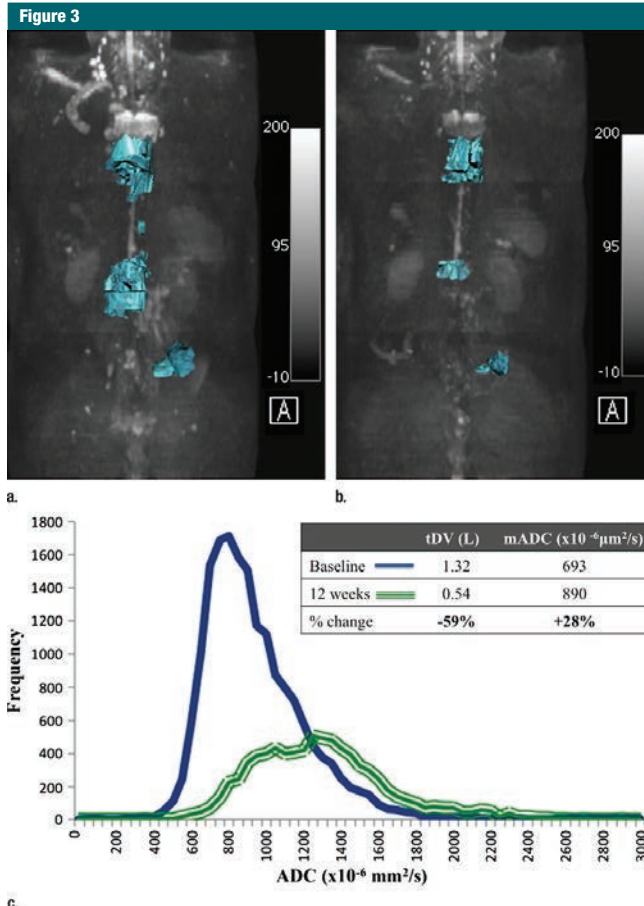


**Figure 3:** (a) Coronal baseline MR image and (b) coronal MR image obtained after 12 weeks of treatment in a 70-year-old man with mCRPC responding to olaparib show a reduction in the abnormal DWI signal intensity ( $b = 900 \text{ sec/mm}^2$ ) extent on maximum intensity projection images. (c) Histogram depicts the ADC values of the tDV at baseline and after 12 weeks of treatment, showing an increase in the median ADC.

responders and nonresponders, are summarized in Table 2; there were no statistically significant differences between the baseline distributions of median ADC between the two groups ( $P = .94$ ). The percentage change in median ADC after 12 weeks of treatment is summarized according to

response status in Table 3 and Figure E1 (online). When comparing the median ADC of the entire axial skeleton (normal and abnormal bone marrow) before and after treatment with olaparib, changes in median ADC were not associated with response to treatment ( $P = .518$ ) (Table 4).

## Discussion

We hypothesized that changes in volume of bone marrow metastases assessed with DWI and changes in median ADC are indicators of response of bone metastases to treatment in patients with mCRPC. In our study, we explored different delineation techniques for assessing bone metastases quantitatively and qualitatively with whole-body DWI. One technique included all the areas of DWI signal abnormality, in keeping with all bone metastases in the axial skeleton (tDV); the other focused on two simpler techniques for assessing five target lesions, based on the widely used RECIST version 1.1 (4), to determine whether a simplified approach may be viable in clinical practice. Finally, we explored whether changes in median ADC that delineate the entire spine and pelvis (including areas of normal and abnormal bone marrow), which may facilitate automated delineation, were associated with response.

We have shown that when delineating all the areas of DWI signal intensity abnormality, in keeping with bone metastases in the axial skeleton (from C4 to midthigh), the changes detected in tDV and median ADC after 12 weeks of treatment allow the identification of responders in mCRPC with bone metastases. Decreases in tDV correlated with decreases in PSA level and CTC count and with overall response, as defined as a composite end point in the TOPARP-A clinical trial (23). Consistent with the fact that tumor cell death results in increased water diffusivity, manifested as higher ADC values, patients who responded to olaparib also showed a greater increase in median ADC when compared with nonresponders. In our population, the results of simpler ways of assessing bone metastases on whole-body DWI images in five selected target lesions (total volume or central section) support further evaluation of this faster and more practical approach in future studies, as decreases in volume and diameter of the five target lesions after 12 weeks of treatment were associated with response. There was also a trend of significance when associating median



ADC increases of the target lesions at 12 weeks and response. Therefore, overall, these data indicate that whole-body DWI may have a role in bone metastases response assessment in mCRPC, without the need for ionizing radiation or intravenous contrast material, potentially allowing the detection of differential responses in visceral or nodal metastases and bone metastases. Clinical qualification of whole-body DWI as a response biomarker in bone metastases would improve assessment of response to treatment in mCRPC, allowing for optimization of patient care, treatment decision making, and drug development in this common disease. Conversely, when delineating the spine and pelvis, including all areas of normal and abnormal bone marrow, increases in median ADC after 12 weeks of treatment were not associated with response, probably because of the fact that changes in median ADC in bone metastases are diluted by the absence of changes in median ADC in normal bone marrow.

We acknowledge the potential limitations of our study. First, because of the small size of this pilot study, only limited exploration of the effect of adjustment for other clinical factors on the association of changes in tDV and median ADC is possible. Analyzing larger populations in multicenter studies is now needed for future validation of these results and to allow multivariate analyses. Second, all our patients were treated with one drug, the poly-(adenosine diphosphate-ribose) polymerase inhibitor olaparib; however, in previous studies, investigators identified similar changes in DWI in bone metastases responding to hormonal therapy and cytotoxic agents (18–21). Prospective studies conducted to replicate our results with established treatments for mCRPC are now needed. Third, it should be noted that ROI delineation depends on the quality of the acquired DWI data, the semiautomatic segmentation tool, and the radiologist's expertise. In prior studies, investigators reported high intrareader reproducibility of DWI analysis by using similar bone metastases delineation methods

(17,25), although this needs to be validated in larger, properly powered studies. Finally, we acknowledge that most of our population had sclerotic bone metastases; only two patients had predominantly lytic bone metastases, and therefore, it was not feasible to perform comparisons between the sclerotic and lytic nature of the bone metastases. Despite these limitations, our study represents the largest prospective series to date in a trial of a novel therapeutic assessment of response to drug treatment in bone metastases in patients with mCRPC by using whole-body DWI. The data presented here highlight the potential of DWI for bone metastases response assessment and warrants further evaluation of whole-body DWI in this disease.

In conclusion, we have shown that assessment of bone metastases with whole-body DWI during anticancer treatment is feasible, with changes in bone metastases volume and median ADC being indicators of response to treatment in mCRPC in our pilot study. Moreover, the more efficient study of five target lesions has substantial practical merit for disease evaluation, which can be more easily adopted into clinical practice. These results support further evaluation of DWI as a response biomarker in prospective mCRPC patient cohorts, ideally embedded into clinical trials (26).

**Acknowledgment:** Raquel Perez-Lopez, MD, MSc, conducted this work in the Medicine Doctorate framework of the Universidad Autonoma de Barcelona.

**Disclosures of Conflicts of Interest:** R.P.L. disclosed no relevant relationships. J.M. disclosed no relevant relationships. H.M. disclosed no relevant relationships. M.D.B. disclosed no relevant relationships. D.J.C. disclosed no relevant relationships. M.R. disclosed no relevant relationships. V.A.M. disclosed no relevant relationships. A.M. disclosed no relevant relationships. S.S. disclosed no relevant relationships. D.L. Activities related to the present article: disclosed no relevant relationships. Activities not related to the present article: author received payment from Janssen, Sanofi, and Bayer. Other relationships: disclosed no relevant relationships. P.R. disclosed no relevant relationships. Z.Z. disclosed no relevant relationships. D.B. disclosed no relevant relationships. N.P. disclosed no relevant relationships. E.H. Activities related to the present article: institution received a grant from AstraZeneca, which also supplied the olaparib. Activ-

ities not related to the present article: institution received grants and nonfinancial support from AstraZeneca, Bayer, Aventis Pharma (Sanofi), and Janssen Diagnostics; institution received nonfinancial support from Astellas. Other relationships: disclosed no relevant relationships. M.O.L. Activities related to the present article: disclosed no relevant relationships. Activities not related to the present article: disclosed no relevant relationships. Other relationships: institution received money for a patent pending. J.S.D.B. Activities related to the present article: author received payment and nonfinancial support from AstraZeneca for honoraria, service on an advisory board, and travel. Activities not related to the present article: disclosed no relevant relationships. Other relationships: disclosed no relevant relationships. D.M.K. disclosed no relevant relationships. N.T. disclosed no relevant relationships.

#### References

1. Ferlay J, Soerjomataram I, Dikshit R, et al. Cancer incidence and mortality worldwide: sources, methods and major patterns in GLOBOCAN 2012. *Int J Cancer* 2015; 136(5):E359–E386.
2. Gandaglia G, Abdollah F, Schiffmann J, et al. Distribution of metastatic sites in patients with prostate cancer: a population-based analysis. *Prostate* 2014;74(2):210–216.
3. Jambor I, Kuusma A, Ramadan S, et al. Prospective evaluation of planar bone scintigraphy, SPECT, SPECT/CT, 18F-NaF PET/CT and whole body 1.5T MRI, including DWI, for the detection of bone metastases in high risk breast and prostate cancer patients: SKELETA clinical trial. *Acta Oncol* 2016;55(1):59–67.
4. Eisenhauer EA, Therasse P, Bogaerts J, et al. New response evaluation criteria in solid tumours: revised RECIST guideline (version 1.1). *Eur J Cancer* 2009;45(2):228–247.
5. Scher HI, Halabi S, Tannock I, et al. Design and end points of clinical trials for patients with progressive prostate cancer and castrate levels of testosterone: recommendations of the Prostate Cancer Clinical Trials Working Group. *J Clin Oncol* 2008;26(7):1148–1159.
6. Berthold DR, Pond GR, Roessner M, et al. Treatment of hormone-refractory prostate cancer with docetaxel or mitoxantrone: relationships between prostate-specific antigen, pain, and quality of life response and survival in the TAX-327 study. *Clin Cancer Res* 2008;14(9):2763–2767.
7. Halabi S, Armstrong AJ, Sartor O, et al. Prostate-specific antigen changes as surrogate for overall survival in men with metastatic castration-resistant prostate cancer treated with second-line chemotherapy. *J Clin Oncol* 2013;31(31):3944–3950.

8. Guo AC, Cummings TJ, Dash RC, Provenza JM. Lymphomas and high-grade astrocytomas: comparison of water diffusibility and histologic characteristics. *Radiology* 2002; 224(1):177-183.
9. Hayashida Y, Hirai T, Morishita S, et al. Diffusion-weighted imaging of metastatic brain tumors: comparison with histologic type and tumor cellularity. *AJNR Am J Neuroradiol* 2006;27(7):1419-1425.
10. Zelhof B, Pickles M, Liney G, et al. Correlation of diffusion-weighted magnetic resonance data with cellularity in prostate cancer. *BJU Int* 2009;103(7):883-888.
11. Liu Y, Ye Z, Sun H, Bai R. Clinical application of diffusion-weighted magnetic resonance imaging in uterine cervical cancer. *Int J Gynecol Cancer* 2015;25(6):1073-1078.
12. Matsubayashi RN, Fujii T, Yasumori K, Muranaka T, Momosaki S. Apparent diffusion coefficient in invasive ductal breast carcinoma: correlation with detailed histologic features and the enhancement ratio on dynamic contrast-enhanced MR images. *J Oncol* 2010;2010:2010.
13. Nonomura Y, Yasumoto M, Yoshimura R, et al. Relationship between bone marrow cellularity and apparent diffusion coefficient. *J Magn Reson Imaging* 2001;13(5):757-760.
14. Thoeny HC, De Keyzer F, Chen F, et al. Diffusion-weighted MR imaging in monitoring the effect of a vascular targeting agent on rhabdomyosarcoma in rats. *Radiology* 2005; 234(3):756-764.
15. Kyriazi S, Collins DJ, Messiou C, et al. Metastatic ovarian and primary peritoneal cancer: assessing chemotherapy response with diffusion-weighted MR imaging—value of histogram analysis of apparent diffusion coefficients. *Radiology* 2011;261(1):182-192.
16. Giles SL, Messiou C, Collins DJ, et al. Whole-body diffusion-weighted MR imaging for assessment of treatment response in myeloma. *Radiology* 2014;271(3):785-794.
17. Perez-Lopez R, Lorente D, Blackledge MD, et al. Volume of bone metastasis assessed with whole-body diffusion-weighted imaging is associated with overall survival in metastatic castration-resistant prostate cancer. *Radiology* 2016;280(1):151-160.
18. Blackledge MD, Collins DJ, Tunariu N, et al. Assessment of treatment response by total tumor volume and global apparent diffusion coefficient using diffusion-weighted MRI in patients with metastatic bone disease: a feasibility study. *PLoS One* 2014;9(4):e91779.
19. Reischauer C, Froehlich JM, Koh DM, et al. Bone metastases from prostate cancer: assessing treatment response by using diffusion-weighted imaging and functional diffusion maps—initial observations. *Radiology* 2010;257(2):523-531.
20. Lee KC, Bradley DA, Hussain M, et al. A feasibility study evaluating the functional diffusion map as a predictive imaging biomarker for detection of treatment response in a patient with metastatic prostate cancer to the bone. *Neoplasia* 2007;9(12):1003-1011.
21. Messiou C, Collins DJ, Giles S, de Bono JS, Bianchini D, de Souza NM. Assessing response in bone metastases in prostate cancer with diffusion weighted MRI. *Eur Radiol* 2011;21(10):2169-2177.
22. Olmos D, Arkenau HT, Ang JE, et al. Circulating tumour cell (CTC) counts as intermediate end points in castration-resistant prostate cancer (CRPC): a single-centre experience. *Ann Oncol* 2009;20(1):27-33.
23. Mateo J, Carreira S, Sandhu S, et al. DNA-repair defects and olaparib in metastatic prostate cancer. *N Engl J Med* 2015;373(18):1697-1708.
24. Vargas HA, Wassberg C, Fox JJ, et al. Bone metastases in castration-resistant prostate cancer: associations between morphologic CT patterns, glycolytic activity, and androgen receptor expression on PET and overall survival. *Radiology* 2014;271(1):220-229.
25. Blackledge MD, Tunariu N, Orton MR, et al. Inter- and intra-observer repeatability of quantitative whole-body, diffusion-weighted imaging (WBDDWI) in metastatic bone disease. *PLoS One* 2016;11(4):e0153840.
26. Yap TA, Sandhu SK, Workman P, de Bono JS. Envisioning the future of early anticancer drug development. *Nat Rev Cancer* 2010;10(7):514-523.

## Supplemental material

**Supplemental Table E1.** Whole-Body MR Imaging Parameters

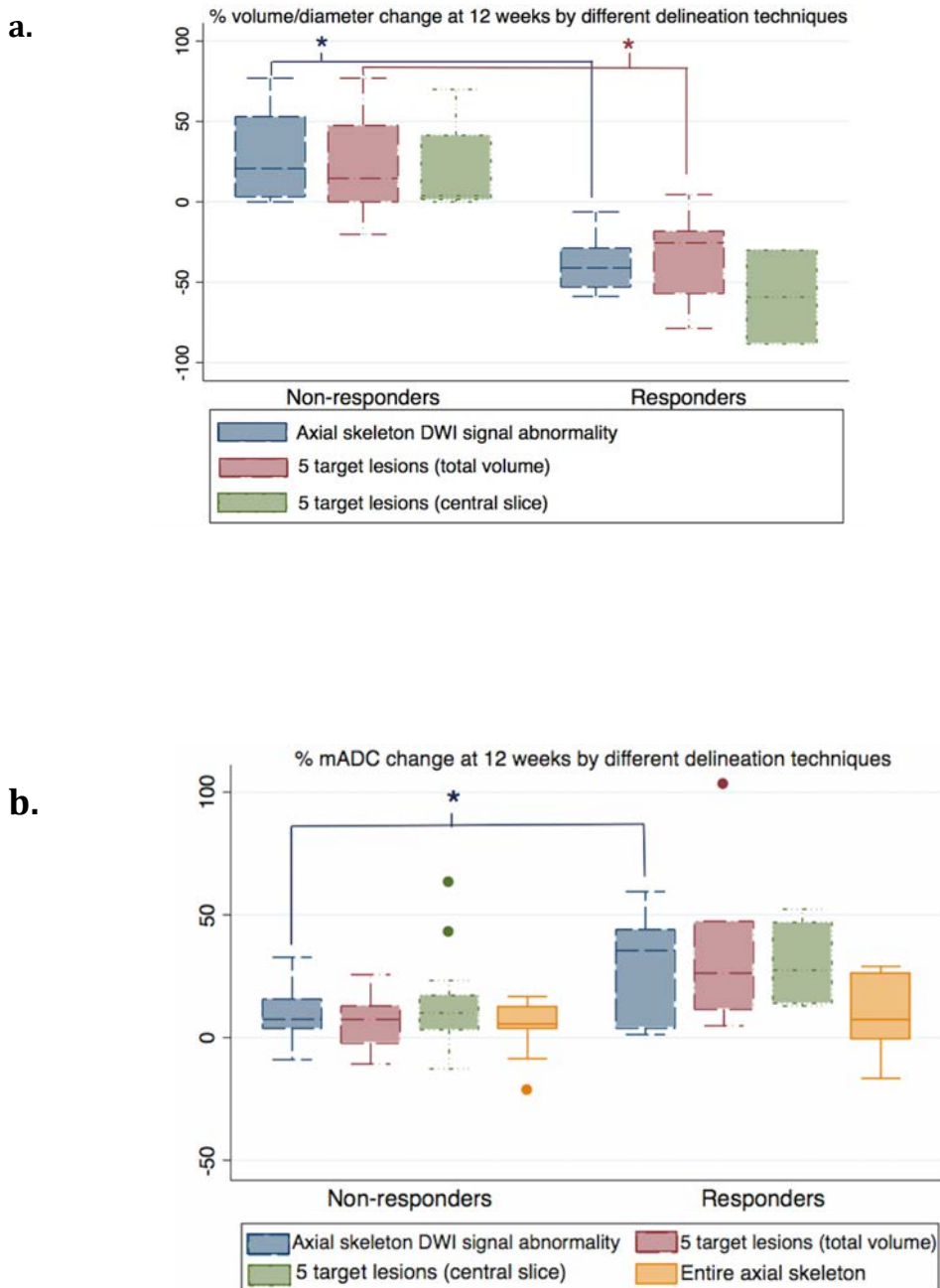
<b>PARAMETER</b>	<b>T1 weighted imaging</b>	<b>DWI</b>
<b>MRI platform</b>	1.5-T scanner (Avanto, Siemens Healthcare)	
<b>Type of pulse sequence</b>	Spoiled gradient echo (FLASH)	Single-shot twice-refocused echo-planar imaging
<b>Respiration</b>	Breath-hold	Free-breathing
<b>Type of acquisition</b>	2D	2D
<b>Field of view (mm)</b>	380-420	380-420
<b>Repetition time (ms)</b>	380	14000
<b>Echo time (ms)</b>	5	68
<b>Inversion time (ms)</b>	NA	180
<b>Flip angle</b>	70	90
<b>Fat suppression</b>	NA	STIR
<b>Receiver bandwidth (Hz/pixel)</b>	331	1800
<b>Number of signal average</b>	1	4
<b>Section thickness (mm)</b>	5	5



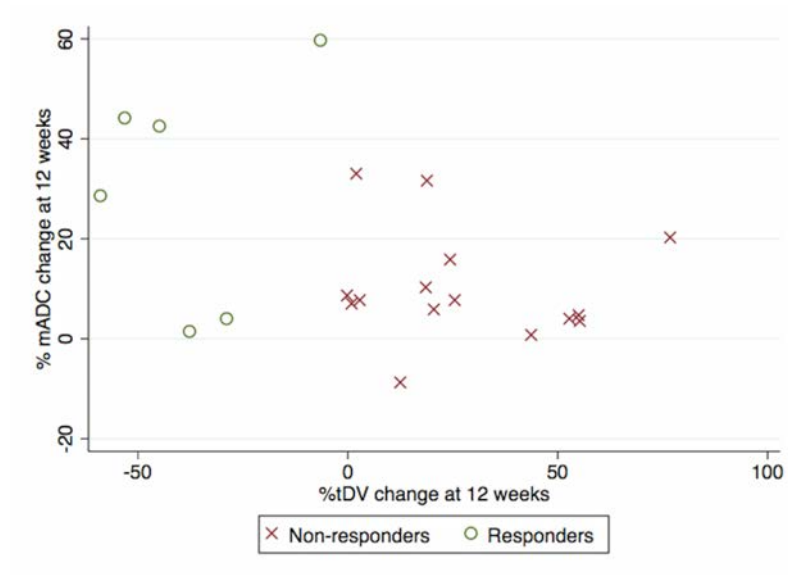
<b>b factors (s/mm<sup>2</sup>)</b>	NA	50 and 900
<b>Number stations</b>	4 (50 slices each)	4 (50 slices each)

Note: A 1.5-T unit (Avanto, Siemens Healthcare) was used for the imaging platform. DWI= Diffusion Weighted Imaging, FLASH = fast low-angle shot, NA = not applicable, STIR = short inversion time inversion recovery, 2D = two-dimensional.

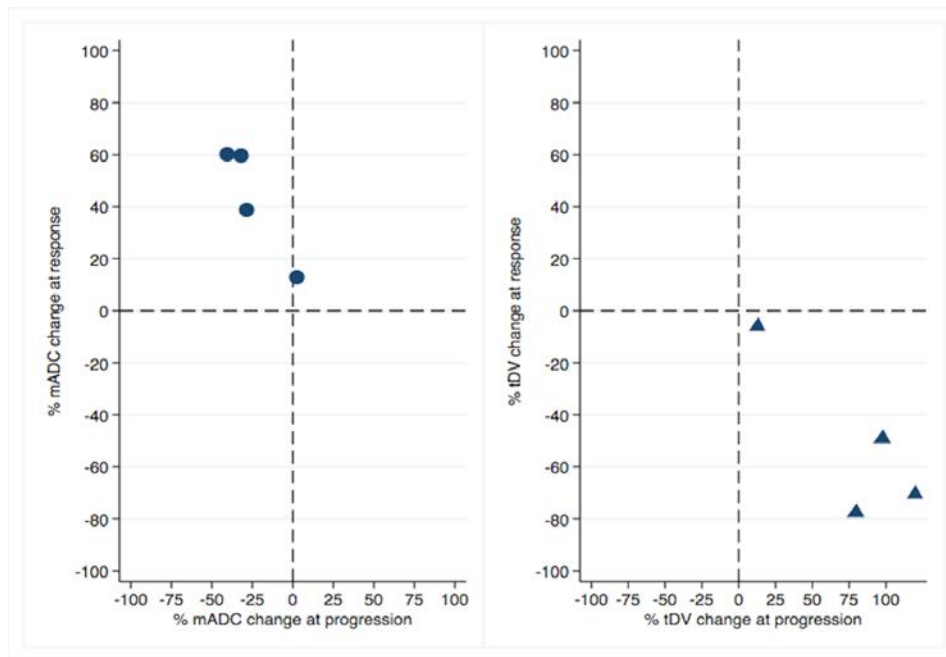
**Supplemental Figure E1.** Box plots of (a) percentage volume and diameter change of bone metastases, delineated on axial DWI images obtained with b values of 900 sec/mm<sup>2</sup>, and (b) median ADC (mADC) at 12 weeks, assessed with different delineation techniques. \* = logistic regression (P < .05).



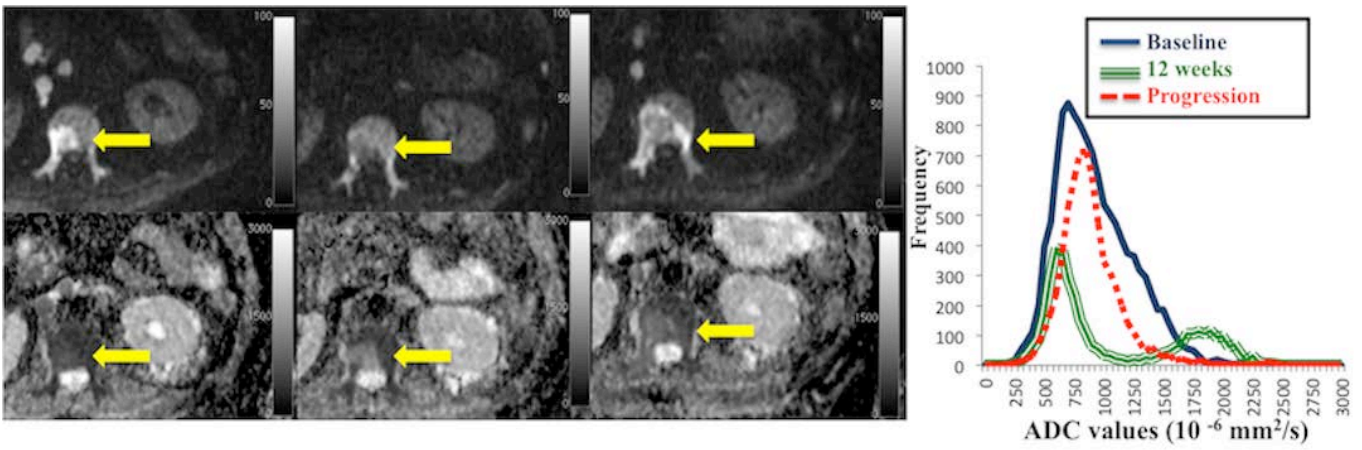
**Supplemental Figure E2.** Scatterplot of tDV and median ADC (mADC) change when delineating axial skeleton abnormal DWI signal intensity in responders (circles) and non-responders (crosses).



**Supplemental Figure E4.** Images in a 70-year-old man with mCRPC (arrows) treated with olaparib. Initially, the 12-week axial MR images showed a reduction in the extent of DWI ( $b = 900 \text{ sec/mm}^2$ ) signal intensity abnormality in the lumbar vertebrae bone metastases and an increase in median ADC values when compared with baseline; subsequently, follow-up MR images showed an increase in the extent of signal intensity abnormality at DWI ( $b = 900 \text{ sec/mm}^2$ ) and a decrease in median ADC values in the same bone metastases, in keeping with disease progression. The histogram depicts the ADC values of the tDV at baseline after 12 weeks of treatment and at progression.



**Supplemental Figure E3:** Scatterplots of percentage change of tDV (triangles) and median ADC (mADC) (circles) at response and disease progression in the four responding patients with evaluable whole-body MR images.



# Discussion



## Discussion

---

Precision medicine aims to improve patient outcomes and optimise the efficacy of medical care by using analytically validated and clinically qualified biomarkers to individualise treatment decisions. My research group, led by my supervisor Professor Johann de Bono, has the primary objective of advancing towards more precise medical care for patients with advanced prostate cancer. During my PhD, I worked on developing imaging cancer biomarkers towards more precise patient care; in particular my research project investigated how whole-body MP MRI including the DWI of bone metastases can aid treatment selection and switch decisions for patients with advanced prostate cancer and bone metastases. Bone involvement in patients with advanced prostate cancer is extremely common, resulting in higher morbidity and mortality in mCRPC patients. Moreover, in many cases, bone represents the only site of metastatic disease, making the assessment of response to anticancer treatment particularly challenging in these patients. It is imperative to develop new imaging prognostic and response biomarkers in mCRPC patients and pursue their analytical and clinical quantification, with the aim of providing new tools to radiologists and clinicians to guide therapeutic decisions.

The studies presented in this thesis were designed to evaluate MP MRI as a prognostic and response biomarker in patients with mCRPC and bone metastases and assess the correlation of MP MRI features with histological and molecular characteristics in bone metastases and non-metastatic bone in patients with CRPC. The data obtained in these studies will be critical for the clinical qualification of this functional imaging assay and future implementation of this test in clinical practice.

First, the presence of visceral and bone metastases is an indicator of poor prognosis in patients with prostate cancer. Moreover, the burden of bone metastases informs on survival in prostate cancer patients. Thus, those patients with a low number of bone metastases (three or less), a condition known as oligometastatic, have a better prognosis and can be considered for focal treatment with stereotactic body radiotherapy, avoiding or delaying systemic treatment (54-56). However, this



condition is defined in standard clinical practice based on the standard of care (CT and BS), which has poor accuracy for bone metastases detection. In order to evaluate the burden of metastatic bone disease it is crucial to apply a highly reliable imaging technique such as whole-body MRI with DWI. We have shown that the volume of bone metastases assessed with whole-body DWI is an indicator of survival in patients with mCRPC. Notably, the volume of bone metastases, quantified by whole-body DWI, correlates with prognostic biomarkers routinely implemented into standard practice such as Hb, PSA and the bone turnover marker alkaline phosphatase. Interestingly, we also detected a correlation with CTC count, an established prognostic biomarker in mCRPC. These findings now need to be corroborated in larger populations. It is also necessary to evaluate and validate prognostic nomograms in mCRPC including the burden of bone metastases by DWI in order to identify those patients with poor outcomes, which will impact treatment decision-making.

Second, CT and BS not only suboptimally assess the true extent of bone metastases but also fail to show reliable changes in response to treatment. We aimed to evaluate if changes in the volume of bone metastases assessed with whole-body DWI or changes in the ADC values of bone metastases were indicators of response in patients with mCRPC and bone metastases. This study was part of an investigator-initiated phase II clinical trial of the PARP inhibitor olaparib in patients with metastatic prostate cancer. Embedding these evaluations into clinical trials is fundamental for obtaining robust data in a prospective manner. The results of this study showed that when delineating all the areas of DWI signal abnormality in keeping with bone metastases in the axial skeleton (from C4 to mid-thigh), the changes detected in the volume of bone metastases and mADC after 12-weeks of treatment allowed the identification of responders and non-responders to the PARP inhibitor olaparib. The utility of whole-body DWI as a response biomarker was further supported by the fact that decreases in the volume of bone metastases strongly correlated with changes in PSA levels and CTC count falls during treatment.

I also explored in the same population alternative, simpler and less time-demanding approaches to evaluate bone metastases on whole-body DWI such as limiting the assessment to five selected target bone lesions (either based on their total volume or the diameter of the central slice). The results were encouraging and

support the further evaluation of this faster and more practical approach in future studies, as decreases in the volume and diameter of the five target lesions after 12 weeks of treatment were found to be associated with response to therapy. There was also a trend of significance when associating mADC increases in the target lesions at 12 weeks with the response. Conversely, when delineating spine and pelvis, including all the areas of normal and abnormal bone marrow, increases in mADC after 12 weeks of treatment were not associated with the response; probably due to the fact that changes in mADC in bone metastases are diluted by the absence of changes in mADC in normal bone marrow. Based on these data, a second clinical trial of the PARP inhibitor olaparib in patients with mCRPC and DNA repair genomic defects implemented whole-body DWI as part of the trial procedures. This trial is currently being conducted in several centres across the United Kingdom. In addition, the whole-body DWI of bone metastases has also been included in an investigator-initiated trial of the radionuclide Radium-223.

Third, in order to fully understand the MP MRI bone metastases features, I pursued a correlative project between the pathology, molecular features and functional imaging characteristics of bone metastases. The aim was to correlate the MP MRI (ADC, nDWI signal intensity and FF) of bone metastases after different lines of treatment and normal bone marrow in CRPC patients with histological and molecular characteristics from bone biopsies. This is crucial to understand the features of MP MRI and to interpret changes in response to treatment to, eventually, clinically qualify this imaging technique as a biomarker of bone metastases in CRPC. These results showed that DWI features including nDWI signal intensity, ADC value and FF are significantly different in normal bone marrow and bone metastases in CRPC. Interestingly, we showed that the ADC values and nDWI signal intensity in the bone correlates with bone metastases cellularity. *Ahmed et al.*, recently showed a high sensitivity of the MP MRI of the prostate gland to detect significant cancers; this maybe extremely helpful in clinical practice guiding in which cases and where to perform prostate biopsies (18). Similarly, the results of our study indicated that we could use DWI to identify those skeletal metastases from which we anticipate to obtain better samples, with higher tumour content, to perform molecular and

genomic tumour characterisation. This is crucial in order to increase the efficiency of biopsies and molecular studies for patient stratification as well as to reduce the discomfort for patients by avoiding biopsies likely to be unsuccessful.

The median ADC values of the bone metastases when delineating the whole axial skeleton bone metastases were similar among the study populations. In the first study population (n=43), the median ADC value in the total bone metastases was  $813 \times 10^{-6} \text{ mm}^2/\text{s}$ ; in the second study population (n=42), the median ADC value of the total bone metastases was  $782 \times 10^{-6} \text{ mm}^2/\text{s}$ . These results are similar to those presented in previous studies of prostate and breast cancer patients (25). However, in the study of MP MRI and bone biopsies correlation, the median ADC value in the area of the bone metastases biopsies (n=43) was  $993 \times 10^{-6} \text{ mm}^2/\text{s}$ . The higher ADC values in the bone metastases in this population may be explained by the fact that these patients had been highly pre-treated; 19/43 (44.2%) patients with previous radiotherapy to the pelvis were included. These differences have to be considered when planning studies assessing single specific lesions versus whole-skeleton assessments, where the median ADC value reflects a mixture of lesions that may be subject to biological intra-patient heterogeneity.

The nDWI b900 signal intensity and ADC values in normal bone marrow in our population were similar to those previously described by *Padhani et al* (42); the ADC in the non-metastatic bone (n=10) was  $601.8 \times 10^{-6} \text{ mm}^2/\text{s}$  (IQR  $545\text{-}667 \times 10^{-6} \text{ mm}^2/\text{s}$ ) and nDWI b900 signal intensity was 1.6 (IQR 1.4-2.7). These are closer to the described values in yellow bone marrow than red bone marrow, in line with the high FF observed in our study. Low signal intensity and the ADC values of yellow bone marrow are likely to be related to an abundance of large fat cells and reduced water proton density. This may account for the advanced age of our population, and critically the long-term exposure to hormonal ablation of prostate cancer patients, which will drive osteoporosis and a higher percentage of fat bone marrow in our population compared with studies in other tumour types. Therefore, these data suggest that prostate cancer-specific studies are needed for the clinical qualification of this assay in this disease, as data from myeloma or breast cancer patients may not be completely transposable to prostate cancer bone metastases.

I acknowledge that these studies have potential limitations that will need to be addressed in future studies before the routine implementation of this assay into clinical practice. First, when evaluating the prognostic and response value of whole-body DWI due to the small population size of these pilot studies, only limited exploration of the effect of adjustment for other clinical factors on the association of the burden of bone metastases and of changes in the volume of bone metastases and the median ADC was possible. Analysing larger populations in multicentre studies is now needed to validate these results and to allow for multivariate analyses. Second, it should be noted that ROI delineation depends on the quality of the acquired DWI data, the semi-automated segmentation tool and the radiologist's expertise. In prior studies, investigators have reported high intrareader reproducibility of DWI analysis by using similar bone metastases delineation methods, although this needs to be validated in larger, properly powered studies. Obviously, the future implementation of this assay into large populations outside academic institutions will need tools to facilitate the homogenisation of assay performance and data interpretation among institutions and radiologists. Third, in the evaluation of whole-body DWI as a response biomarker, all our patients were treated with one drug, the PARP inhibitor olaparib, in the context of one clinical trial. Prospective studies conducted to replicate our results with established treatments for mCRPC are now needed, and some of them have been initiated already by our group. Finally, we acknowledge that most of our population had sclerotic bone metastases; therefore, it was not feasible to perform comparisons between the sclerotic and lytic nature of the bone metastases.

Despite these limitations, the studies presented in this thesis represent the largest series assessing mCRPC bone metastasis with DWI, and the first including a prospective clinical trial assessing the performance of this assay as a response biomarker. Moreover, the study presented in this thesis is the first describing the MP MRI features of normal bone marrow and bone metastases in CRPC and correlating these with histological findings. The data presented here highlight the potential of DWI for bone metastases prognosis and response assessment and herein support the further evaluation of whole-body DWI in this disease and eventually its validation as a non-invasive imaging biomarker in patients with mCRPC and bone metastases, which can aid towards delivering more precise care for patients with advanced prostate cancer.

## **Further work needed for the clinical qualification of whole-body DWI as a prognostic and response biomarker of prostate cancer bone metastases**

- To validate the ADC values and DWI signal intensity threshold of non-infiltrated bone marrow and metastatic bone marrow in patients with prostate cancer.
- To implement studies of whole-body DWI to assess the response in patients with prostate cancer and bone metastases treated with standard treatments.
- To perform whole-body MRI studies embedded into multicentre prospective trials in order to assess the feasibility of whole-body MRI protocol implementation.
- To evaluate patients' acceptance of whole-body MRI studies in order to assess the feasibility of the implementation of whole-body MRI as the standard of care in clinical practice.
- To develop simpler-whole body MRI data analysis techniques, including software development for automatic segmentation tools, in order to being able to standardise data analysis.
- To take into account intra-patient heterogeneity in response to treatment between different metastases in whole-body MRI. This could be achieved by introducing colour-coded ADC maps and ADC histograms studies and developing existing bioinformatics tools.
- To define the optimal timings for response assessment by whole-body MRI. In order to do this, we will need clinical trials testing whole-body MRI at

different time points on treatment (from a few days to several weeks) and correlate MRI changes with patient outcomes.



# Conclusions





## Conclusions

---

### 9.1. General conclusions

---

One practical conclusion of the studies presented in this thesis is the demonstration of the feasibility of performing whole-body DWI in reasonably short data acquisition times (25 minutes), without the need for contrast media, radioactive materials or ionising radiation. Moreover, whole-body DWI is a robust technique; data acquisition is relatively simple and the protocols can be implemented in most commonly used MRI scanners. This facilitates multicentre and longitudinal studies and eventually the implementation of whole-body DWI in everyday clinical practice.

Moreover, the delineation of the whole-body metastatic bone disease is feasible with semi-automated segmentation tools such as that developed by OsiriX. Assessing metastatic bone disease from prostate cancer with whole-body DWI is currently possible allowing us to analyse the whole tumour burden and its spatial heterogeneity in reasonable acquisition and imaging analysis times.

The positive results of these studies, indicating that whole-body DWI has a prognostic and response value in patients with CRPC and bone metastases and that DWI parameters correlate with histological features in bone metastases, represent relevant steps towards the validation and clinical implementation of whole-body DWI as a prognostic and response biomarker in mCRPC. The next steps are now to replicate these studies in larger prospective cohorts with standard treatments in prostate cancer. In parallel it is crucial to optimise and standardise a whole-body DWI protocol in multicentre studies.

### 9.2. Specific conclusions

---

1. Assessment of the total volume of bone metastases by whole-body DWI informs on the overall survival of mCRPC patients.

2. Volume of bone metastases assessed by whole-body DWI correlates with established prognostic biomarkers for patients with advanced mCRPC, including CTC count.
3. DWI and DIXON quantitative chemical shift imaging derived FF differentiates bone metastases and non-metastatic bone in patients with prostate cancer. In our cohort, the median ADC and muscle-normalised DWI signal were significantly higher and the median FF was significantly lower in bone metastases than in non-metastatic bone in patients with CRPC (median  $993 \times 10^{-6} \text{ mm}^2/\text{s}$  vs.  $601.75 \times 10^{-6} \text{ mm}^2/\text{s}$ , 4 AU vs. 1.6 AU and 16% vs. 63% respectively);  $p < 0.001$ .
4. In bone metastases from prostate cancer, DWI and DIXON quantitative chemical shift imaging-derived FF differentiates metastases with detectable cancer and those with no detectable tumour cells in the bone biopsy. In our cohort, the median ADC and FF were significantly lower and median nDWI signal was significantly higher in biopsies with cancer cells than in those with no detectable tumour cells (median  $898 \times 10^{-6} \text{ mm}^2/\text{s}$  vs.  $1617 \times 10^{-6} \text{ mm}^2/\text{s}$ , 11.45% vs. 62% and 5.25 AU vs. 2.3 AU respectively);  $p < 0.001$  in all cases.
5. Decreases in the total volume of bone metastases assessed with whole-body DWI indicate response to treatment with PARP inhibitors in metastatic prostate cancer. Responding patients showed a decrease in total diffusion volume (median: -41.1%; range: -58.8%, -6.3%), but no decrease was observed in non-responders (median: +20.7%; range +0.0%, +76.9%); this difference between responders and non-responders was significant ( $p = 0.001$ ).

6. Increases in the whole-body median ADC of bone metastases after 12 weeks of treatment were associated with the response to olaparib in metastatic prostate cancer (OR: 1.08, 95% CI 1.00, 1.15,  $p=0.04$ ).
7. Limited assessment of up to five target bone metastases instead of whole-skeleton assessment can still inform on response to treatment (OR: 0.89, 95% CI 0.80, 0.99,  $p=0.04$ ). This may facilitate the implementation of the assay into large populations by simplifying data analysis.
8. The ADC and DWI signal at a single metastasis level are indicators of the cell burden in prostate cancer bone metastases. There was an inverse correlation between histological cellularity burden as an ordinal variable and the ADC ( $r=-0.57$ ;  $p<0.001$ ) and FF ( $r=-0.59$ ;  $p<0.001$ ), as well as a positive correlation with nDWI signal intensity ( $r=0.59$ ;  $p<0.001$ ).
9. FF in single metastases assessed by MRI correlates with the histological fat content in the bone biopsies in prostate cancer bone metastases. There was a positive correlation between the median FF on MRI and percentage of histological fat content in the bone biopsies ( $r=0.60$ ;  $p<0.001$ ).
10. In patients with bone biopsies taken prior to and during treatment with different anticancer therapies, MP MRI changes in prostate cancer bone metastases paralleled histological changes in response to treatment.



# **Bibliography**



## 10. Bibliography

---

1. Huggins C, Hodges CV. Studies on prostatic cancer. I. The effect of castration, of estrogen and androgen injection on serum phosphatases in metastatic carcinoma of the prostate. *CA Cancer J Clin.* 1972;22(4):232-40.
2. de Bono JS, Logothetis CJ, Molina A, Fizazi K, North S, Chu L, et al. Abiraterone and increased survival in metastatic prostate cancer. *N Engl J Med.* 2011;364(21):1995-2005.
3. Scher HI, Fizazi K, Saad F, Taplin ME, Sternberg CN, Miller K, et al. Increased survival with enzalutamide in prostate cancer after chemotherapy. *N Engl J Med.* 2012;367(13):1187-97.
4. de Bono JS, Oudard S, Ozguroglu M, Hansen S, Machiels JP, Kocak I, et al. Prednisone plus cabazitaxel or mitoxantrone for metastatic castration-resistant prostate cancer progressing after docetaxel treatment: a randomised open-label trial. *Lancet.* 2010;376(9747):1147-54.
5. Tannock IF, de Wit R, Berry WR, Horti J, Pluzanska A, Chi KN, et al. Docetaxel plus prednisone or mitoxantrone plus prednisone for advanced prostate cancer. *N Engl J Med.* 2004;351(15):1502-12.
6. Parker C, Nilsson S, Heinrich D, Helle SI, O'Sullivan JM, Fossa SD, et al. Alpha emitter radium-223 and survival in metastatic prostate cancer. *N Engl J Med.* 2013;369(3):213-23.
7. Mateo J, Carreira S, Sandhu S, Miranda S, Mossop H, Perez-Lopez R, et al. DNA-Repair Defects and Olaparib in Metastatic Prostate Cancer. *N Engl J Med.* 2015;373(18):1697-708.
8. Sternberg CN, Petrylak DP, Sartor O, Witjes JA, Demkow T, Ferrero JM, et al. Multinational, double-blind, phase III study of prednisone and either satraplatin or placebo in patients with castrate-refractory prostate cancer progressing after prior chemotherapy: the SPARC trial. *J Clin Oncol.* 2009;27(32):5431-8.
9. Cheng HH, Pritchard CC, Boyd T, Nelson PS, Montgomery B. Biallelic Inactivation of BRCA2 in Platinum-sensitive Metastatic Castration-resistant Prostate Cancer. *Eur Urol.* 2016;69(6):992-5.



10. Emmett L, Willowson K, Violet J, Shin J, Blanksby A, Lee J. Lutetium 177 PSMA radionuclide therapy for men with prostate cancer: a review of the current literature and discussion of practical aspects of therapy. *J Med Radiat Sci.* 2017;64(1):52-60.
11. Graff JN, Alumkal JJ, Drake CG, Thomas GV, Redmond WL, Farhad M, et al. Early evidence of anti-PD-1 activity in enzalutamide-resistant prostate cancer. *Oncotarget.* 2016;7(33):52810-7.
12. Gandaglia G, Abdollah F, Schiffmann J, Trudeau V, Shariat SF, Kim SP, et al. Distribution of metastatic sites in patients with prostate cancer: A population-based analysis. *Prostate.* 2014;74(2):210-6.
13. Eisenhauer EA, Therasse P, Bogaerts J, Schwartz LH, Sargent D, Ford R, et al. New response evaluation criteria in solid tumours: revised RECIST guideline (version 1.1). *Eur J Cancer.* 2009;45(2):228-47.
14. Scher HI, Morris MJ, Stadler WM, Higano C, Basch E, Fizazi K, et al. Trial Design and Objectives for Castration-Resistant Prostate Cancer: Updated Recommendations From the Prostate Cancer Clinical Trials Working Group 3. *J Clin Oncol.* 2016;34(12):1402-18.
15. Halabi S, Armstrong AJ, Sartor O, de Bono J, Kaplan E, Lin CY, et al. Prostate-specific antigen changes as surrogate for overall survival in men with metastatic castration-resistant prostate cancer treated with second-line chemotherapy. *J Clin Oncol.* 2013;31(31):3944-50.
16. Berthold DR, Pond GR, Roessner M, de Wit R, Eisenberger M, Tannock AI, et al. Treatment of hormone-refractory prostate cancer with docetaxel or mitoxantrone: relationships between prostate-specific antigen, pain, and quality of life response and survival in the TAX-327 study. *Clin Cancer Res.* 2008;14(9):2763-7.
17. Stejskal EO TJ. Spin diffusion measurements: spin echoes in the presence of time-dependent field gradient. *J Chem Phys.* 1965;42(1):288-92.
18. Ahmed HU, El-Shater Bosaily A, Brown LC, Gabe R, Kaplan R, Parmar MK, et al. Diagnostic accuracy of multi-parametric MRI and TRUS biopsy in prostate cancer (PROMIS): a paired validating confirmatory study. *Lancet.* 2017;389(10071):815-22.
19. Thoeny HC, De Keyzer F, Oyen RH, Peeters RR. Diffusion-weighted MR imaging of kidneys in healthy volunteers and patients with parenchymal diseases: initial experience. *Radiology.* 2005;235(3):911-7.

20. Kyriazi S, Collins DJ, Messiou C, Pennert K, Davidson RL, Giles SL, et al. Metastatic ovarian and primary peritoneal cancer: assessing chemotherapy response with diffusion-weighted MR imaging--value of histogram analysis of apparent diffusion coefficients. *Radiology*. 2011;261(1):182-92.
21. Giles SL, Messiou C, Collins DJ, Morgan VA, Simpkin CJ, West S, et al. Whole-body diffusion-weighted MR imaging for assessment of treatment response in myeloma. *Radiology*. 2014;271(3):785-94.
22. Jambor I, Kuisma A, Ramadan S, Huovinen R, Sandell M, Kajander S, et al. Prospective evaluation of planar bone scintigraphy, SPECT, SPECT/CT, 18F-NaF PET/CT and whole body 1.5T MRI, including DWI, for the detection of bone metastases in high risk breast and prostate cancer patients: SKELETA clinical trial. *Acta Oncol*. 2016;55(1):59-67.
23. Koh DM, Blackledge M, Padhani AR, Takahara T, Kwee TC, Leach MO, et al. Whole-body diffusion-weighted MRI: tips, tricks, and pitfalls. *AJR Am J Roentgenol*. 2012;199(2):252-62.
24. Padhani AR, Lecouvet FE, Tunariu N, Koh DM, De Keyzer F, Collins DJ, et al. METastasis Reporting and Data System for Prostate Cancer: Practical Guidelines for Acquisition, Interpretation, and Reporting of Whole-body Magnetic Resonance Imaging-based Evaluations of Multiorgan Involvement in Advanced Prostate Cancer. *Eur Urol*. 2017;71(1):81-92.
25. Blackledge MD, Collins DJ, Tunariu N, Orton MR, Padhani AR, Leach MO, et al. Assessment of treatment response by total tumor volume and global apparent diffusion coefficient using diffusion-weighted MRI in patients with metastatic bone disease: a feasibility study. *PLoS One*. 2014;9(4):e91779.
26. Perez-Lopez R, Lorente D, Blackledge MD, Collins DJ, Mateo J, Bianchini D, et al. Volume of Bone Metastasis Assessed with Whole-Body Diffusion-weighted Imaging Is Associated with Overall Survival in Metastatic Castration-resistant Prostate Cancer. *Radiology*. 2016;280(1):151-60.
27. Reischauer C, Froehlich JM, Koh DM, Graf N, Padevit C, John H, et al. Bone metastases from prostate cancer: assessing treatment response by using diffusion-weighted imaging and functional diffusion maps--initial observations. *Radiology*. 2010;257(2):523-31.

28. Guo AC, Cummings TJ, Dash RC, Provenzale JM. Lymphomas and high-grade astrocytomas: comparison of water diffusibility and histologic characteristics. *Radiology*. 2002;224(1):177-83.
29. Hayashida Y, Hirai T, Morishita S, Kitajima M, Murakami R, Korogi Y, et al. Diffusion-weighted imaging of metastatic brain tumors: comparison with histologic type and tumor cellularity. *AJNR Am J Neuroradiol*. 2006;27(7):1419-25.
30. Zelhof B, Pickles M, Liney G, Gibbs P, Rodrigues G, Kraus S, et al. Correlation of diffusion-weighted magnetic resonance data with cellularity in prostate cancer. *BJU Int*. 2009;103(7):883-8.
31. Liu Y, Ye Z, Sun H, Bai R. Clinical Application of Diffusion-Weighted Magnetic Resonance Imaging in Uterine Cervical Cancer. *Int J Gynecol Cancer*. 2015;25(6):1073-8.
32. Matsubayashi RN, Fujii T, Yasumori K, Muranaka T, Momosaki S. Apparent Diffusion Coefficient in Invasive Ductal Breast Carcinoma: Correlation with Detailed Histologic Features and the Enhancement Ratio on Dynamic Contrast-Enhanced MR Images. *J Oncol*. 2010;2010.
33. Nonomura Y, Yasumoto M, Yoshimura R, Haraguchi K, Ito S, Akashi T, et al. Relationship between bone marrow cellularity and apparent diffusion coefficient. *J Magn Reson Imaging*. 2001;13(5):757-60.
34. Hillengass J, Bauerle T, Bartl R, Andrulis M, McClanahan F, Laun FB, et al. Diffusion-weighted imaging for non-invasive and quantitative monitoring of bone marrow infiltration in patients with monoclonal plasma cell disease: a comparative study with histology. *Br J Haematol*. 2011;153(6):721-8.
35. Blackledge MD, Tunariu N, Orton MR, Padhani AR, Collins DJ, Leach MO, et al. Inter- and Intra-Observer Repeatability of Quantitative Whole-Body, Diffusion-Weighted Imaging (WBDWI) in Metastatic Bone Disease. *PLoS One*. 2016;11(4):e0153840.
36. Halabi S, Kelly WK, Ma H, Zhou H, Solomon NC, Fizazi K, et al. Meta-Analysis Evaluating the Impact of Site of Metastasis on Overall Survival in Men With Castration-Resistant Prostate Cancer. *J Clin Oncol*. 2016;34(14):1652-9.
37. Robinson D, Van Allen EM, Wu YM, Schultz N, Lonigro RJ, Mosquera JM, et al. Integrative clinical genomics of advanced prostate cancer. *Cell*. 2015;161(5):1215-28.

38. Lorente D, Omlin A, Zafeiriou Z, Nava-Rodrigues D, Perez-Lopez R, Pezaro C, et al. Castration-Resistant Prostate Cancer Tissue Acquisition From Bone Metastases for Molecular Analyses. *Clin Genitourin Cancer*. 2016.
39. Liu LP, Cui LB, Zhang XX, Cao J, Chang N, Tang X, et al. Diagnostic Performance of Diffusion-weighted Magnetic Resonance Imaging in Bone Malignancy: Evidence From a Meta-Analysis. *Medicine (Baltimore)*. 2015;94(45):e1998.
40. Park SH, Choi HY, Hahn SY. Correlations between apparent diffusion coefficient values of invasive ductal carcinoma and pathologic factors on diffusion-weighted MRI at 3.0 Tesla. *J Magn Reson Imaging*. 2015;41(1):175-82.
41. Chen L, Liu M, Bao J, Xia Y, Zhang J, Zhang L, et al. The correlation between apparent diffusion coefficient and tumor cellularity in patients: a meta-analysis. *PLoS One*. 2013;8(11):e79008.
42. Padhani AR, van Ree K, Collins DJ, D'Sa S, Makris A. Assessing the relation between bone marrow signal intensity and apparent diffusion coefficient in diffusion-weighted MRI. *AJR Am J Roentgenol*. 2013;200(1):163-70.
43. Messiou C, Collins DJ, Morgan VA, Desouza NM. Optimising diffusion weighted MRI for imaging metastatic and myeloma bone disease and assessing reproducibility. *Eur Radiol*. 2011;21(8):1713-8.
44. Dietrich O, Geith T, Reiser MF, Baur-Melnyk A. Diffusion imaging of the vertebral bone marrow. *NMR Biomed*. 2015.
45. Perez-Lopez R, Lorente D, Blackledge MD, Collins DJ, Mateo J, Bianchini D, et al. Volume of Bone Metastasis Assessed with Whole-Body Diffusion-weighted Imaging Is Associated with Overall Survival in Metastatic Castration-resistant Prostate Cancer. *Radiology*. 2016:150799.
46. Perez-Lopez R, Mateo J, Mossop H, Blackledge MD, Collins DJ, Rata M, et al. Diffusion-weighted Imaging as a Treatment Response Biomarker for Evaluating Bone Metastases in Prostate Cancer: A Pilot Study. *Radiology*. 2016:160646.
47. Le Ster C, Gambarota G, Lasbleiz J, Guillin R, Decaux O, Saint-Jalmes H. Breath-hold MR measurements of fat fraction, T1, and T2\* of water and fat in vertebral bone marrow. *J Magn Reson Imaging*. 2016;44(3):549-55.
48. Daldrup-Link HE, Henning T, Link TM. MR imaging of therapy-induced changes of bone marrow. *Eur Radiol*. 2007;17(3):743-61.

49. Teman CJ, Wilson AR, Perkins SL, Hickman K, Prchal JT, Salama ME. Quantification of fibrosis and osteosclerosis in myeloproliferative neoplasms: a computer-assisted image study. *Leuk Res.* 2010;34(7):871-6.
50. Ferraldeschi R, Nava Rodrigues D, Riisnaes R, Miranda S, Figueiredo I, Rescigno P, et al. PTEN protein loss and clinical outcome from castration-resistant prostate cancer treated with abiraterone acetate. *Eur Urol.* 2015;67(4):795-802.
51. Rosset A, Spadola L, Ratib O. OsiriX: an open-source software for navigating in multidimensional DICOM images. *J Digit Imaging.* 2004;17(3):205-16.
52. Insight Segmentation and Registration Toolkit (ITK). Available via: <http://itk.org/>  
[
53. Ulmert D, Kaboteh R, Fox JJ, Savage C, Evans MJ, Lilja H, et al. A novel automated platform for quantifying the extent of skeletal tumour involvement in prostate cancer patients using the Bone Scan Index. *Eur Urol.* 2012;62(1):78-84.
54. Hellman S, Weichselbaum RR. Oligometastases. *J Clin Oncol.* 1995;13(1):8-10.
55. Ost P, Bossi A, Decaestecker K, De Meerleer G, Giannarini G, Karnes RJ, et al. Metastasis-directed therapy of regional and distant recurrences after curative treatment of prostate cancer: a systematic review of the literature. *Eur Urol.* 2015;67(5):852-63.
56. Ost P, Jereczek-Fossa BA, As NV, Zilli T, Muacevic A, Olivier K, et al. Progression-free Survival Following Stereotactic Body Radiotherapy for Oligometastatic Prostate Cancer Treatment-naïve Recurrence: A Multi-institutional Analysis. *Eur Urol.* 2016;69(1):9-12.

# **Annexes**



## 11. Annexes

---

### Other publications co-authored by the candidate during the PhD program

---

1. Mateo J, Carreira S, Sandhu S, Miranda S, Mossop H, **Perez-Lopez R**, Nava Rodrigues D, Robinson D, Omlin A, Tunariu N, Boysen G, Porta N, Flohr P, Gillman A, Figueiredo I, Paulding C, Seed G, Jain S, Ralph C, Protheroe A, Hussain S, Jones R, Elliott T, McGovern U, Bianchini D, Goodall J, Zafeiriou Z, Williamson CT, Ferraldeschi R, Riisnaes R, Ebbs B, Fowler G, Roda D, Yuan W, Wu YM, Cao X, Brough R, Pemberton H, A'Hern R, Swain A, Kunju LP, Eeles R, Attard G, Lord CJ, Ashworth A, Rubin MA, Knudsen KE, Feng FY, Chinnaiyan AM, Hall E, de Bono JS. **DNA-Repair Defects and Olaparib in Metastatic Prostate Cancer.** *N Engl J Med.* 2015 Oct 29;373(18):1697-708.

*The candidate performed a central review of imaging assays (CT and BS) as part of the primary endpoint analysis for the TOPARP-A phase II multicentre clinical trial of olaparib in prostate cancer. Additionally, the candidate performed soft-tissue biopsies of nodal and visceral metastases for genomic sequencing and the molecular characterisation of the tumour.*

2. Robinson D, Van Allen EM, Wu YM, Schultz N, Lonigro RJ, Mosquera JM, Montgomery B, Taplin ME, Pritchard CC, Attard G, Beltran H, Abida W, Bradley RK, Vinson J, Cao X, Vats P, Kunju LP, Hussain M, Feng FY, Tomlins SA, Cooney KA, Smith DC, Brennan C, Siddiqui J, Mehra R, Chen Y, Rathkopf DE, Morris MJ, Solomon SB, Durack JC, Reuter VE, Gopalan A, Gao J, Loda M, Lis RT, Bowden M, Balk SP, Gaviola G, Sougnez C, Gupta M, Yu EY, Mostaghel EA, Cheng HH, Mulcahy H, True LD, Plymate SR, Dvinge



H, Ferraldeschi R, Flohr P, Miranda S, Zafeiriou Z, Tunariu N, Mateo J, **Perez-Lopez R**, Demichelis F, Robinson BD, Schiffman M, Nanus DM, Tagawa ST, Sigaras A, Eng KW, Elemento O, Sboner A, Heath EI, Scher HI, Pienta KJ, Kantoff P, de Bono JS, Rubin MA, Nelson PS, Garraway LA, Sawyers CL, Chinnaiyan AM. **Integrative clinical genomics of advanced prostate cancer.** *Cell.* 2015 May 21;161(5):1215-28. doi: 10.1016/j.cell.2015.05.001.

*The candidate was involved in performing imaging-guided biopsies of nodal and visceral metastases for genomic sequencing and the molecular characterisation of the tumour. This paper is considered to be the landscape study of genomics in advanced prostate cancer.*

3. Ferraldeschi R, Nava Rodrigues D, Riisnaes R, Miranda S, Figueiredo I, Rescigno P, Ravi P, Pezaro C, Omlin A, Lorente D, Zafeiriou Z, Mateo J, Altavilla A, Sideris S, Bianchini D, Grist E, Thway K, **Perez Lopez R**, Tunariu N, Parker C, Dearnaley D, Reid A, Attard G, de Bono J. **PTEN Protein Loss and Clinical Outcome from Castration-resistant Prostate Cancer Treated with Abiraterone Acetate.** *Eur Urol.* 2015 Apr;67(4):795-802.

*The candidate performed imaging-guided biopsies for the molecular characterisation of the tumour and reviewed the CT and MRI scans of the patients included in this study.*

4. D. Lorente, A. Omlin, R. Ferraldeschi, C. Pezaro, **R. Perez-Lopez**, J. Mateo, Altavilla A, Zafeirou Z, Tunariu N, Parker C, Dearnaley D, Gillessen S, de Bono J, Attard G. **Tumour responses following a steroid switch from prednisone to dexamethasone in castration-resistant prostate cancer patients progressing on abiraterone.** *Br J Cancer.* 2014 Dec 9;111(12):2248-53.

*The candidate performed imaging-guided biopsies for the molecular characterisation of the tumour and reviewed the CT and MRI scans of the patients included in this study.*

5. C. Pezaro, A. Omlin, **R. Perez-Lopez**, D. Mukherji, G. Attard, D. Bianchini, D., Lorente D., Parker C., Dearneley D., de Bono JS, Sohaib A, Tunariu N. **Progressive computed tomography (CT) appearances preceding malignant spinal cord compression (MSCC) in men with castration-resistant prostate cancer.** *Clin Radiol.* 2015 Apr; 70(4):359-65. doi: 10.1016/j.crad.2014.05.104.

*The candidate participated in the study design and data generation and interpretation.*

6. Lorente D, Mateo J, **Perez-Lopez R**, de Bono JS, Attard G. **Sequencing of agents in castration-resistant prostate cancer.** *Lancet Oncol.* 2015 Jun;16(6):e279-92. doi: 10.1016/S1470-2045(15)70033-1.

*The candidate reviewed the manuscript on the state-of-the-art for management and response assessment in advanced prostate cancer.*

7. Frenel JS, Carreira S, Goodall J, Roda D, **Perez-Lopez R**, Tunariu N, Riisnaes R, Miranda S, Figueiredo I, Nava-Rodrigues D, Smith A, Leux C, Garcia-Murillas I, Ferraldeschi R, Lorente D, Mateo J, Ong M, Yap TA, Banerji U, Gasi Tandefelt D, Turner N, Attard G, de Bono JS. **Serial Next-Generation Sequencing of Circulating Cell-Free DNA Evaluating Tumor Clone Response To Molecularly Targeted Drug Administration.** *Clin Cancer Res.* 2015 Oct 15;21(20):4586-96.

*The candidate participated in the study design, set up, data generation, collection and interpretation. The candidate analysed responses of the imaging assays to several new anticancer therapies being tested in clinical trials to identify areas of intra-patient heterogeneity in response to therapy in parallel with the assessment of the genomic profiling of circulating DNA samples from the same patients.*

8. Rescigno P, Lorente D, Bianchini D, Ferraldeschi R, Kolinsky MP, Sideris S, Zafeiriou Z, Sumanasuriya S, Smith AD, Mehra N, Jayaram A, **Perez-Lopez R**, Mateo J, Parker C, Dearnaley DP, Tunariu N, Reid A, Attard G, de Bono JS. **Prostate-specific Antigen Decline After 4 Weeks of Treatment with Abiraterone Acetate and Overall Survival in Patients with Metastatic Castration-resistant Prostate Cancer.** *Eur Urol.* 2016 Mar 7.

*The candidate participated in the data generation and interpretation and review of CT and BS from the study population during treatment with abiraterone acetate.*

9. Lorente D, Omlin A, Zafeiriou Z, Nava Rodrigues D, **Perez-Lopez R**, Pezaro C, Mehra N, Sheridan E, Figueiredo I, Riisnaes R, Miranda S, Crespo M, Flohr P, Mateo J, Altavilla A, Ferraldeschi R, Bianchini D, Attard G, Tunariu N, de Bono J. **Castration-Resistant Prostate Cancer Tissue Acquisition From Bone Metastases for Molecular Analyses.** *Clin Genitourin Cancer.* 2016. 14(6):485-493.

*The candidate participated in the study design, data generation and analyses.*